NGU
Norges geologiske undersøkelse
Geological Survey of Norway

GEOLOGI FOR SAMFUNNET
GEOLOGY FOR SOCIETY

NGU Report 2013.025

Pockmarks, gas flares, carbonate crusts and their relation to tectonic and stratigraphic evolution of southwestern Barents Sea

NGU
Norges geologiske undersøkelse
Geological Survey of Norway

Geological Survey of Norway
NO-7491 Trondheim, Norway
Tel.: 47 73 90 40 00
Telefax 47 73 92 16 20

REPORT

Report no.: 2013.025 | ISSN 0800-3416 | Grading: Confidential until April 2014

Title:
Pockmarks, gas flares, carbonate crusts and their relation to tectonic and stratigraphic evolution of southwestern Barents Sea

Authors:
Shyam Chand, Terje Thorsnes, Aivo Lepland, Leif Rise, Reidulv Bøe

Client:
Lundin Norway AS

County:
Norway

Commune:
Trondheim

Map-sheet name (M=1:250.000)

Map-sheet no. and -name (M=1:50.000)

Deposit name and grid-reference:

Number of pages: 60 Price (NOK): *260*
Map enclosures: 0

Fieldwork carried out:

Date of report:
29th April, 2013

Project no.:
341300

Person responsible:
Jan J. Gamer

Summary:

The project's aim is to achieve a better understanding of shallow geological/seabed conditions and processes to support technical and environmental aspects of exploration and production along the southwestern margin of the Barents Sea, including the Hammerfest Basin, the Loppa High, the Polheim Subplatform, the Tromsø Basin/Ingøydjupet area and along the Finnmark Platform.

The project had the following subgoals:

- Cruise planning and preparations.
- Testing of methane sniffers at already known gas plume locations along the Norwegian offshore.
- Detection of water column gas flares at identified locations.
- Mapping of bathymetry and identification of neotectonic features on the seafloor and their relation to the subsurface.
- Sampling of seep gas and carbonate crusts from pockmarks and adjacent seabed for the follow-up study that will assess the potential of these crusts as proxies of the timing and intensity of leakage.
- Gas hydrate modeling.

The project has the following results:

- Three cruises were planned and carried out in April, August and September 2012, respectively.
- A total of 10 gas flares from the Polheim Subplatform were identified from water column data collected using the multibeam echosounder system during the cruise in April 2012.
- Carbonate crusts were identified in three areas using the HUGIN HUS system during the cruise in April 2012, and carbonate crusts, seep gas samples and short sediment cores were collected during the ROV cruise in September 2012.
- Pockmarks and gas flare like anomalies were identified from the Finnmark Platform during the cruise in August 2012.
- A new Quaternary sediments thickness map is compiled from existing data.

Keywords: Marine Geology	Gas hydrate	Gas Flare
Pockmark	Seismic	Shallow Gas
Multibeam bathymetry	Water column gas anomaly	Neotectonic faulting

Contents

1. INTRODUCTION

The Barents Sea is an epicontinental sea bounded by a sheared and rifted Tertiary margin to the west (Eldholm et al., 1984). Mesozoic and early Cenozoic sedimentation took place in intracratonic basins. After the early Eocene opening of the Norwegian Sea, the Tertiary sediment transport bypassed these basins, and depocentres were established on the continental margin (Spencer et al., 1984). The Bear Island Trough (Bjørnøyrenna) was formed through extensive glacial erosion (Nøttvedt et al., 1988; Eidvin and Riis, 1989; Vorren et al., 1991; Riis and Fjeldskaar, 1992) and the bulk of the eroded sediments were deposited on the continental slope on the Bear Island Trough Mouth Fan (Vorren et al., 1991; Faleide et al., 1996). The morphology of the Barents Sea has been interpreted as a submerged, inherited fluvial landscape, formed in preglacial times and later modified by glacial erosion (Nansen, 1904; Lastochkin, 1977; Vorren et al., 1986, 1991; Laberg et al., 2011). Recent drilling and coring show that the main part of the erosion took place in the late Plio-Pleistocene (<2.7 Ma) and that the corresponding sediments have mainly a glacial affinity (Eidvin and Riis, 1989; Eidvin et al., 1993, 1998; Mørk and Duncan, 1993; Hald et al., 1990; Knies et al., 2009).

Estimates show that about 1000 m of sediments may have been removed by the glacial erosion (Nøttvedt et al., 1988; Vorren et al., 1991; Riis and Fjeldskaar, 1992; Løseth et al., 1992; Nyland et al., 1992). The erosion produced a prominent erosion surface, the upper regional unconformity, URU (Solheim and Kristoffersen, 1984; Vorren et al., 1986). An upper glacigenic sediment sequence of varying thickness covers the URU (Solheim and Kristoffersen, 1984; Vorren et al., 1986). It reaches a maximum thickness of about 1000 m at the present shelf edge, and has a secondary maximum on the inner shelf, adjacent to the Norwegian coast, where it fills a large glacial trough (Vorren et al., 1989, 1990). Associated with erosion, considerable late Cenozoic uplift took place, modeled by Riis and Fjeldskaar (1992) to 900-1400 m in the western Barents Sea. A major part of the fan is of late Pliocene and Pleistocene age (Eidvin and Riis, 1989; Eidvin et al., 1993), which implies very high erosion and sedimentation rates. High erosion rates in the mid-late Pleistocene were also inferred by Vorren et al. (1991), with 150 m regionally, and as much as 400 m locally, during the last 0.8 Ma, and by Sættem et al. (1992), who suggest erosion of 200-250 m or more for the last 0.44 Ma. Seismostratigraphic interpretations indicate that grounded glaciers may have reached the shelf break of the southern Barents Sea 5-10 times during the Pleistocene (Solheim and Kritoffersen, 1984; Vorren et al., 1988; Sættem et al., 1992).

The present study is focused on two small regions along the southwestern Barents Sea. The first study includes the western margin of the Hammerfest Basin, the Loppa High and the Tromsø Basin/Ingøydjupet area. The second study focusses on the Finnmark Platform (Fig. 1). The project's aim is to achieve a better understanding of the shallow subsurface and seabed geological conditions and processes to support technical and environmental aspects of hydrocarbon exploration within the study area. The project has the following subgoals:

- To detect seep-related features, including pockmarks on the seafloor and gas flares in the water column.
- To map faults and other neo-tectonic structures and assess their nature.
- To identify carbonate crusts at the seafloor and assess their potential as indicators of fluid fluxes and timing.
- To study the Quaternary stratigraphy of the southwestern Barents Sea.

2. STUDY AREAS

The study focuses on two locations in the southwestern Barents Sea. The first location covers the previously studied (Chand et al., 2009, 2012a) region along the western margin of the Hammerfest Basin/Loppa High and the Tromsø Basin/Ingøydjupet areas and further north, hereafter referred to as the Loppa High area (Fig. 1). The Loppa High area is underlain by numerous regional faults oriented in the N-S direction and some of them branching out in the E-W direction (Fig. 1). The area is hydrocarbon prone with the recent discovery of the Skrugard and the Havis hydrocarbon fields. The northern part of the study area is also unique with a large number of subsurface gas anomalies and gas hydrate related bottom simulating reflectors (BSRs).

The region was under the influence of a thick ice sheet during the last Glacial Maximum (LGM), inferred to be 750-1000 m thick from modeling results (Siegert et al., 2001) (Fig. 1). The glaciers retreated from this region around 18 000-20 000 cal years BP (14 000-16 000 C^{14} yrs) which resulted in huge release of ice load as well as deposition of glaciomarine and marine sediments. The exact timing of the retreat is still debated, but an early retreat was suggested by Aagard Sørensen et al. (2010) based on dating of a core from Ingøydjupet. The sedimentation rates during the glaciomarine period varied between 40 and 70 cm/kyr while it settled to a modest rate of 6 cm/kyr during the last 9000 cal years BP (Aagard Sørensen et al., 2010). The study area is also located along the northernmost boundary of the Ingøydjupet depression where the basin shallows to a morainal high which represents the boundary of the stage II glaciations during the late Weichselian (Winsborrow et al., 2010) (Fig. 3). The northernmost part of the study area touches the southern boundary of the Bear Island Trough and hence is a location where many glacial advances coincide creating a chaotic pattern of depositional features (Winsborrow et al., 2010).

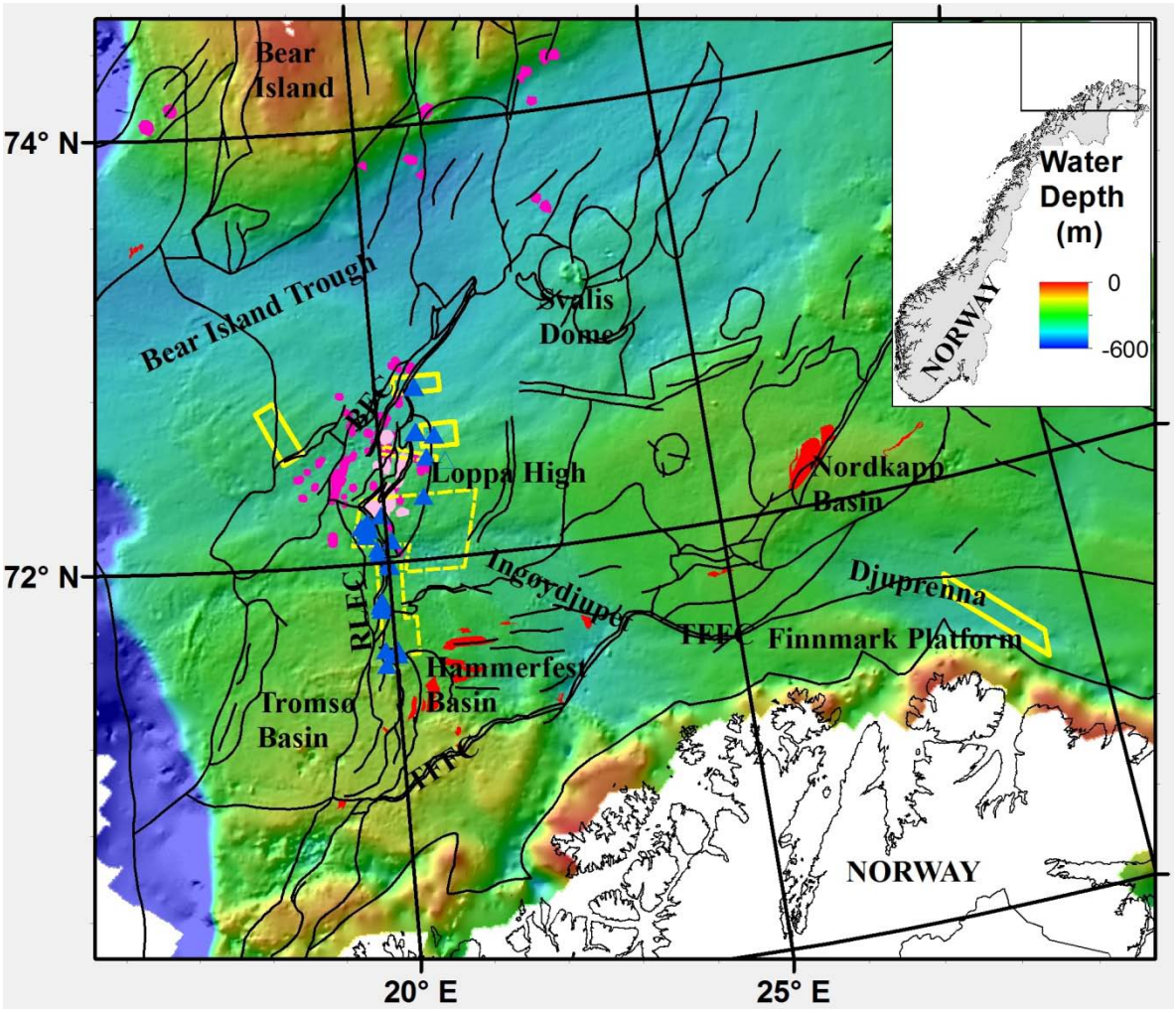

Figure 1. Bathymetry map of the SW Barents Sea showing the study areas. Also shown are areas surveyed earlier in Lundin projects using EM710 multibeam echosounder (yellow dashed polygons), gas flares (blue triangles), new study areas (yellow polygons), BSR occurrences (pink filled polygon), gas anomalies (purple filled polygons) (Andreassen and Hansen, 1995), faults at URU level (black lines) and hydrocarbon discoveries (red filled polygons). RLFC – Ringvassøy Loppa Fault Complex, BFC – Bjørnøyrenna Fault Complex, TFFC – Troms Finnmark Fault Complex.

The second study area is located along the eastern part of the Finnmark Platform south of the Nordkapp Basin, hereafter referred as Finnmark Platform area (Fig. 1). The bedrock is of Permocarboniferous to Cretaceous age with steeply dipping boundaries towards the south with glacial/postglacial sediments on top (Fig. 2). The regional Troms- Finmark Fault Complex (TFFC) cuts across the study area (Fig. 1). The region was under the influence of a thicker ice sheet (1000-1250 m) compared to the Loppa High study area (Siegert et al., 2001).

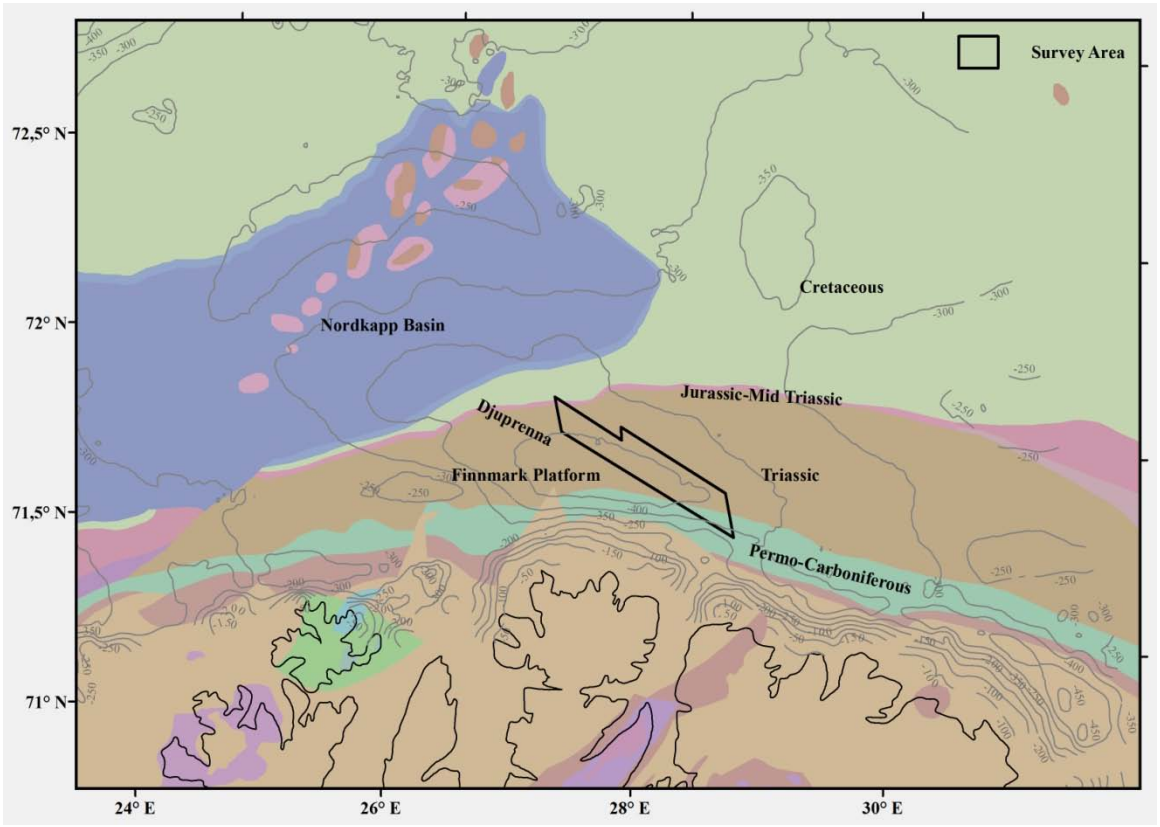

Figure 2. Structural and subcrop map of the SW Barents Sea showing the study area (black polygon) and bathymetry (contours)(Sigmond, 1992).

3. MATERIALS AND METHODS

3.1 **Bathymetry/backscatter**

The multibeam bathymetry (MBB) data in the study areas were collected by the Norwegian Defence Research Establishment (FFI) using EM710 echosounder (Figs. 1 & 3). The main advantage of this multibeam echosounder system is that it can record the water column data also. The operating frequency (70-100 kHz) is also advantageous for the intermediate water depths, between 200 m and 1000 m, where other systems usually need a change in frequency. The operating frequency of 70-100 kHz and water depths of ca. 350 m give a Fresnel zone diameter (foot print) of around 4 m thus mapping 16 m^2 by each beam. As a general rule, features smaller than the size of one fourth the wavelength cannot be resolved (Sheriff, 1980). Hence, features larger than 1 meter in diameter can be theoretically detected using the system. The water column data recorded by the system can be used for detection of active gas seeps and also detection of fauna. The presences of fish schools (air in bladder) can be easily identified and is hence useful to estimate the energy loss in the water column during detailed backscatter processing. FlederMaus (FM) Midwater package was used to analyse water column data for detecting and analysing gas anomalies. The MBB data can also be used to derive the seafloor reflection (i.e., backscatter) properties which will indirectly give an indication of sediment type/grain size and/or hardness of the sea bottom. The FM Geocoder

package was used to process the MBB data for backscatter. A 25m grid of bathymetry was already available for the major part of the Finnmark Platform study area making it easier to define the interesting locations for detailed MBB acquisition and HUGIN survey (Fig. 4).

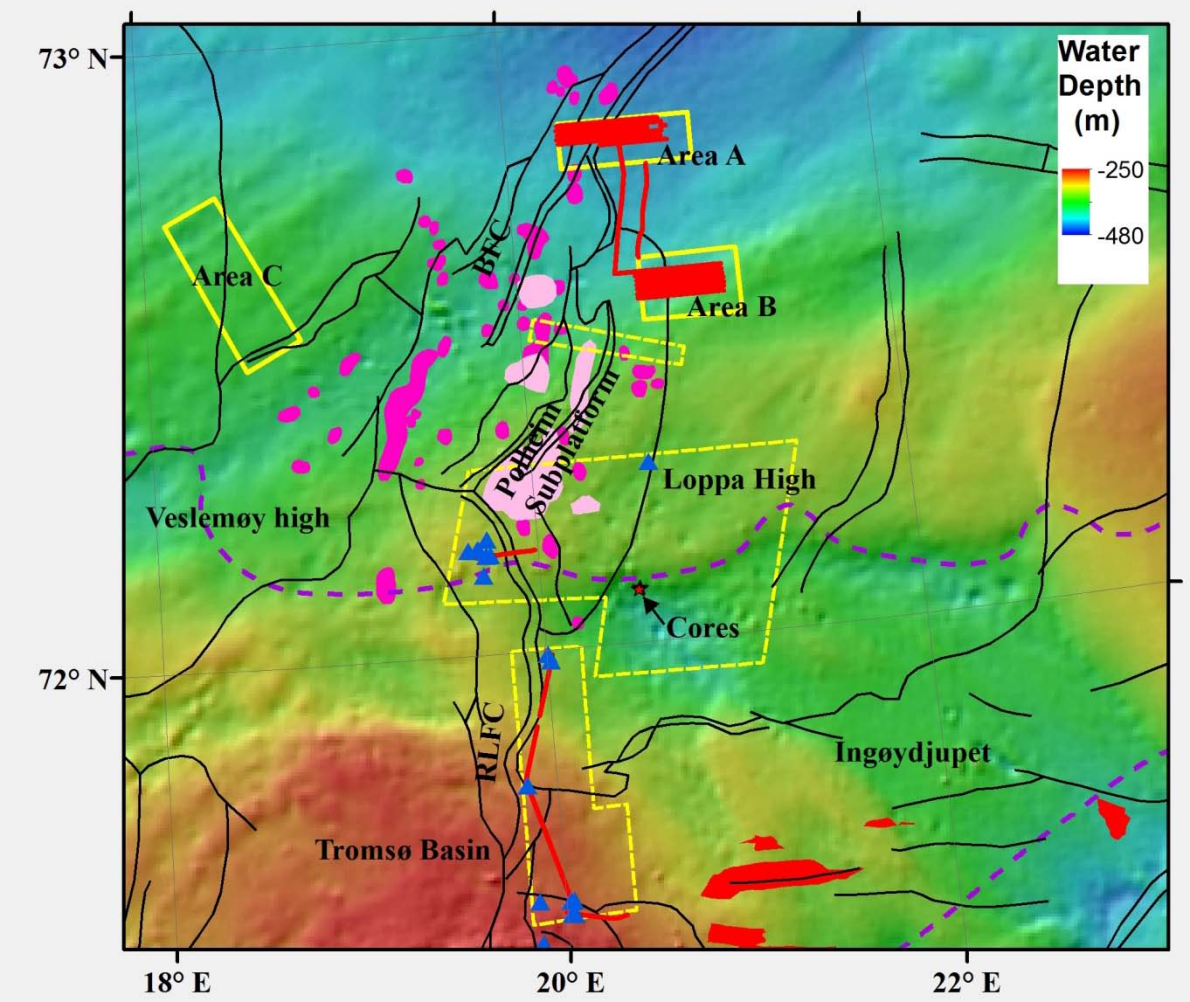

Figure 3. Bathymetry of the Loppa High study areas (yellow polygons) showing the locations of airgun data (red lines), BSR occurrences (pink filled polygons), gas anomalies (purple polygons) (Andreassen and Hansen, 1995), faults at URU level (black lines), hydrocarbon discoveries (red filled polygons), cores and subbottom profiler data (red star) and gas flares from 2008/2009 MBB data(Chand et al., 2012a,b) (blue triangles). RLFC – Ringvassøy Loppa Fault Complex, BFC – Bjørnøyrenna Fault Complex.

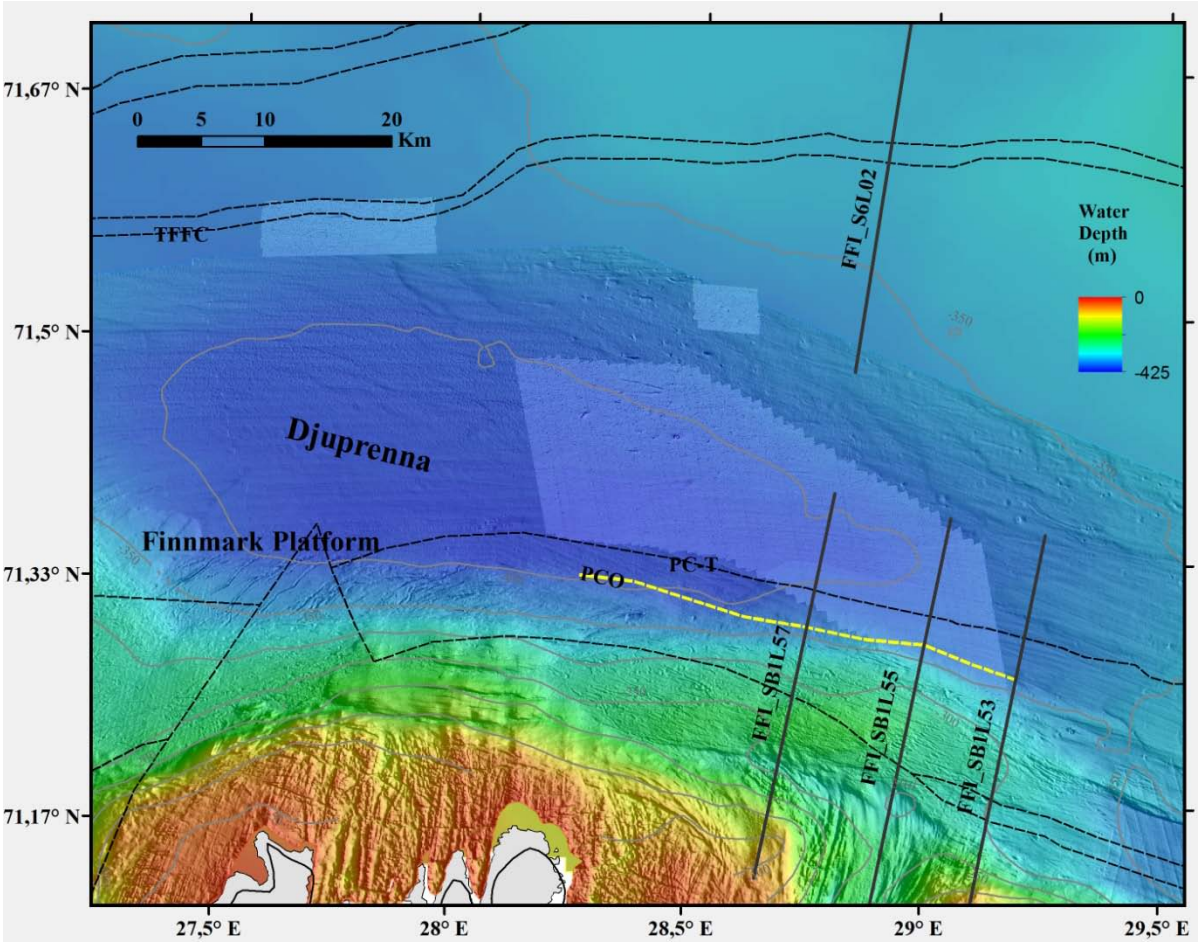

Figure 4. Multibeam bathymetry of the Finnmark study area from MAREANO data showing locations of FFI airgun seismic (black lines), bedrock formation boundaries (black dashed lines) (Sigmond, 1992), multibeam data from the HU Sverdrup II cruise in August 2012 (overlay) and seafloor outcrop of Permo-Carboniferous bedrock (PCO) mapped from FFI 2D seismic (yellow line).

3.2 **HUGIN Payloads**

The HUGIN AUV was equipped with the following payloads: 1) An EdgeTech 2200 high resolution full spectrum chirp sub-bottom profiler (SBP), 2) HISAS, 3) Methane Sniffer, 4) Turbidity sensor, 5) B&W photo camera. The SBP was used to profile interesting features of the immediate subsurface in very high resolution (Fig. 3). The HUGIN HUS was flown ~10 m above the seafloor at a constant speed giving 50 cm horizontal resolution and a vertical resolution of less than 100 microseconds (~10 cm) with the SBP system. The HUGIN EdgeTech data are available to the user as Segy files, needing however a correction for water depth. The data were corrected for water depth using the Vista Seismic Processing package. In house software was used for converting the geographic coordinates to UTM coordinates with centimeter accuracy and converted coordinates were uploaded to the header of the Segy files.

HISAS 1030 is a high resolution interferometric synthetic aperture sonar system capable of providing very high resolution images and detailed bathymetry of the seabed. The system has a range-independent resolution of approximately 3x3 cm out to a distance of 200 m from both sides of the AUV at a speed of 2 m/s. The data were processed onboard. Raw, unprocessed sidescan sonar data in xtf format were ready within a few hours. Processed high resolution mosaics in geotiff format were available for inspection in Reflection and/or ArcMap within 10 hours of HUGIN recovery.

Multibeam echo sounder data were collected by HUGIN using the Kongsberg EM2000 system. Data were stored in .all format for further processing of bathymetry and backscatter using Fledermaus DMagic and Fledermaus GeoCoder.

The methane sniffer (METS) has a methane sensitive detector located in a detector room in the sensor head. The detector room is protected against water and pressure by a silicone membrane. The gas molecules diffuse through the membrane, following the partial pressure gradient between water and detector room, according to Henry's law. Hence, the concentration in the detector room is directly correlated to the concentration in the outside water. The sensitivity in the pumped flow-through mode is 1nM – 500nM. The reaction time is within a few seconds (METS product sheet, from www.franatech.com). The T90 time (time to reach 90% of the end-value) for this version of METS is typically within 5 min in pumped-through mode (Michel Masson, Franatech – pers comm.)

The methane sniffer was used to estimate the amount of leakage at locations where gas flares have been identified during previous cruises. In addition to the methane sniffer, HUGIN also carried temperature, turbidity, salinity and visibility sensors. Data set deliveries included GeoTiff files and ASCII text files. The TFish B&W camera provided very high resolution image of the seafloor. The TFish images were available co-registered with the HISAS data within hours through the Reflection software system on-board HU Sverdrup.

3.3 **2D Seismic**

26 airgun seismic lines (Fig. 3) were collected from different parts of the study are at the Loppa High using two 40 cubic inch air guns. Data were stored using Delph Seismic v. 2., and stored as *. par and *.tra files. The tar files were in the SEGY format, and a few lines were inspected using SeisView2 in order to make sure that the quality was satisfactory. The data were used to interpret the Quaternary stratigraphy and the subsurface structural set-up at gas flare locations. Industry 2D seismic from the study area was evaluated for subsurface anomalies. 2D single channel seismic lines from FFI surveys partially covering the Finnmark Platform study area were used to delineate the location of faults and formation boundaries (Fig. 4).

3.4 **ROV**

Sampling of the gas, crusts and adjacent sediments was undertaken using the ROV deployed from the M/V Fugro Meridian in September, 2012. The Hugin data collected during the HU Sverdrup II cruise in April 2012 provided unambiguous evidence for gas seepage and the occurrence of carbonate crusts at the seabed in several areas of the Loppa High. The ROV work was focussed on five localities, PR1-PR5 (Fig. 5) including two pockmarks (PR2, PR5) and three localities outside of pockmark areas where carbonates crusts have been identified by Hugin. Gas samples were obtained from one locality (PR1) using hydraulically operated syringe sampler. Hugin profiling had indicated active gas bubbling also at the PR4 locality, but poor visibility due the easily resuspendable sediment at the locality hindered finding the bubbling sites by ROV. Short, c. 20 cm long sediment cores were obtained adjacent to the crust by pushing the plastic tube into the sediment (Fig. 6). Active bubbling typically accompanied the sediment sampling indicating the gas-saturated nature of the sediments. A total of 18 carbonate crust samples was collected from four localities.

Sediment cores were upon recovery immediately frozen on board. Frozen sediment cores were shipped to GFZ German Research Centre for Geosciences, Helmhotz Centre Potsdam in November 2012 where the cores were subsampled for organic and inorganic geochemical analyses. Sediment analyses on parallel subsamples will be undertaken in laboratories at GFZ and NGU. Carbonate crust samples were sliced by sawing at NGU in November 2012. A total of 71 petrographic thin sections have been made of all crust samples whereas selected specimens have been delivered for biomarker analyses at GFZ and U-Th dating and Sr isotope analyses at Natural Environmental Research Council (NERC) Isotope Geosciences Laboratory (NIGL). Analyses of two gas samples (carbon and hydrogen isotopic composition of CH_4 is presented below) has been arranged by Lundin AS using the Applied Petroleum Technology AS facility.

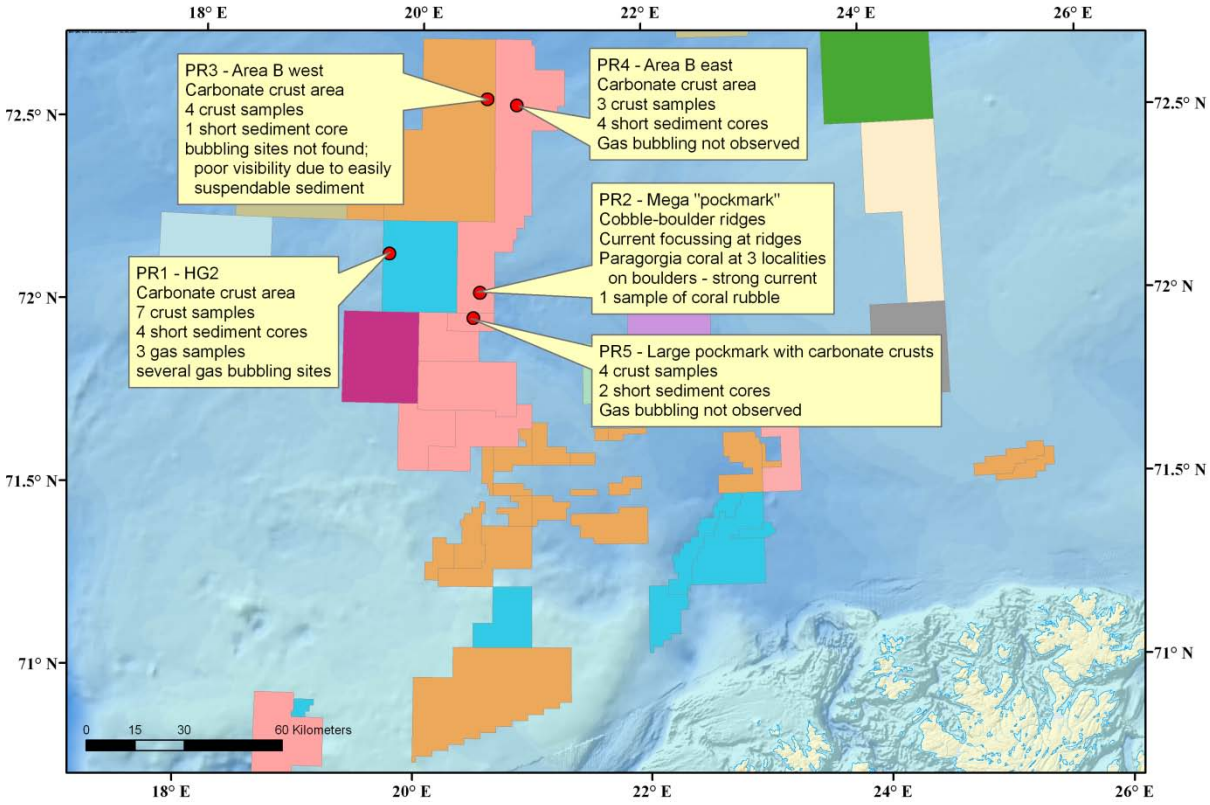

Figure 5. ROV survey areas and list of materials collected during the M/V Fugro Meridian cruise in the Loppa High area in September 2012.

Figure 6. ROV sampling of sediments by push-in tubes adjacent to the carbonate crusts.

3.5 **Hydrate Stability Modelling**

Present thickness of the methane hydrate stability zone (MHSZ) for the Barents Sea was modelled using a modified version of the gas hydrate stability modelling program CSMHYD (Sloan, 1990; Chand et al., 2008). A smooth bathymetry model available for the whole southwestern Barents Sea (Fig. 1), available heat flow values (Bugge et al., 2002) and measured bottom water temperature values (WOD, 2005) were used to predict the present MHSZ thickness. Gas hydrate stability zone (GHSZ) thickness for detailed study areas were modelled using geothermal gradient and gas composition values from nearby wells.

4. POCKMARKS, GAS FLARES, GAS HYDRATES, NEOTECTONICS AND QUATERNARY STRATIGRAPHY

4.1 **General morphology**

4.1.1. Loppa High

Multibeam bathymetry data were collected on the northern part of the Loppa High in April 2012 at two study areas, Area A and Area B ((Fig. 7). Water depths range from 350 m to 480 m, with largest depths in the northernmost part of the new datasets (Fig. 7). Both areas are located on the upper northern flank of the wide topographical ridge between Ingøydjupet and Bjørnøyrenna (Fig. 7).

In Area A at the Loppa High, an area of c. 175 square kilometers was mapped using the EM710 multibeam echo sounder. The water depth varied between 412 and 480 m (Fig. 8). A number of pockmarks with diameter up to 20 m occur in the eastern, deepest parts. The seabed is mainly composed of till, heavily incised by iceberg plough marks. Judging from the TFish photos, the dominant sediment type is gravelly sandy mud. Somewhat finer sediments in the deeper eastern parts is indicated by slightly lower backscatter and presence of pockmarks. The backscatter map (Fig. 9) reveals that the flanks of the plough marks have a higher backscatter than the unploughed areas, while occurrence of softer sediments in the plough marks is indicated by low backscatter. HUGIN surveys using SAS, the methane sniffer and the TFish system were run in the central southern part of Area A (Fig. 7). At the time of planning the HUGIN dives, the gas flare had not been identified in the EM710 data, and therefore HUGIN surveys did unfortunately not cover the flare site.

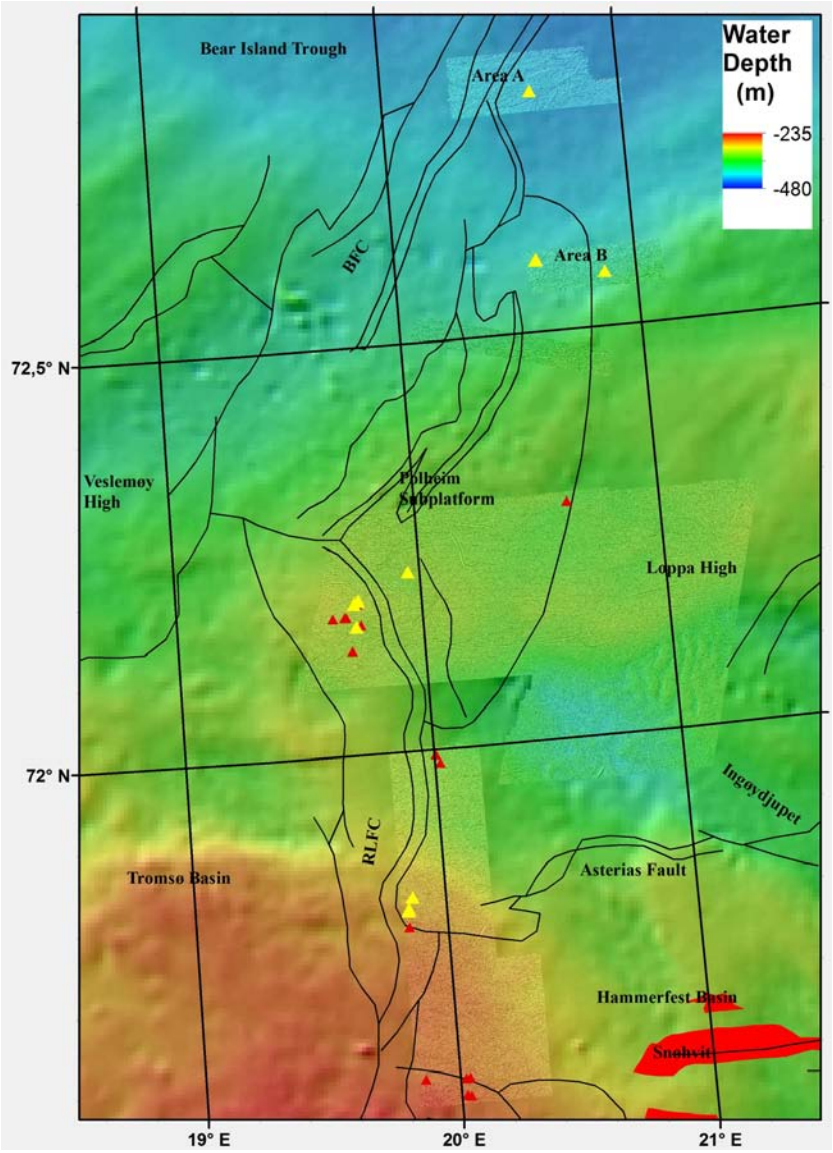

Figure 7. Bathymetry of the study area showing area where detailed multibeam bathymetry have been collected, flares mapped using water column data from 2008 and 2009 (red triangles) and 2012 (yellow triangles), hydrocarbon discoveries (red polygons) and regional faults (black lines). RLFC – Ringvassøy Loppa Fault complex, BFC – Bjørnøyrenna Fault Complex.

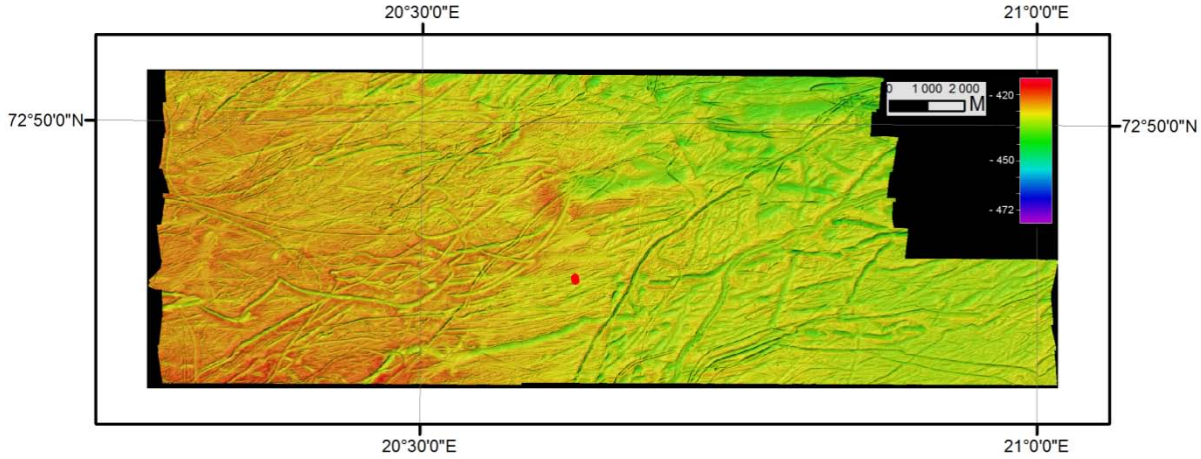

Figure 8: Shaded relief image from Area A. The gas flare (red dot) occurs in an area with no pockmarks.

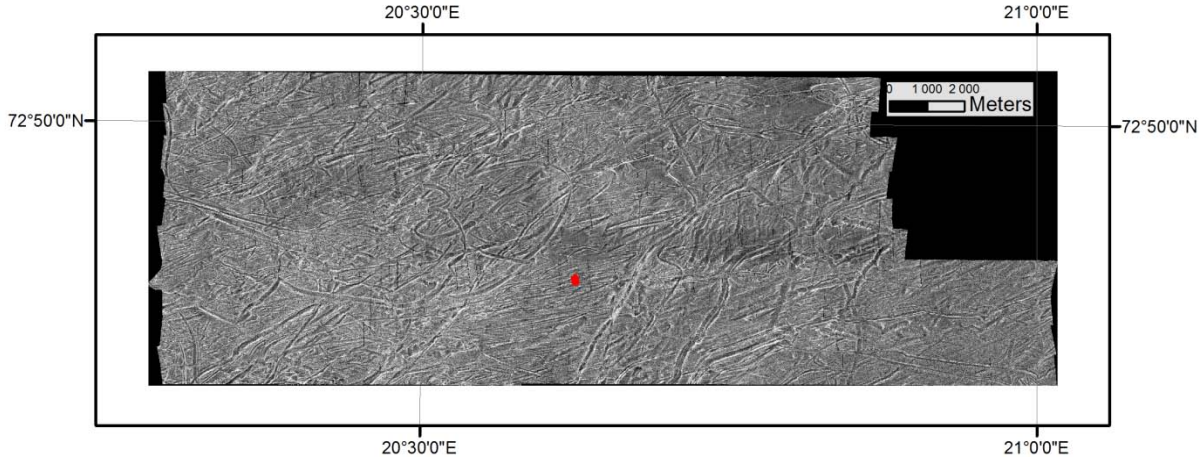

Figure 9: Backscatter map, Area A. Gas flare is marked in red.

Some unusual features were observed in the HUGIN data sets. Irregular elogated depressions in the sea floor were observed, being up to 10 m long, and a few tens of centimeters *deep* (Fig 10). These can be whale feeding marks. Gray whales have been reported to create similar marks, formed by the whales stirring up or easting, and filtering sediments (Oliver et al., 1984). A whale skeleton was also found. This was first observed in the SAS data, and thereafter confirmed by TFish photos (Fig. 11).

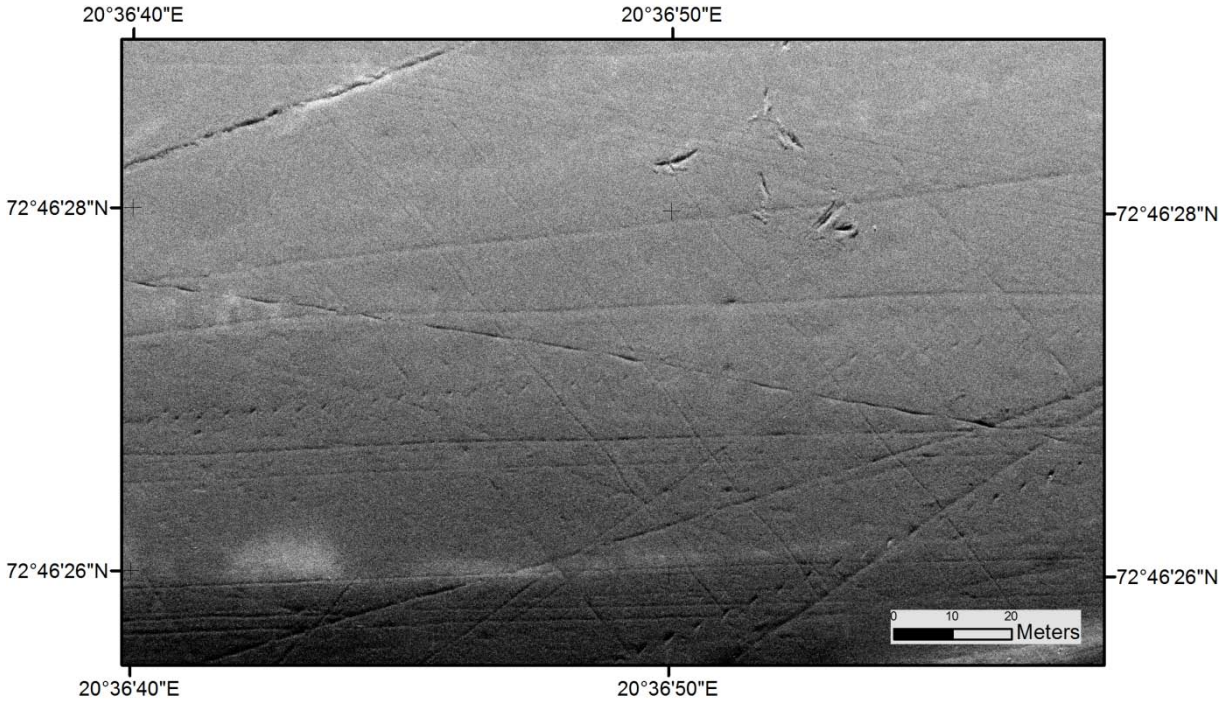

Figure 10. Whale feeding marks. Note criss-crossing trawl marks.

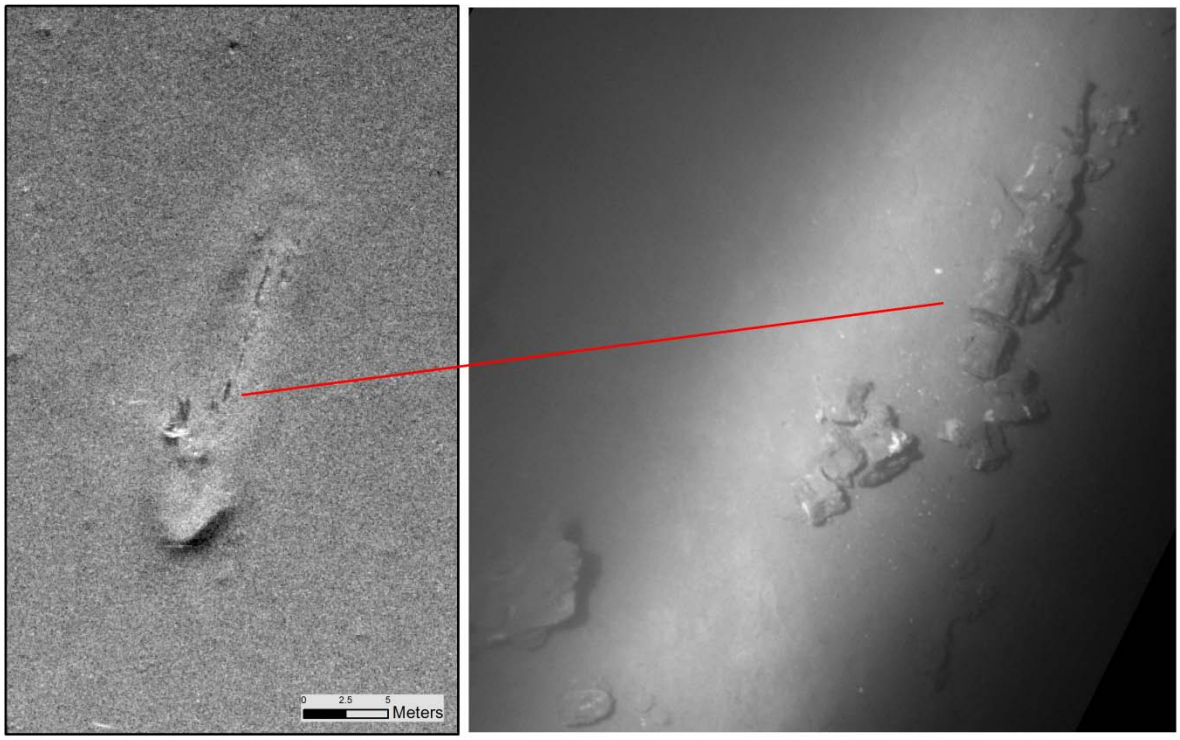

Figure 11. Whale skeleton, imaged by SAS (left) and TFish photo (right, 3 m wide).

In Area B at the Loppa High, c. 105 square kilometers were mapped using the EM710 multibeam echosounder. The water depth varies between 355 and 414 m (Fig. 12). The seabed is mainly composed of till, heavily incised by iceberg plough marks. Pockmarks are irregularly distributed over the entire area at water depths greater than c. 400 m. Judging from

the TFish photos, the dominant sediment type is gravelly sandy mud. HUGIN surveys using SAS, the methane sniffer and the TFish system were run in E-W lines covering both flare locations and a well location in the SE part.

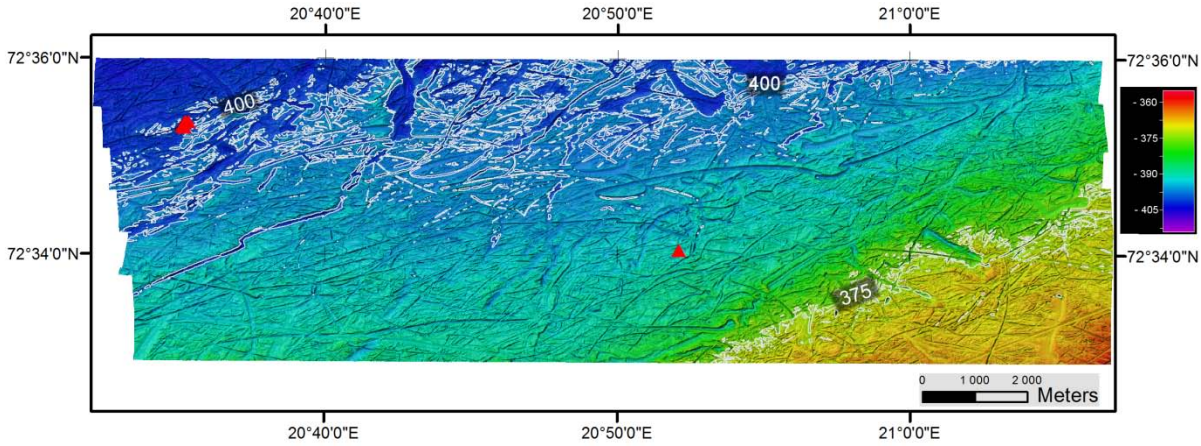

Figure 12. Shaded relief bathymetry from Area B. Gas flares in red.

The seabed sediments consist of till with abundant iceberg plough marks and boulders up to a few meters. Dominant surface sediments are muddy gravelly sand, with finer material in the iceberg plough marks, and coarser sediments on the plough mark flanks.

4.1.2. Finnmark Platform

Bathymetry data from MAREANO were used to analyse special features (Fig. 4). Water depths range from 50 to 425 m with the deepest part centrally in the study area. Water depths increase from the coast towards the Djuprenna and then decrease further northwards. The study area has a large number of pockmarks located north of the deepest part of the Djuprenna (Fig. 13). Some iceberg prodmarks and ploughmarks can be observed along the middle part.

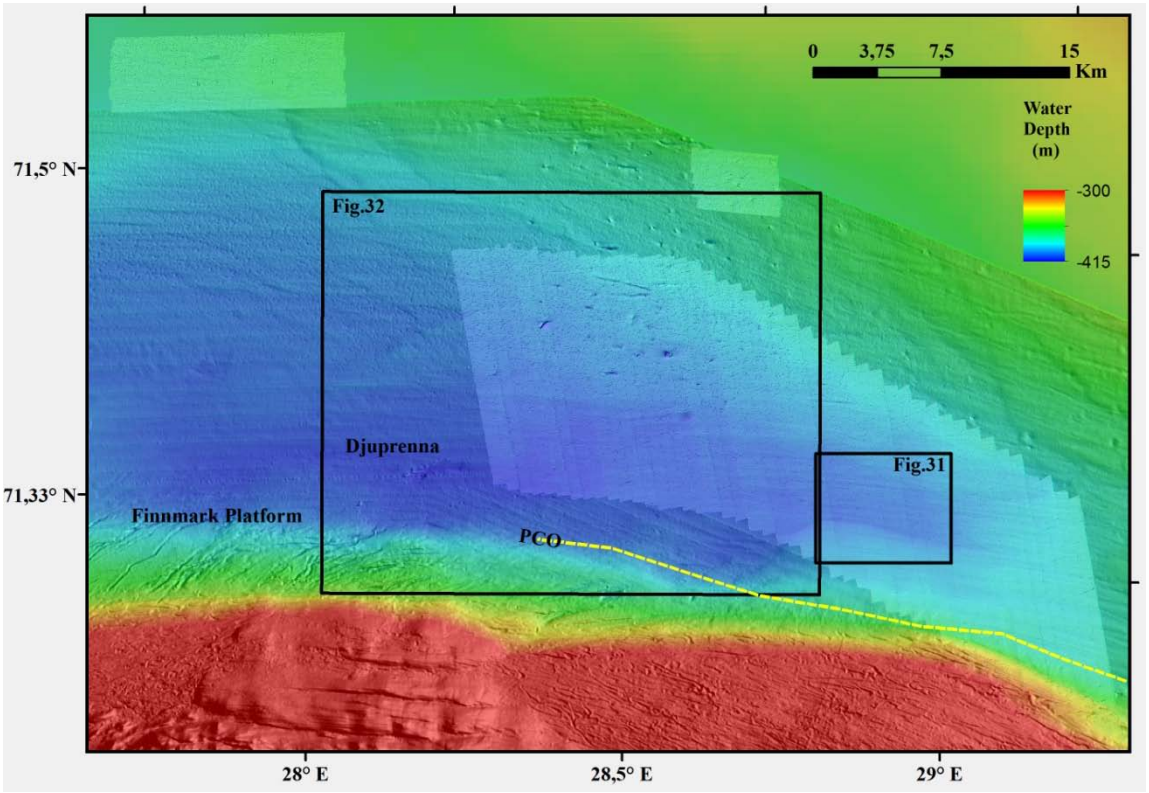

Figure 13. MAREANO multibeam bathymetry from the Finnmark study area showing multibeam data (overlay) from the HU Sverdrup II cruise in August 2012. PCO - Seafloor outcrop of Permo-Carboniferous bedrock.

4.2 **Quaternary stratigraphy of the Barents Sea**

The Quaternary stratigraphy of the SW Barents was presented in earlier NGU project reports (Chand et al., 2009 & 2012a). The compilation in this report included new airgun and TOPAS seismic lines acquired during shipborne surveys in 2008. In this report we compiled all information available up to now and produced digital map versions on some of the units mentioned in the earlier report. Interpretation of new seismic data acquired during a cruise in 2012 from this region is used to identify these units. The western and eastern parts of the SW Barents Sea are defined with different names of seismic units (Fig. 14). A regional geological profile across the western Barents Sea show their juxtaposition in relation to various other underlying units as well as units extending eastward (Fig. 14). We attempted a correlation between the units in the east and the west in the last report, and present this again here (Table 1).

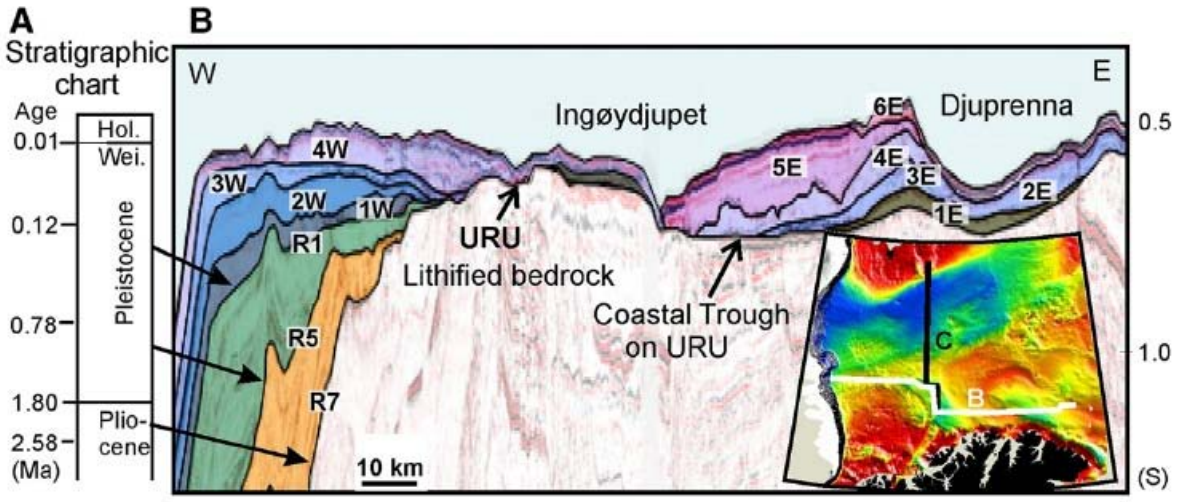

Figure 14. Geological cross section across the western Barents sea showing various Quaternary units (Andreassen et al., 2008). Notice that our study area is west of Ingøydjupet partially covering units marked 1W to 4W north of this line.

Seismo-stratigraphic interpretations along the western part of the southwestern Barents Sea indicated four major Quaternary units along the Loppa High study area (Lebesbye, 2000) (Fig. 14). The Quaternary sediment thickness map of the SW Barent Sea indicates depocentres along the Finnmark Platform area extending along the Tromsø Basin and into the Sørvestnaget Basin (Fig. 15). The deposition pattern of various units indicated show that the glaciers were active from different directions.

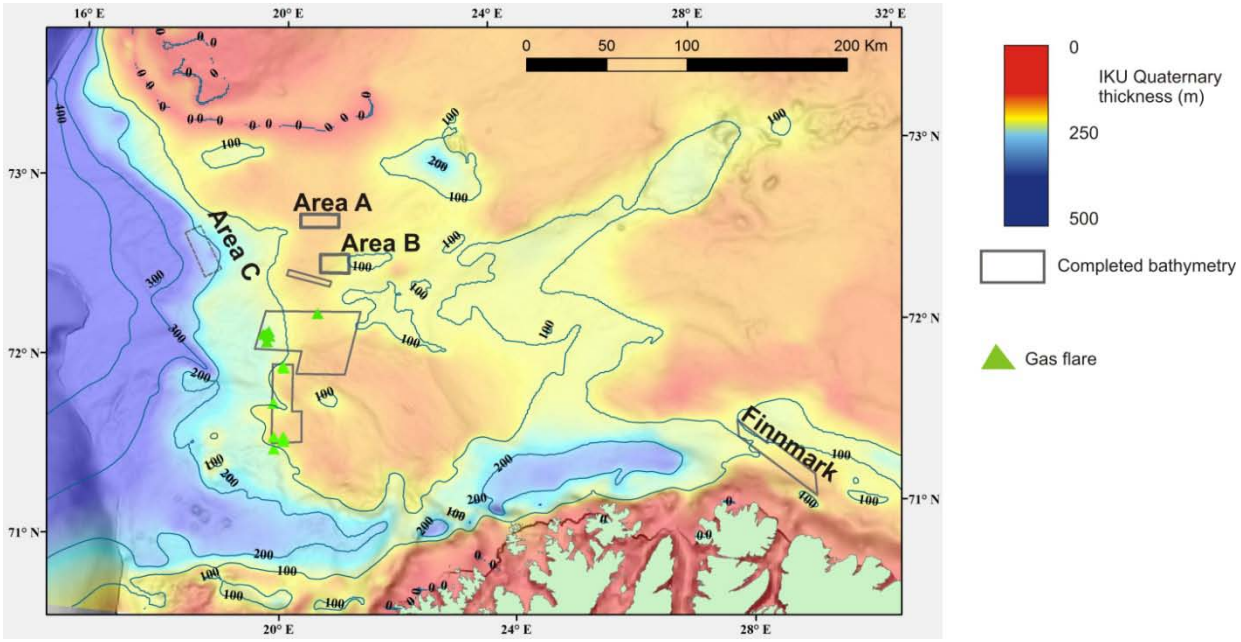

Figure 15. Quaternary sediment thickness map compiled from IKU contour map.

Table 1. Correlation of various Quaternary sedimentary units from the western Barents Sea based on information from previous studies (Lebesbye 2000; Butt et al. 2000; Solheim et al. 1998; Sættem et al. 1992) and interpretations made in this study.

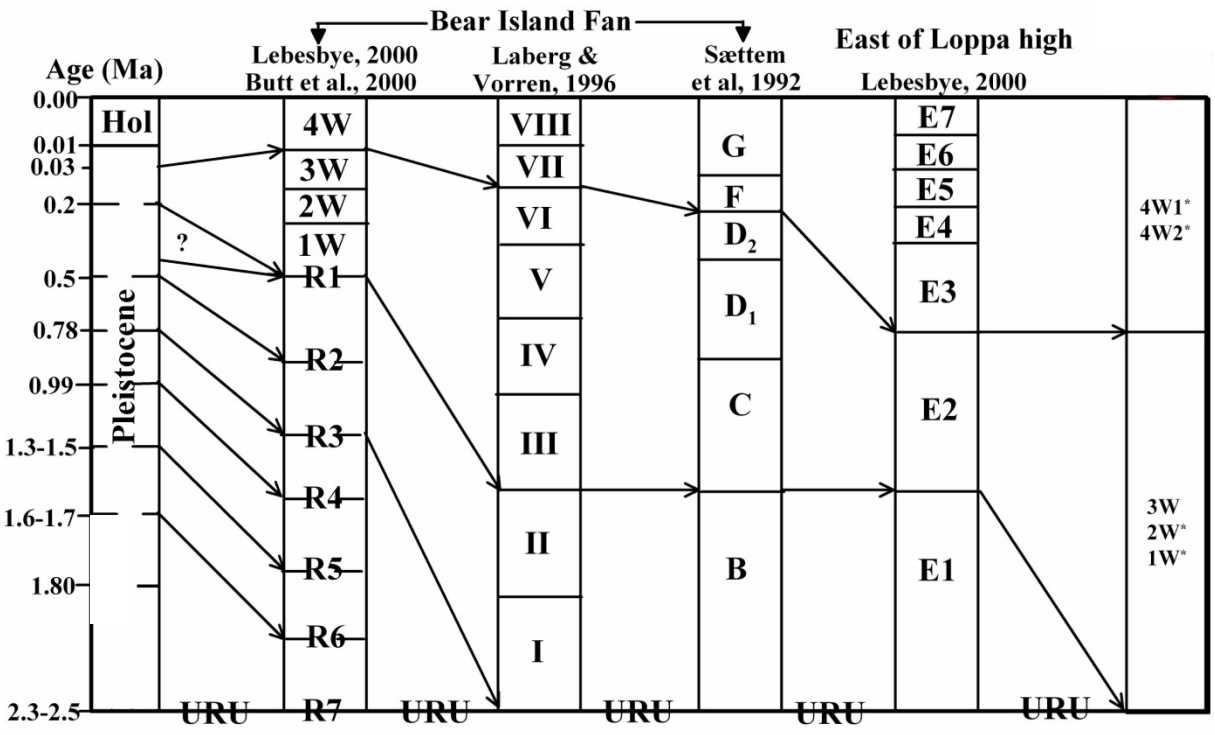

The general glaciation model for the southwestern Barents Sea based on seismo-stratigraphic interpretations and dating results is shown by Lebesbye (2000) and Chand et al. (2009). The model proposed by Lebesbye (2000) indicates the following sequence of events: A) Ice margins covering Ingøydjupet during GA2 and 3 and related deposition of unit E2, B) Ice margins up to the present Barents shelf edge during GA5 and related deposition of units E3 and E4 during the following phases: 1) The initial advance outside the coast, 2) phase during the advance when sedimentation took place in Ingøydjupet and at its periphery, 3) LGM1 (23 ^{14}C ka BP) marks the terminal position of the ice sheet at the shelf edge, C) Ice margins again reaching the Barents shelf edge during GA6-9 and units E5 and E6 were deposited (Lebesbye, 2000) during the following phases: 1) Approximate ice position when large parts of unit E5 and parts of E6 were deposited, 2) ice maximum position (LGM II (18 ^{14}C ka BP)), partly along the shelf edge, D) Ice margin position during the last deglaciation: 1) ice margin during deposition of most of the unit E7, 2) the Risvik substage (Lebesbye, 2000).

4.2.1.Loppa High

The areas covered by multibeam sonar surveys during 2008 and 2009 are underlain by units 4W and 1W while the those surveyed in 2012 (Area A and Area B) are underlain by Unit 4W and 2W (Fig. 16). The general character and thicknesses of the units are shown on seismic data collected during 2012 below (Figs. 17-26).

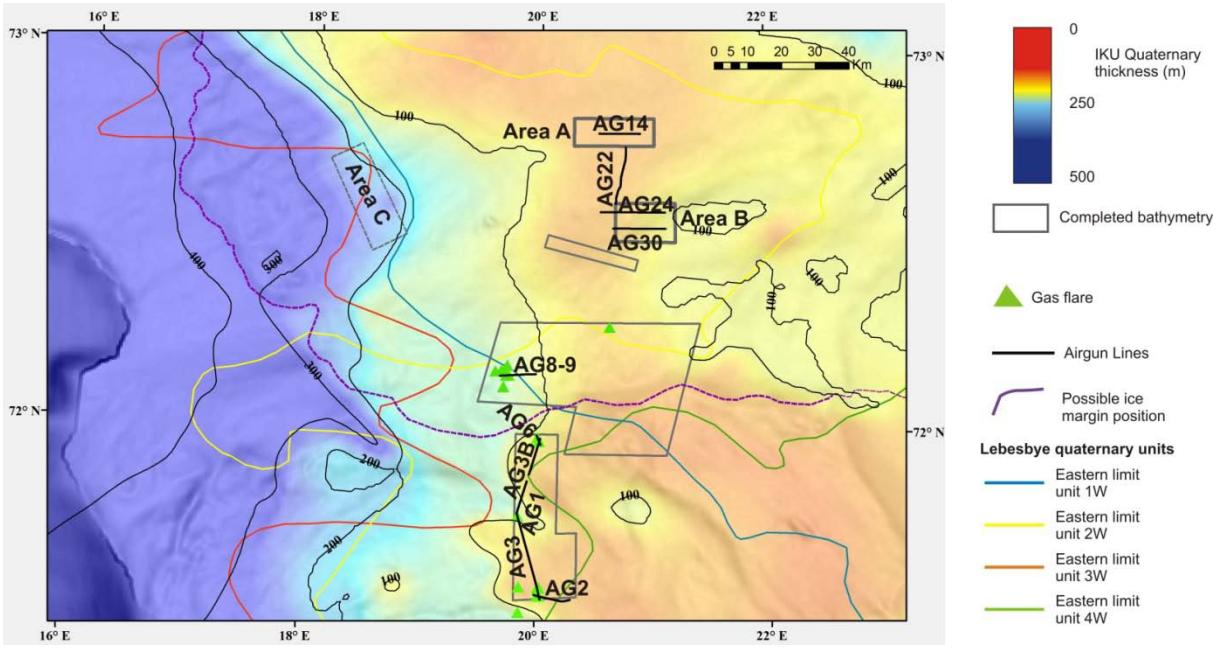

Figure 16. Quaternary sediment thickness map of the Loppa High study area showing the location of seismic lines, multibeam data from 2008, 2009 and 2012 (Area A and B), proposed pilot study area (Area C) and eastern limit of various glacigenic units.

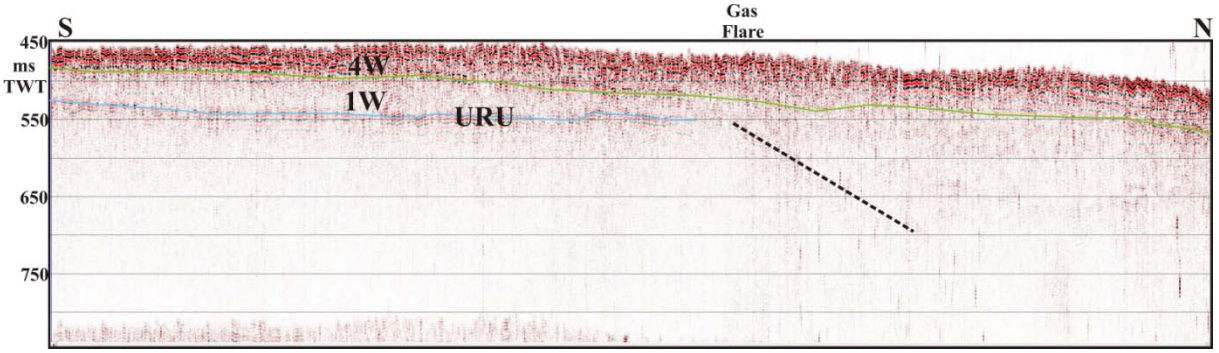

Figure 17. Airgun seismic profile AG1 across one of the gas flares identified in the 2009 MBB data. Notice the two Quaternary units, Unit 1W and 4W underlying the gas flare area. The gas flare is located close to the pinch out of the Quaternary units (Fig. 16).

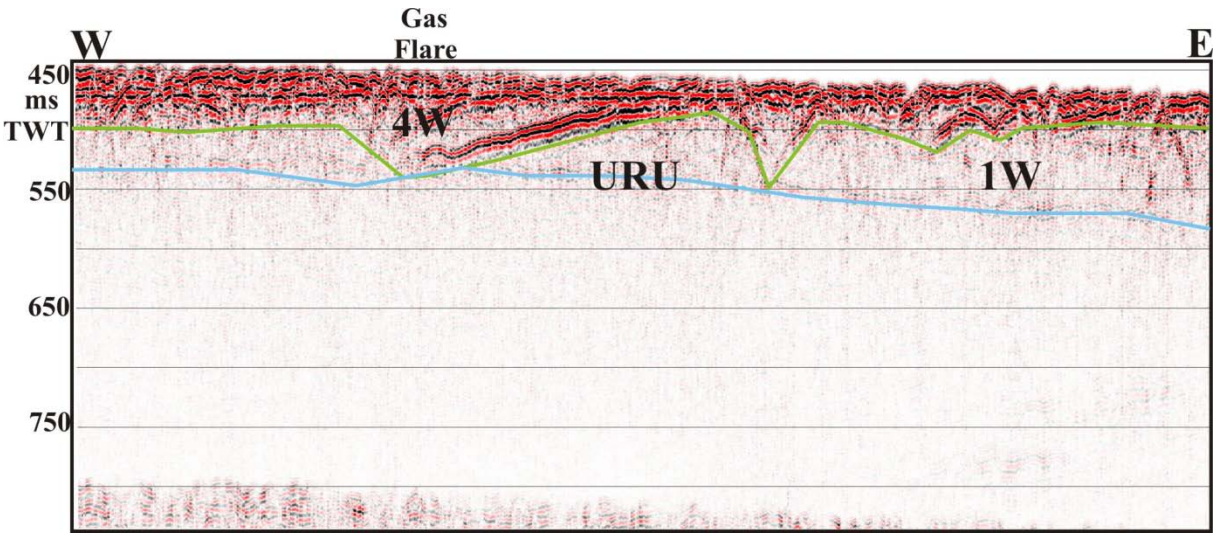

Figure 18. Airgun seismic line AG2 across one of the gas flares identified in the 2009 MBB data. Notice the two Quaternary units, Unit 1W and 4W underlying the gas flare area. The gas flare is located close to a large depression in Unit I and close to the pinchout of the Quaternary units (Fig. 16).

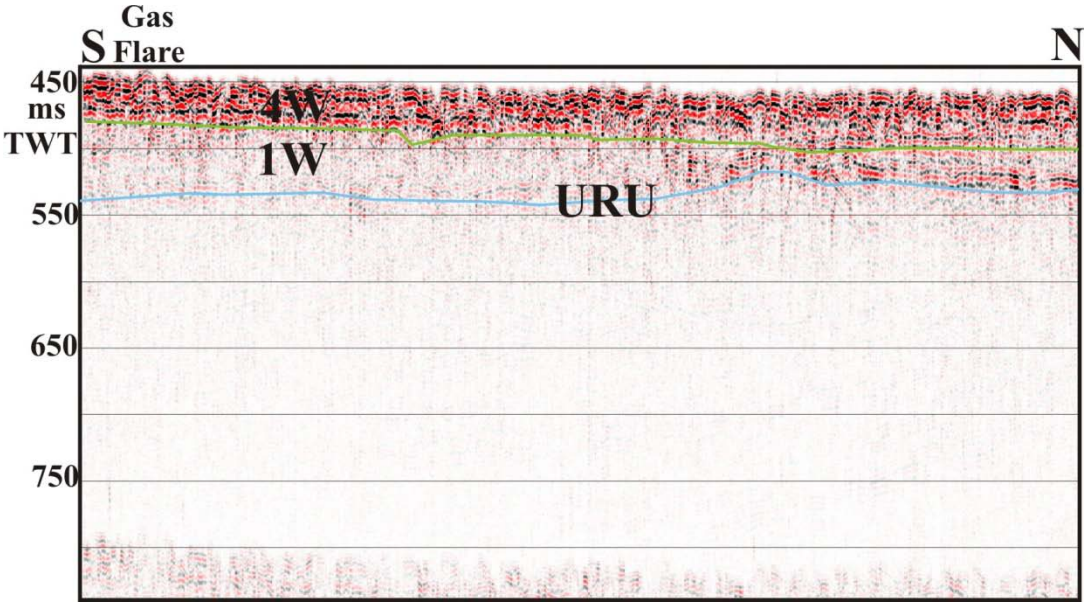

Figure 19. Airgun seismic line AG3 across one of the gas flares identified in the 2009 MBB data. Notice the two Quaternary units, Unit 1W and 4W underlying the gas flare area. The gas flare is located close to the pinchout of the Quaternary units (Fig. 16).

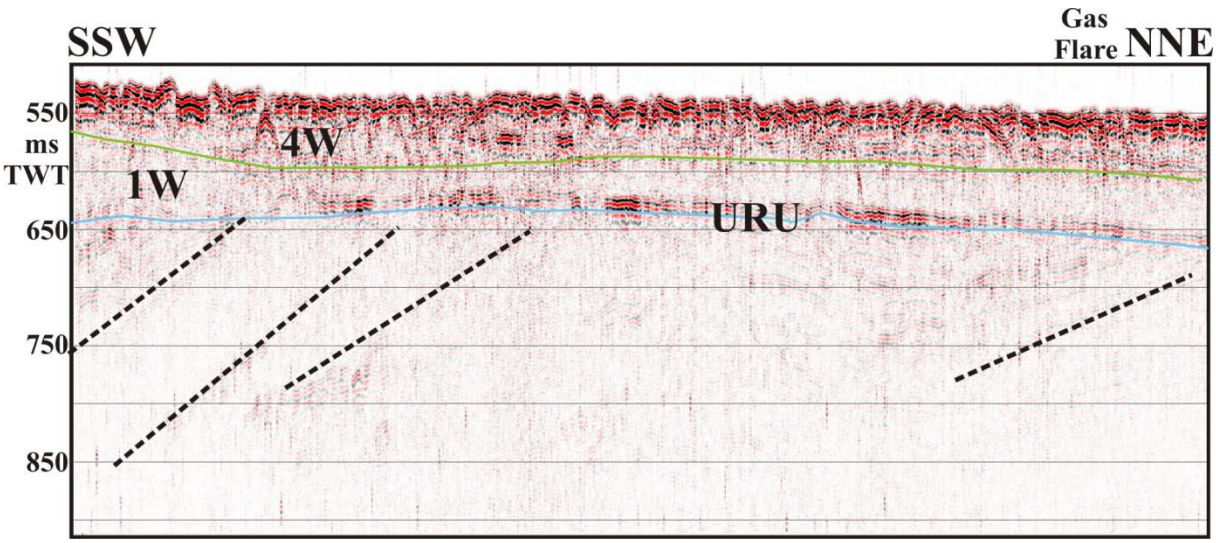

Figure 20. Airgun seismic line AG3b across one of the gas flares identified in the 2009 MBB data. Notice the two Quaternary units, Unit 1W and 4W underlying the gas flare area. The gas flare is located close to the pinchout of the Quaternary units (Fig. 16).

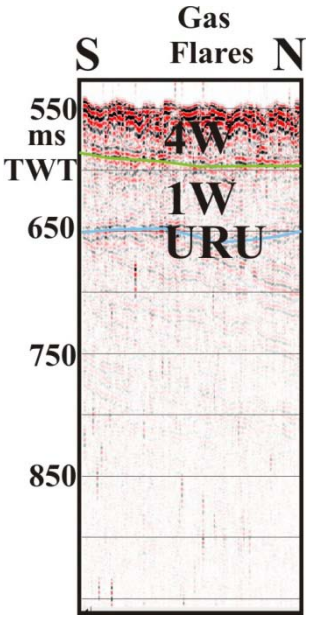

Figure 21. Airgun seismic line AG6 across two gas flares identified in the 2009 MBB data. Notice the two Quaternary units, Unit 1W and 4W underlying the gas flare area. The gas flare is located close to the pinchout of the Quaternary units as in other gas flare locations (Fig. 16).

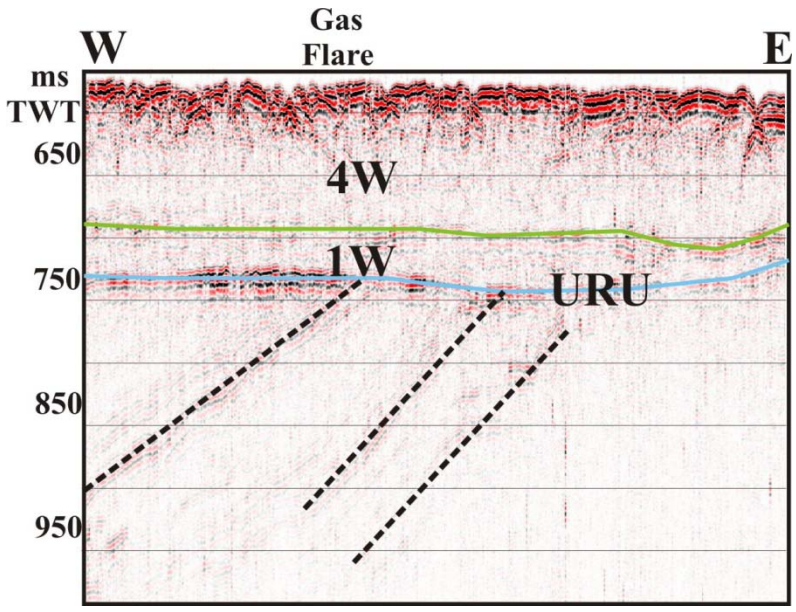

Figure 22. Airgun seismic line AG8_9 across one of the gas flares identified in the 2008 MBB data. Notice the two Quaternary units, Unit 1W and 4W underlying the gas flare area. The gas flare is located close to the pinchout of the Quaternary units (Fig. 16). Also the Tertiray units are subcropping under URU and high amplitude gas anomalies can be seen.

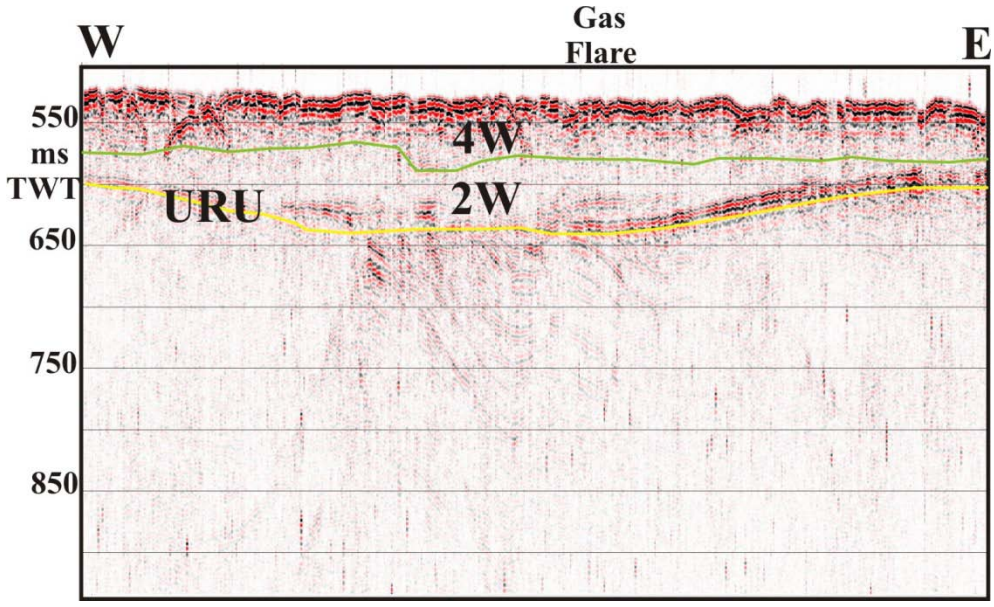

Figure 23. Airgun seismic line AG14 across one of the gas flares identified in the 2012 MBB data in Area A. Notice the two Quaternary units, Unit 2W and 4W underlying the gas flare area. The gas flare is located close to the pinchout of the Quaternary units (Fig. 16). Also notice subcrop of older units below the URU (below 2W).

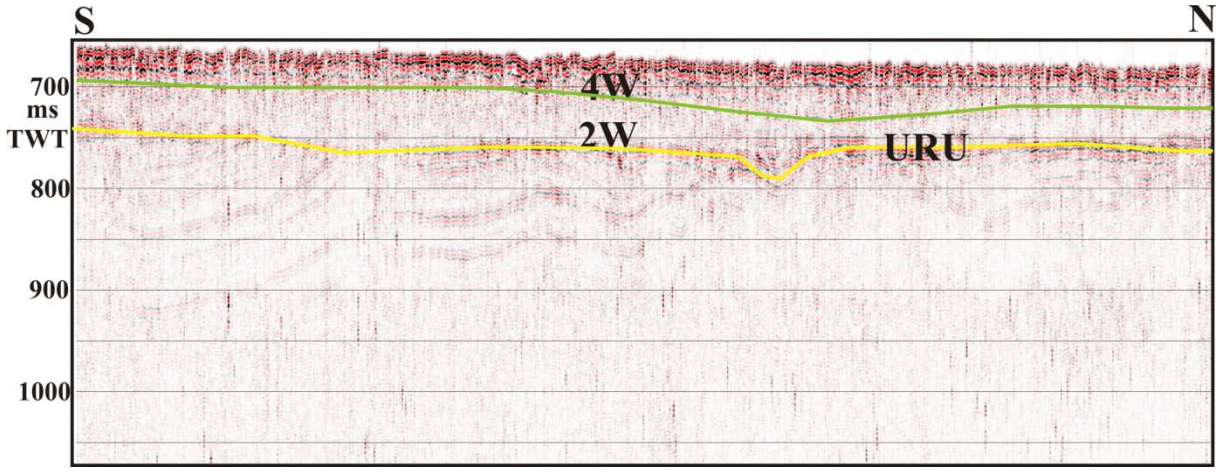

Figure 24. Airgun seismic line AG22 connecting Area A and Area B in the 2012 MBB data. Notice the two Quaternary units, Unit 2W and 4W underlying the seafloor with uniform thcikness. The deeper older units subcrop below the URU (below unit 2W).

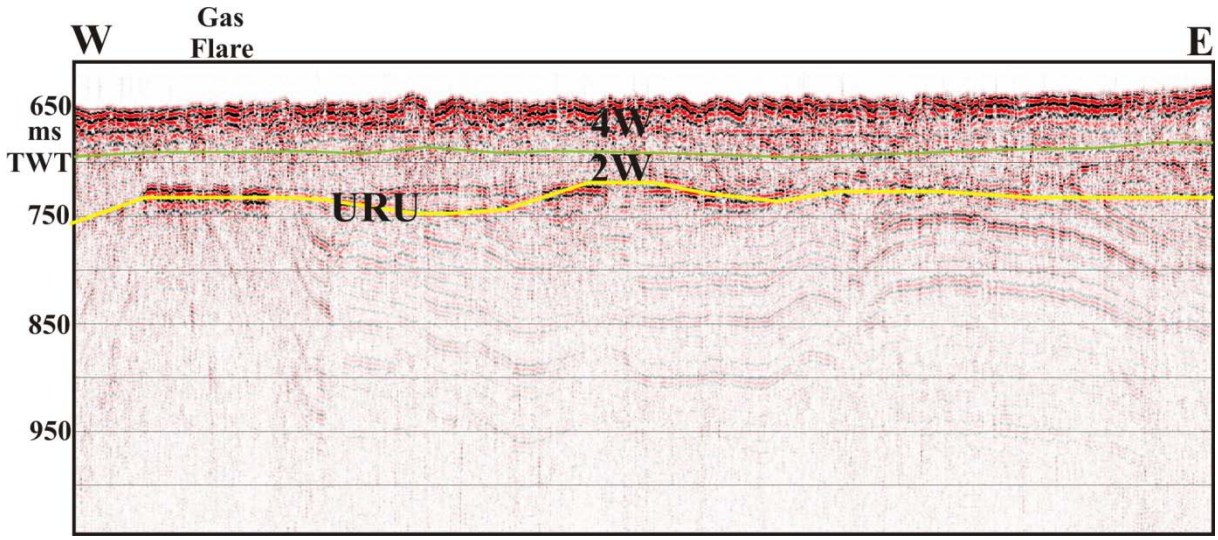

Figure 25. Airgun seismic line AG24 across one of the gas flares identified in the 2012 MBB data in Area B. Notice the two Quaternary units, Unit 2W and 4W underlying the gas flare area. The gas flare is located close to the pinchout of Quaternary units (Fig. 16). Also notice the subcrop of older units below URU (below 2W) and high amplitude gas anomalies.

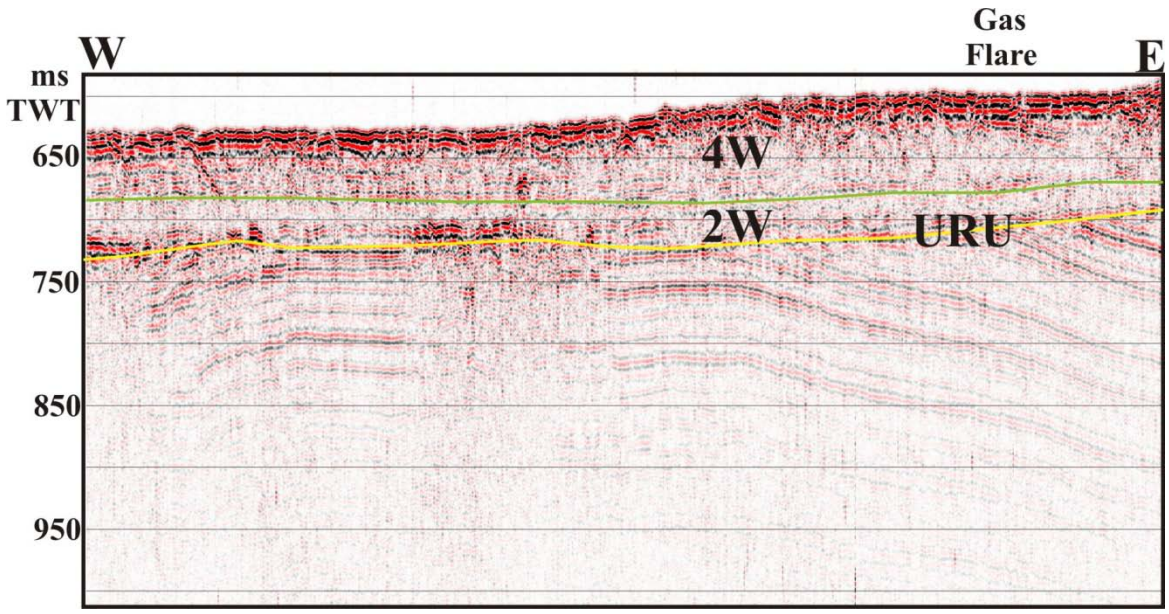

Figure 26. Airgun seismic line AG30 across one of the gas flares identified in the 2012 MBB data in Area B. Notice the two Quaternary units, Unit 2W and 4W underlying the gas flare area. The gas flare is located close to the pinchout of Quaternary units in the study area (Fig. 16). Also notice the subcrop of older units below URU (below 2W).

4.2.2 Finnmark Platform

The Finnmark study area is located slightly east of a Quaternary depocentre (Fig. 27). Five out of seven Quaternary glacial units of various thicknesses occur in this area. Major units include E1 (~50 m) and E2 (~100m), spanning the period from 2.5 Ma to 30 ka (Table 1) covering the initial start up of glacial related erosion and deposition in the Barents Sea (Lebesbye et al., 2000). No dating of these sediments have been performed, but atleast the oldest of the units (E1) may be older than the last Weichselian glaciations (i.e. > 100 ka). Unit E2 is equivalent to units 1W to 3W in the Loppa High study area. Unit E3 is very thin and occurs along the western part of the study area. Unit E4 is inferred to represent a late glacial advance (LGM I). Unit E5 is absent in the study area, while unit E6 (~25m) is interpreted to represent the latest glacial advance towards the shelf edge (LGM II) (Lebesbye et al., 2000). Unit E7 (~15 m) comprises soft clays from the last deglaciation (Lebesbye et al 2000) (Table 1).

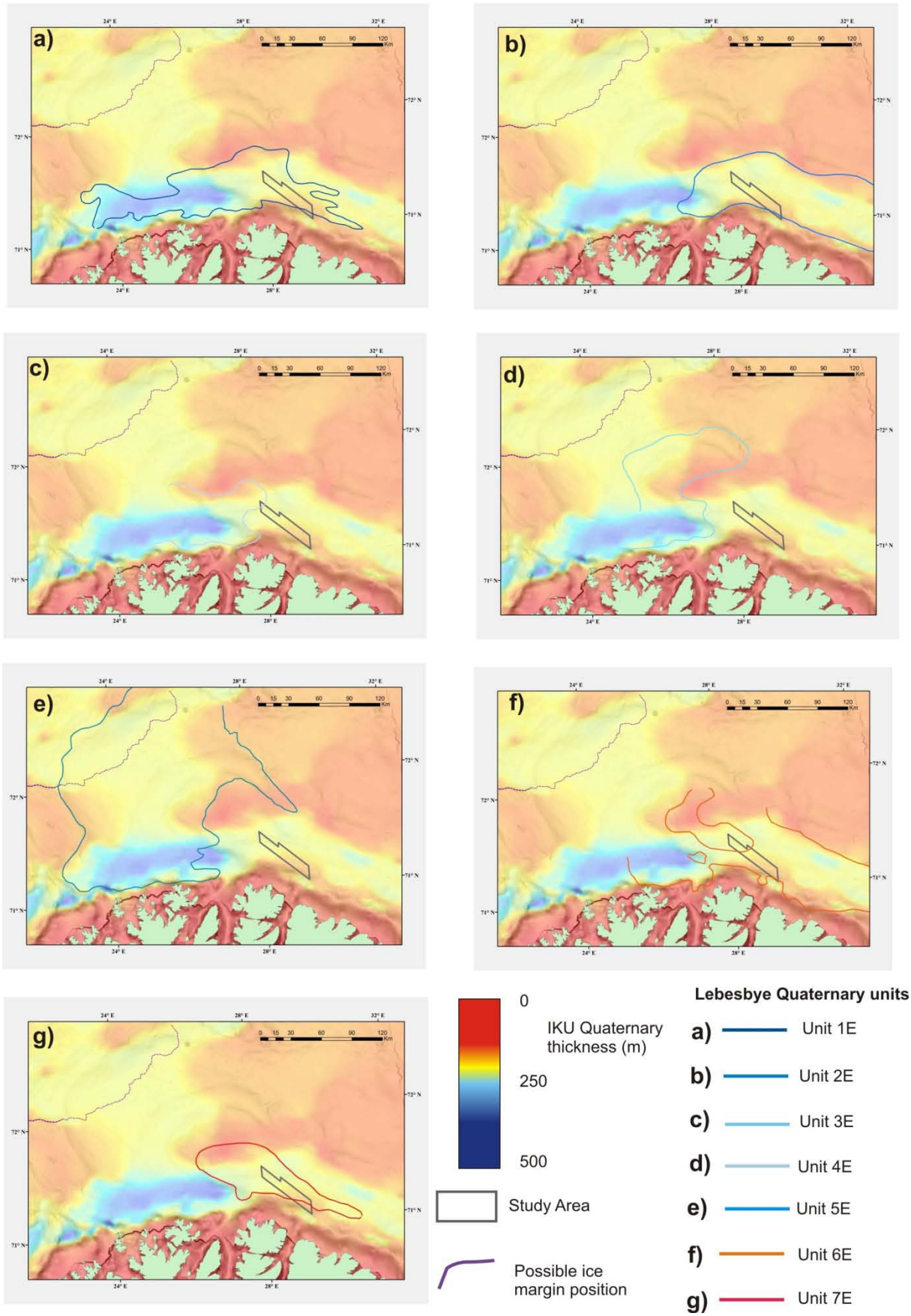

Figure 27. Lateral extent of the various Quaternary units in the Finnmark study area shown on the Quaternary sediment thickness map. Units 1E, 2E and parts of units 6E and 7E cover the study area. A correlation of these units to those on Loppa High is given in Table 1.

4.3 **Pockmarks**

4.3.1. Loppa High

Pockmarks have been mapped in the Loppa High area, especially in depressions with accumulation of fine-grained sediments. Diameter and depth of pockmarks increase towards deeper parts of depressions implying that the thickness of the soft sediments play a role for their formation and geometry. Correlation of the cores collected inside and outside of the pockmarks decipher the mechanism and timing of their origin (Figs. 28, 29 & 30). Pockmarks are observed in the new MBB areas concentrated along iceberg ploughmarks, but they are scarcely distributed within the main part of the two new survey areas. Pockmarks occur in higher density beyond the 400 m depths.

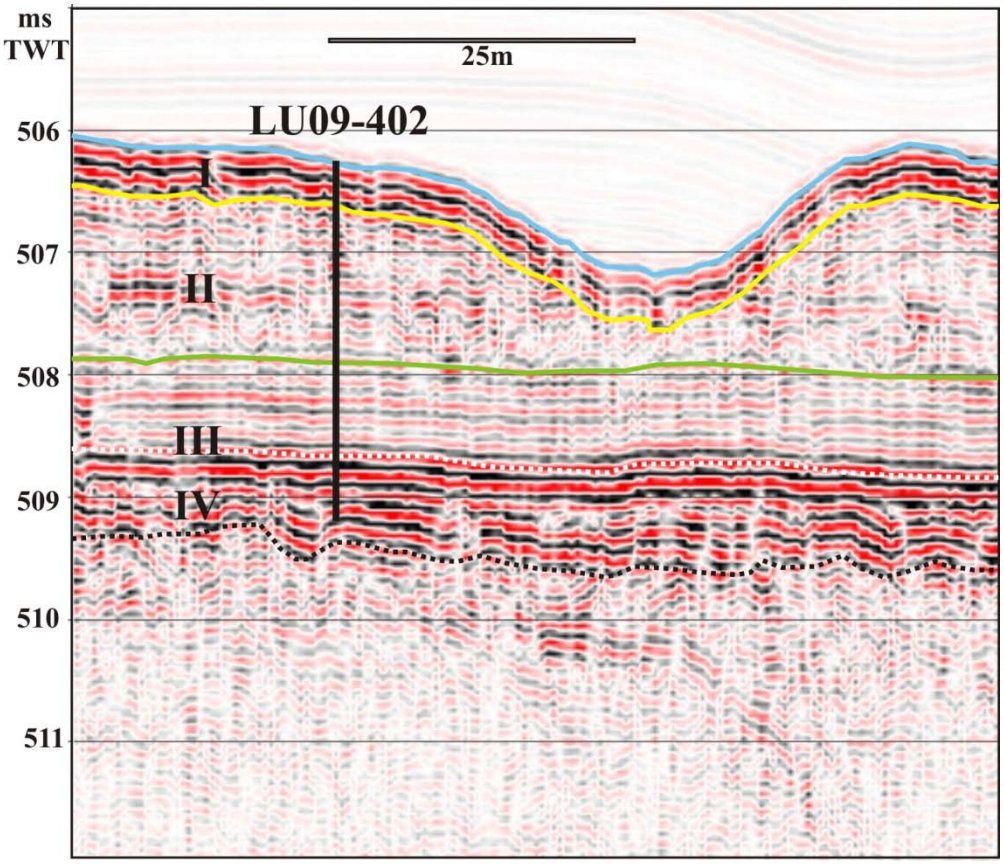

Figure 28. HUGIN Edgetech subbottom profiler data across the location of core LU09-402. Location shown in Fig. 3. Correlation of various units are given in Fig. 30.

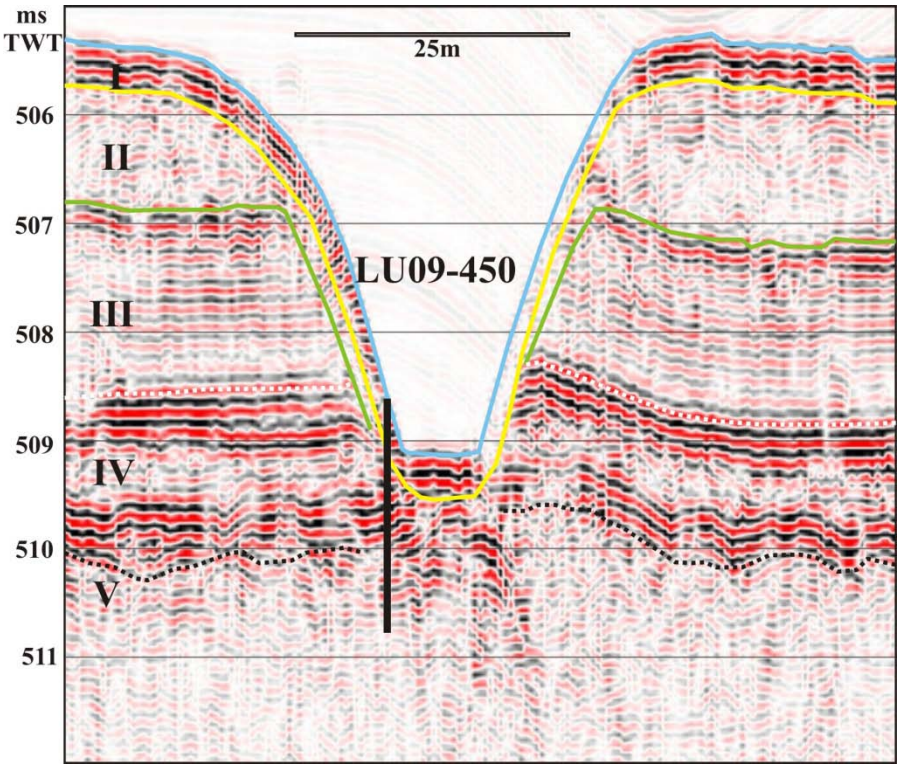

Figure 29. HUGIN Edgetech subbottom profiler line across the location of core LU09-450.Location shown in Fig. 3. Correlation of various units are given in Fig. 30.

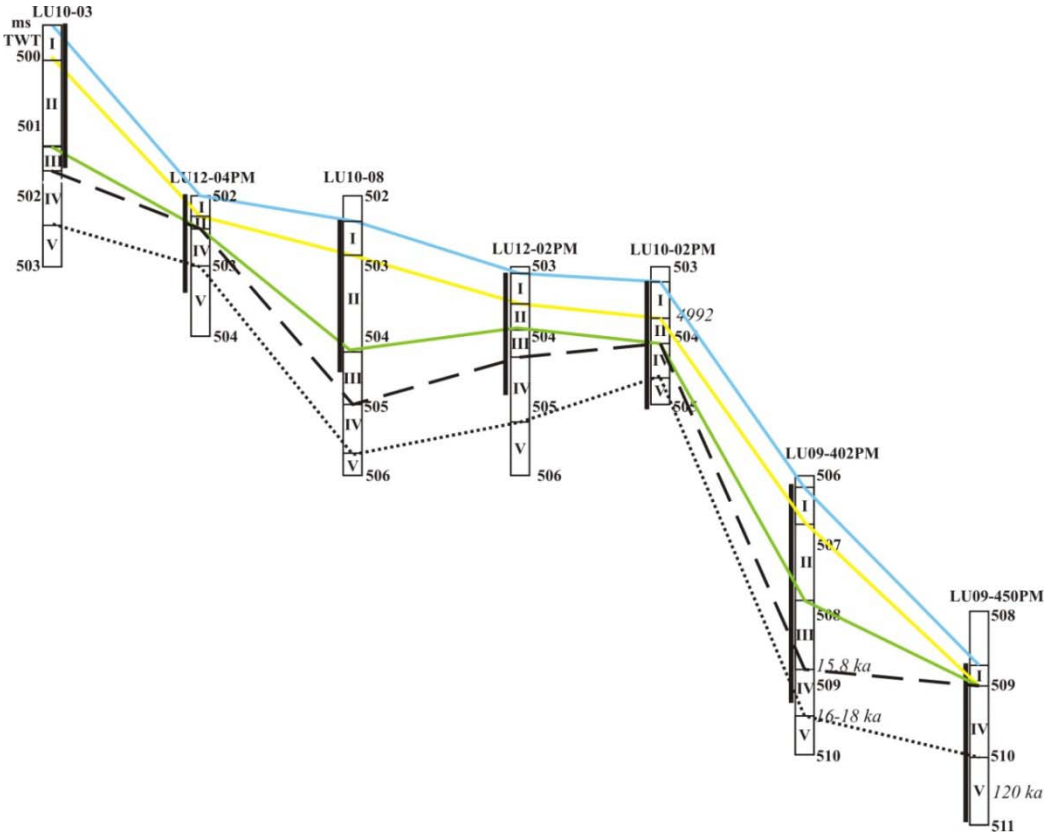

Figure 30. Correlation diagram showing various units tied between cores in the Loppa High pockmark area. Location of cores are shown in Fig. 3.

4.3.2. Finnmark Platform

The Finnmark Platform study area is peculiar with large numbers of pockmarks located north of the deepest area (Fig. 31 & 32). The Troms-Finnmark Fault Complex (Fig. 1) cuts across the northern part of the study area. The pockmarks occur north of where the Permo-Carboniferous to Triassic boundary subcrop on the seafloor (Fig. 33) implying a possible connection to focussed fluid flow along this boundary. The pockmarks range in size (~ 50m) and shape, and occur ~60 per sqkm while larger prodmarks are observed on bathymetric highs.

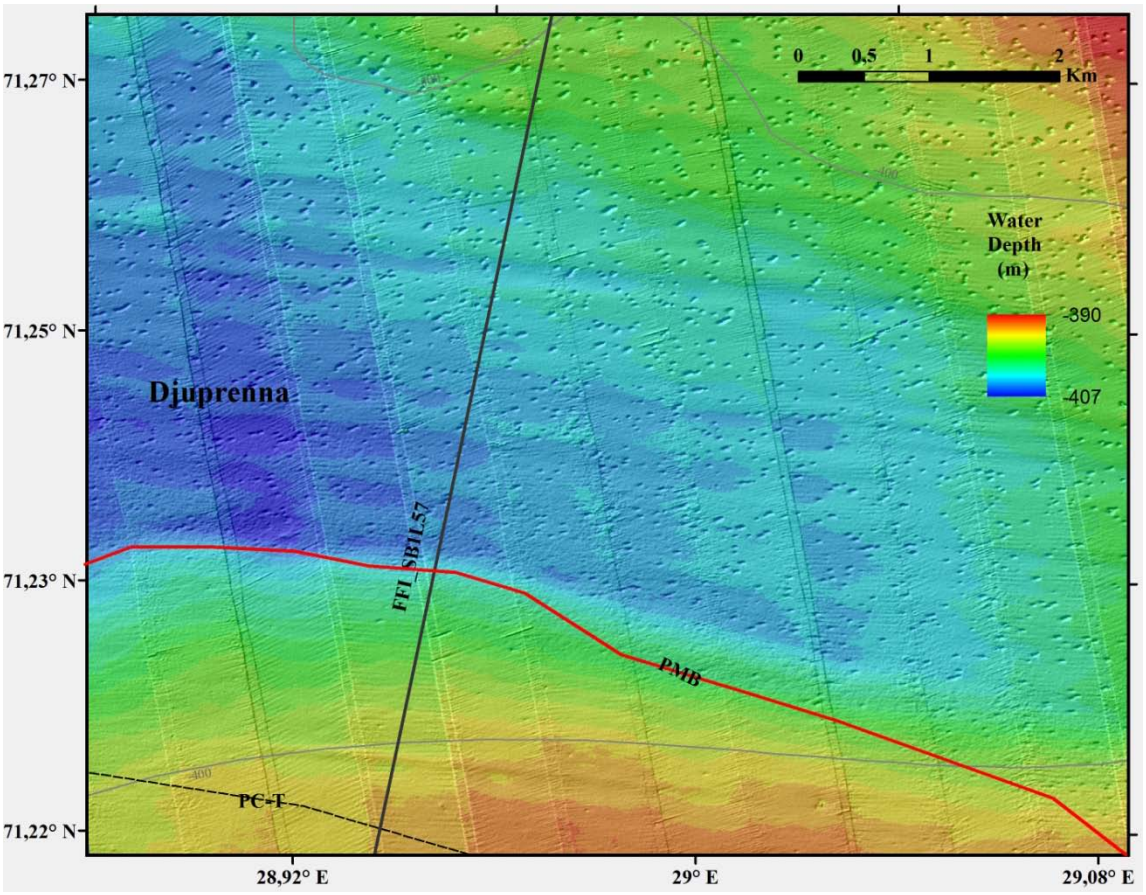

Figure 31. Pockmarks in the Finnmark study area. The pockmarks are located NE of the deepest part (see Fig. 32) of Djuprenna and north of the Permo-Carboniferous to Triassic (PC-T) boundary (dashed line) (see Fig. 13 for location). PMB – Pockmark region southern boundary.

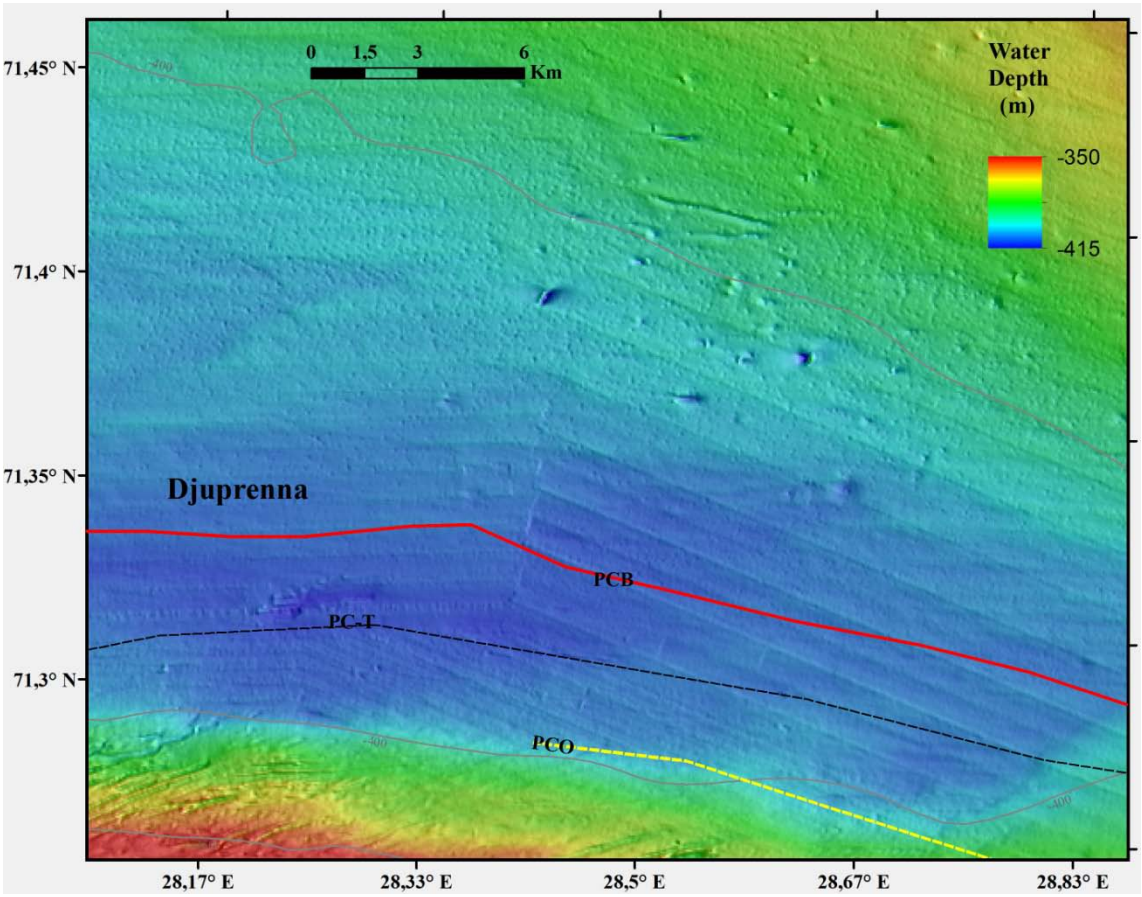

Figure 32. Pockmarks in the Finnmark study area. The pockmarks are located NE of the deepest part of Djuprenna and north of the Permo-Carboniferous to Triassic (PC-T) boundary (dashed black line).The seafloor outcrop of the top of the Permo-Carboniferous boundary (PCO) is also shown (yellow dashed line). The big depression-high pairs observed on top right of the figure are possibly prodmarks.(see Fig. 13 for location). PCB – Pockmark region southern boundary.

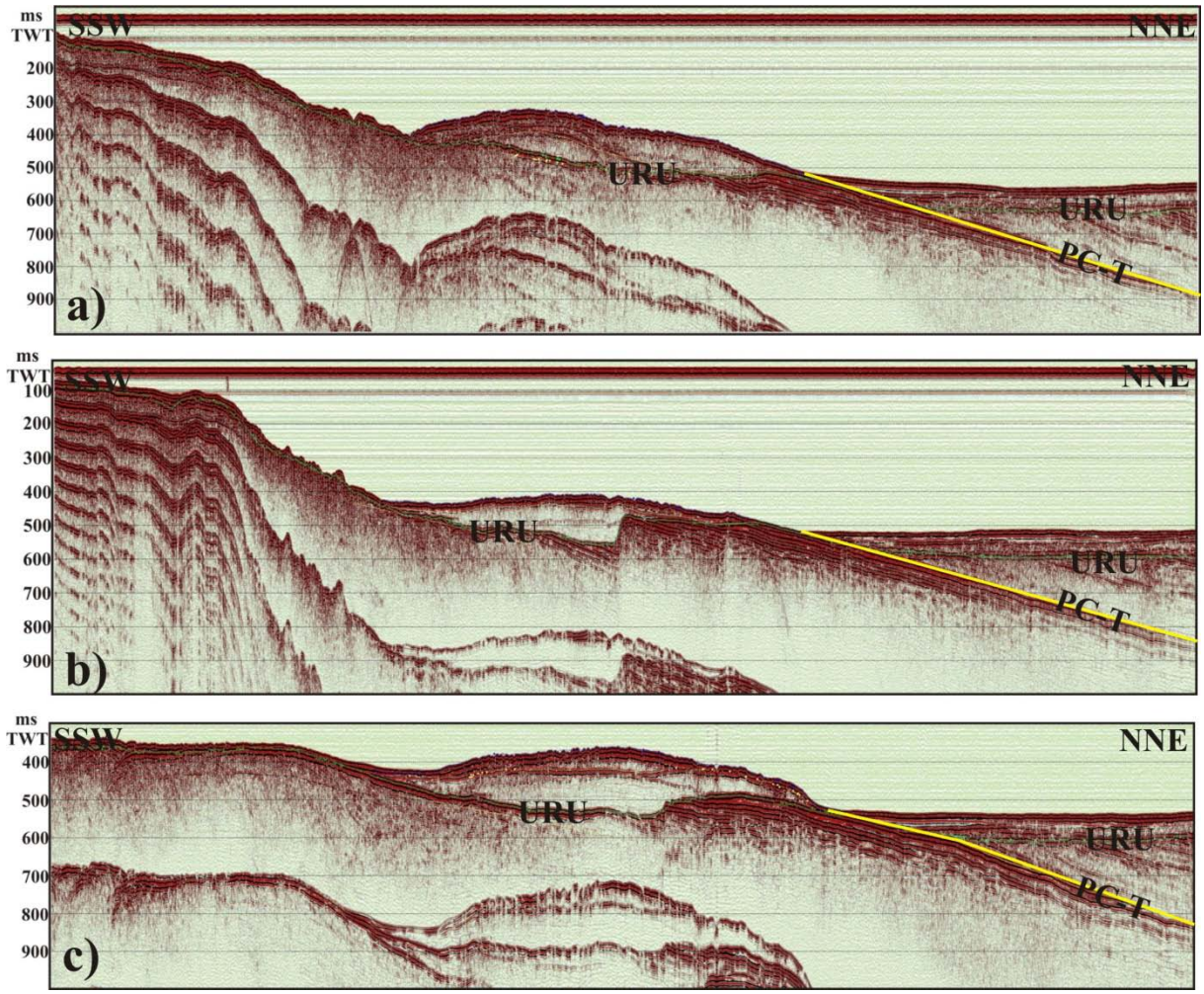

Figure 33 . Seismic air gun lines a) FFI_SB1L57, b) FFI_SB1L55 and c) FFI_SB1L57 (see Fig. 4 for location) across the Permo-Carboniferous to Triassic boundary (PC-T). The green line indicates the base of the Plio-Pleistocene (URU) sediments.

4.4 **Gas flares and methane anomalies**

4.4.1. Hammerfest Basin, Polheim Sub-platform and Loppa High

Water column data analysed using the FlederMaus Midwater package indicate 12 new acoustic gas flares in the area covered by the multibeam data collected in 2012 (Table 2, Fig 34).

Table 2: Details of gas flares located in the 2012 EM710 MBB data.

Name	Area	Latitude WGS84	Longitude WGS84	Comments
2012.1a	Hammerfest Basin	71.805103	19.847538	2200 m NNE of previously observed gas flare
2012.1b	Hammerfest Basin	71.807084	19.849525	230 m NNE of GF1a
2012.2	Hammerfest Basin	71.821456	19.86772	100 m long elongated flare NNE-SSW
2012.HG2_center_crust	Polheim	72.157837	19.727	Same structure
2012.HG2_Center_flare	Polheim Sub-platform	72.157963	19.728515	
2012.HG4_1a	Polheim Sub-platform	72.186332	19.724893	
2012.HG4_1b	Polheim Sub-platform	72.189869	19.742924	
2012.3	Polheim Sub-platform	72.220345	19.953043	
2012.Area_A	Loppa High, Area A	72.796403	20.625149	
2012.Area_B_1	Loppa High, Area B	72.567632	20.86851	Eastern flare
2012.Area_B_2a	Loppa High, Area B	72.588263	20.586593	Western flare, largest
2012.Area_B_2b	Loppa High, Area B	72.588465	20.585241	Western flare
2012.Area_B_2c	Loppa High, Area B	72.58921	20.58709	Western flare, just NE of largest crust field
2012.Area_B_2d	Loppa High, Area B	72.589218	20.588904	Western flare

Three flares were found in the southernmost area (Hammerfest Basin), 4 gas flares were found in the central area (Polheim Sub-platform), 5 flares were detected in Area B on the Loppa High, and one in Area A. Some of the flare locations are new, while positions of others are close to flares described by Chand et al. (2012a,b). Some survey lines during the April 2012 cruise crossed localities where gas flares were previously reported by Chand et al. (2012b), but no signs of gas were recorded. This probably shows the discontinuous nature of the gas flares.

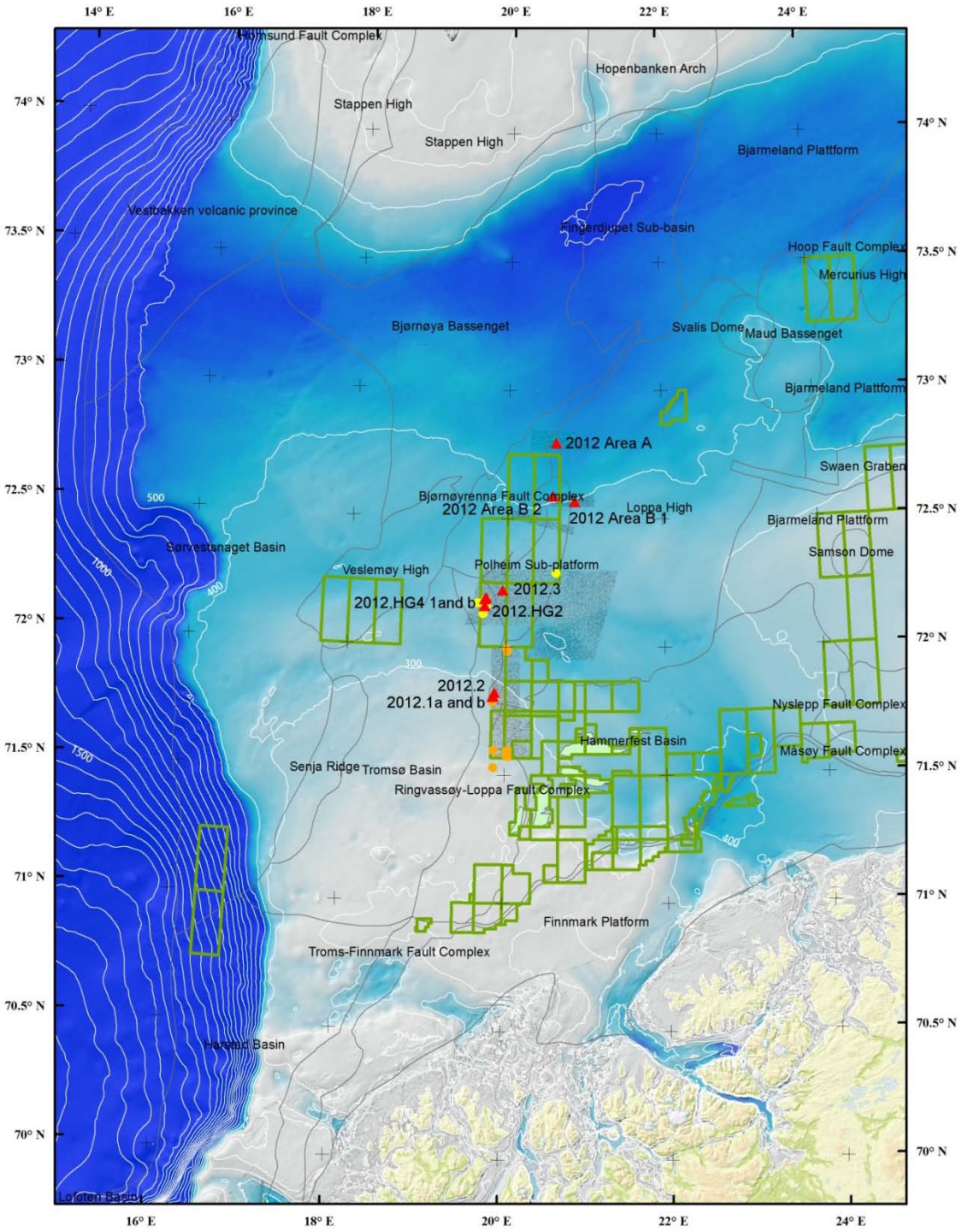

Figure 34. Overview map showing the Barents sea between Finnmark and Bear Island, with NPD blocks, major structural provinces, areas surveyed with multibeam bathymetry, and gas flares (yellow dots – EM710 data from 2008; orange dots – EM710 data from 2009; red triangles –EM710 data from 2012). Labels starting with 2012 refer to Table 2.

In the southern area (Hammerfest Basin), three flares (2012.1a and b, 2012.2) were identified from EM710 transit lines. The gas flares occur within a few kilometers of a flare previously reported in Chand et al. (2012b). In the Polheim Sub-platform area (Fig. 34 & 35), 6 flares have previously been identified. A survey using HUGIN with SAS, METS and TFish was conducted, covering the flare sites (HG1-HG4) and two additional areas of special interest

(HG5-HG6). EM710 lines were collected from the sites. Four flares were detected (2012.HG2, 2012.HG41a and b, 2012.3).

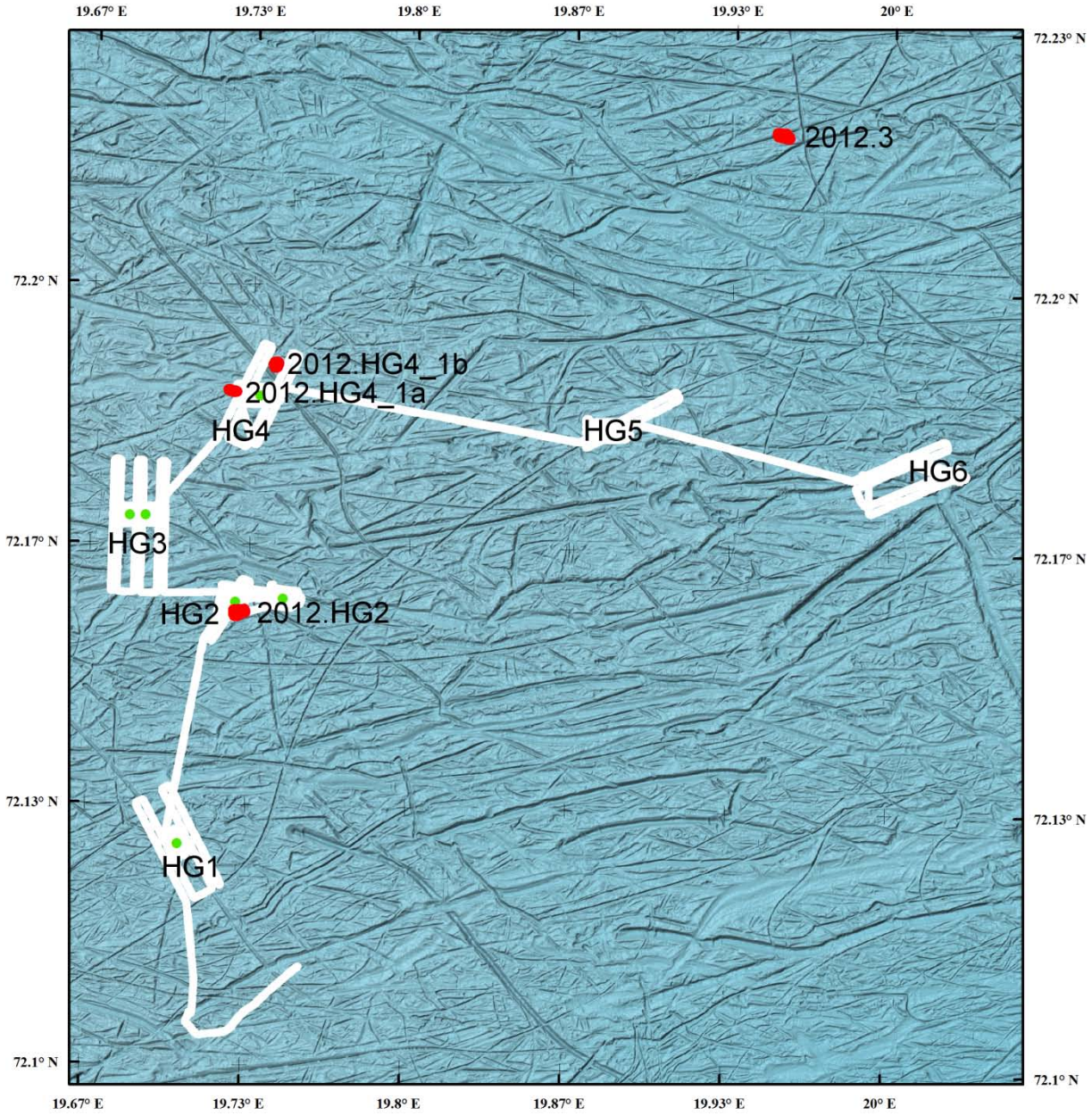

Figure 35.Overview map showing the HUGIN tracks, the HG1-HG6 areas, and gas flares (green dots – MB data from 2008; red dots – this cruise).

HG1 did not show any signs of gas leakage from the METS sensor, the SAS or TFish. The SAS imagery showed a rugged seabed, with angular blocks up to 5 m (Fig. 36). Inspection of the TFish images indicated that the blocks are sandstone blocks. The interpretation is that this block field represents a glaciotectonic feature, where rafts from the underlying sedimentary rocks have been removed and transported for some distance before disintegrating.

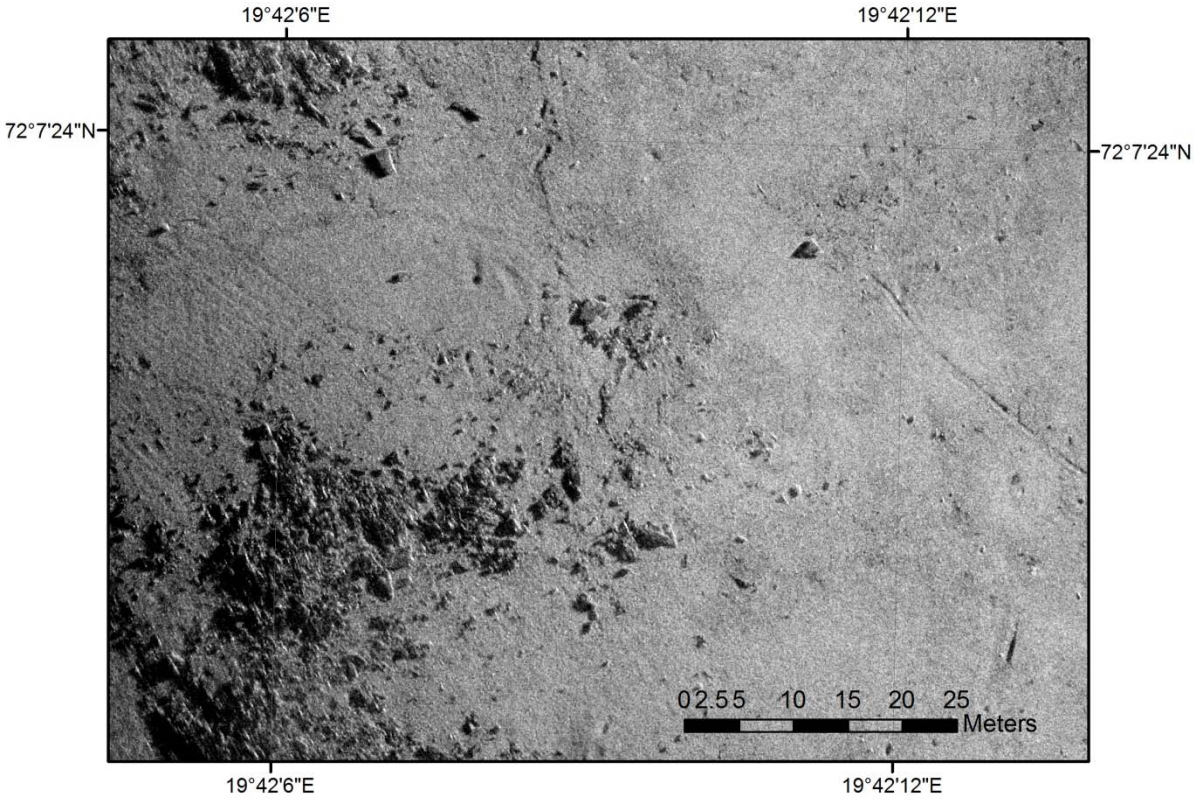

Figure 36. SAS imagery showing the sandstone blocks in HG1. Note NW-SE trending trawl marks.

The survey in HG2 revealed far more interesting features. The METS sensor showed a clear anomaly (Fig. 37), an irregular carbonate crust pavement could be identified from the SAS imagery (Fig. 38), and the TFish sensor recorded images of gas bubbling from below the carbonate crusts (Fig. 39). Abundant fish (mainly *Sebastes Marinus)* can be observed (Fig. 40). The area of the carbonate crust field is c. 200 m^2. The carbonate crust pavement consists of individual crust pieces which may be up to several meters in diameter. The outlines of the crusts are jagged. Parts of the crusts can be as much as 50 cm above the surrounding seabed and can have cavites of c. 10 cm under parts of it.

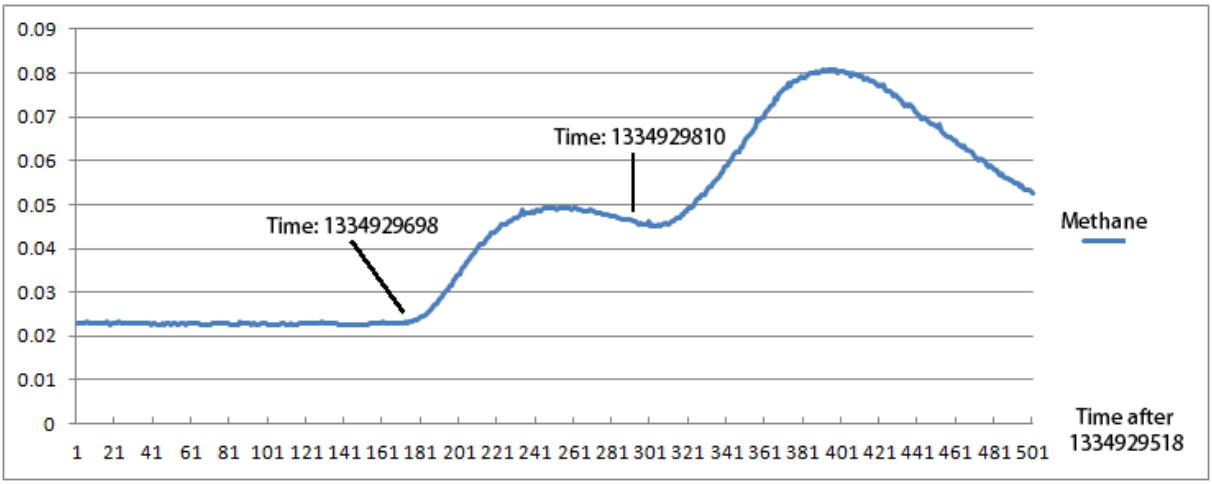

Figure 37. XY plot of CH4 values (µmol/litre) versus time (seconds) for HG2. The time for the initial increase (1334929698) corresponds the time label in Fig. 38 and shows that the METS sensor responds within tens of seconds after passing the carbonate crust field. The time is given in seconds.

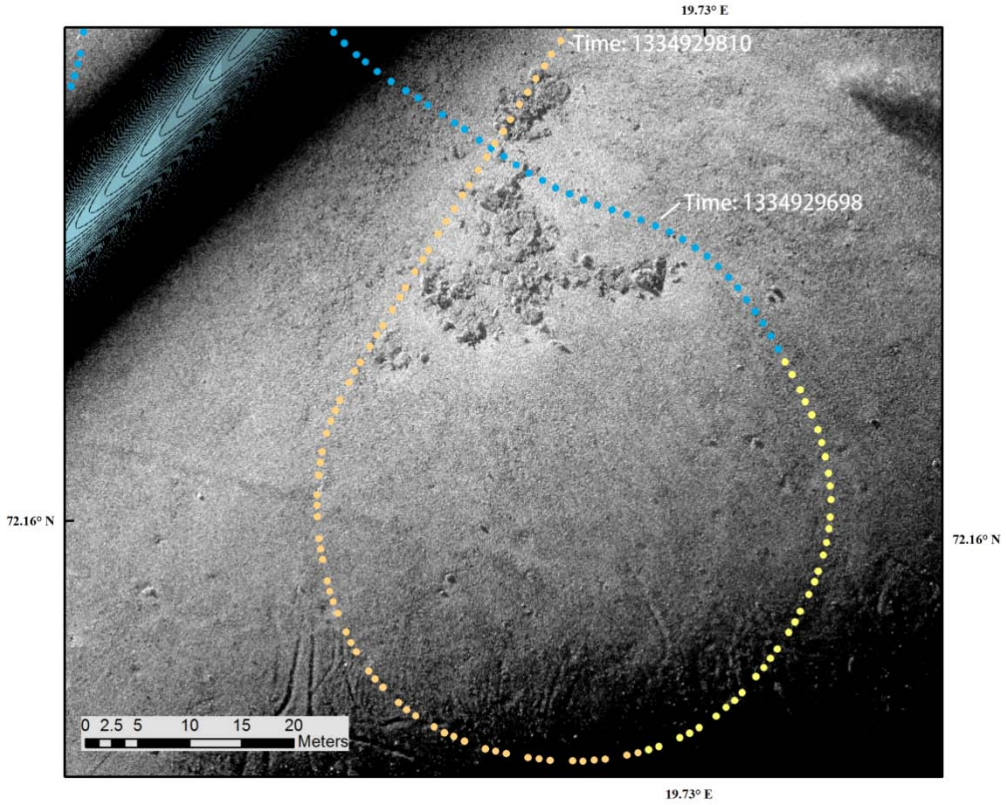

Figure 38. SAS imagery from HG2 showing the carbonate crust field (central upper part) and the CH4 values from the METS sensor (blue values: below 0.027; yellow dots: 0.027- 0.045; orange dots: 0.045-0.060). HUGIN entered the imaged area from upper left and exited the area in the upper central part. Time labels correspond to the labels in Fig. 37.

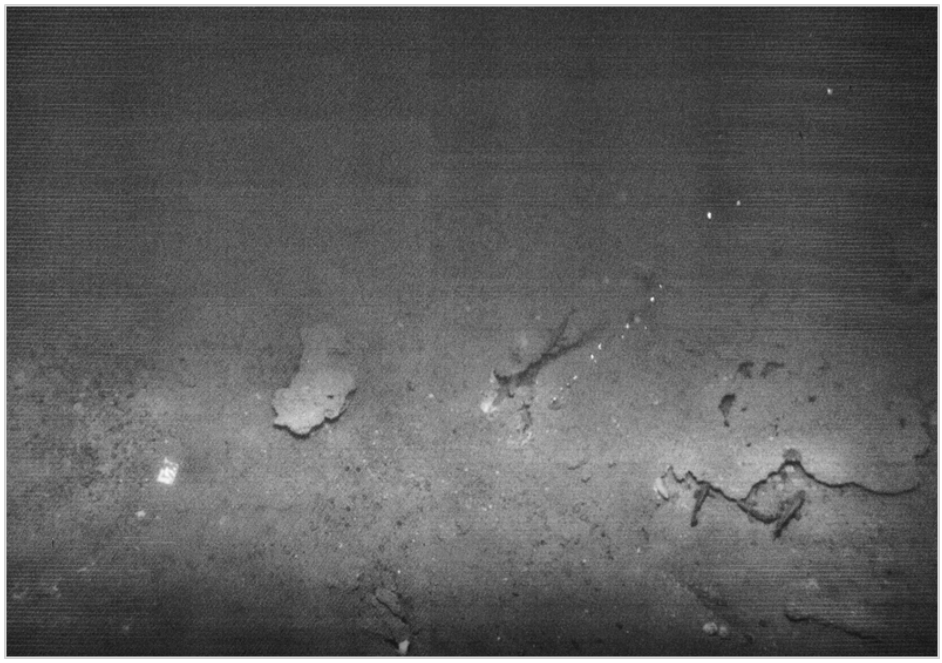

Figure 39. TFish photo from HG, showing carbonate crusts and gas bubbles. The photo is ca. 7 m wide.

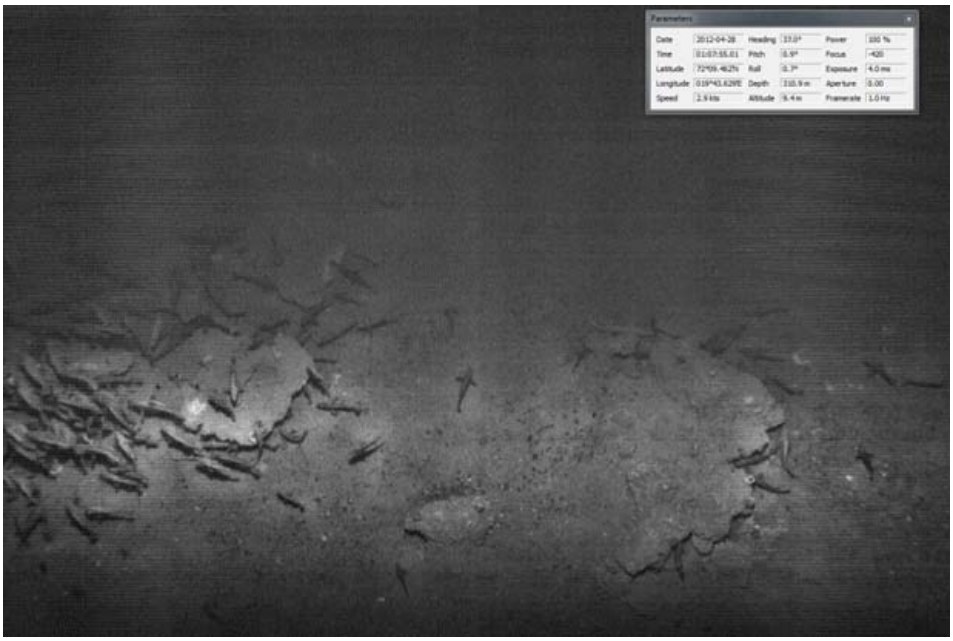

Figure 40. TFish image from the HG2 carbonate crust field showing abundant fish (probably Sebeastes marinus).

After the initial discovery and identification of gas seepage and carbonate crusts in HG2 area, a second HUGIN survey was conducted to collect more photos, imagery and CH_4 data. The METS data from the second survey are presented in Fig. 41 and show the maximum value of 13.4064 *µmol/L* and the median of 0.0199 *µmol/L*, considered to represent the average background value. These values are in contrast to the first survey, where the maximum value

is 0.08352 µmol/L, and the median value is 0.02469 µmol/L. This means that the surveys record comparable background levels, the maximum levels in the first survey are close to background level, while that in the second survey is 160 times higher. This suggests that the gas leakage during the second survey was considerably higher than during the first, or that HUGIN passed closer to the seepage site with highest bubble concentration.

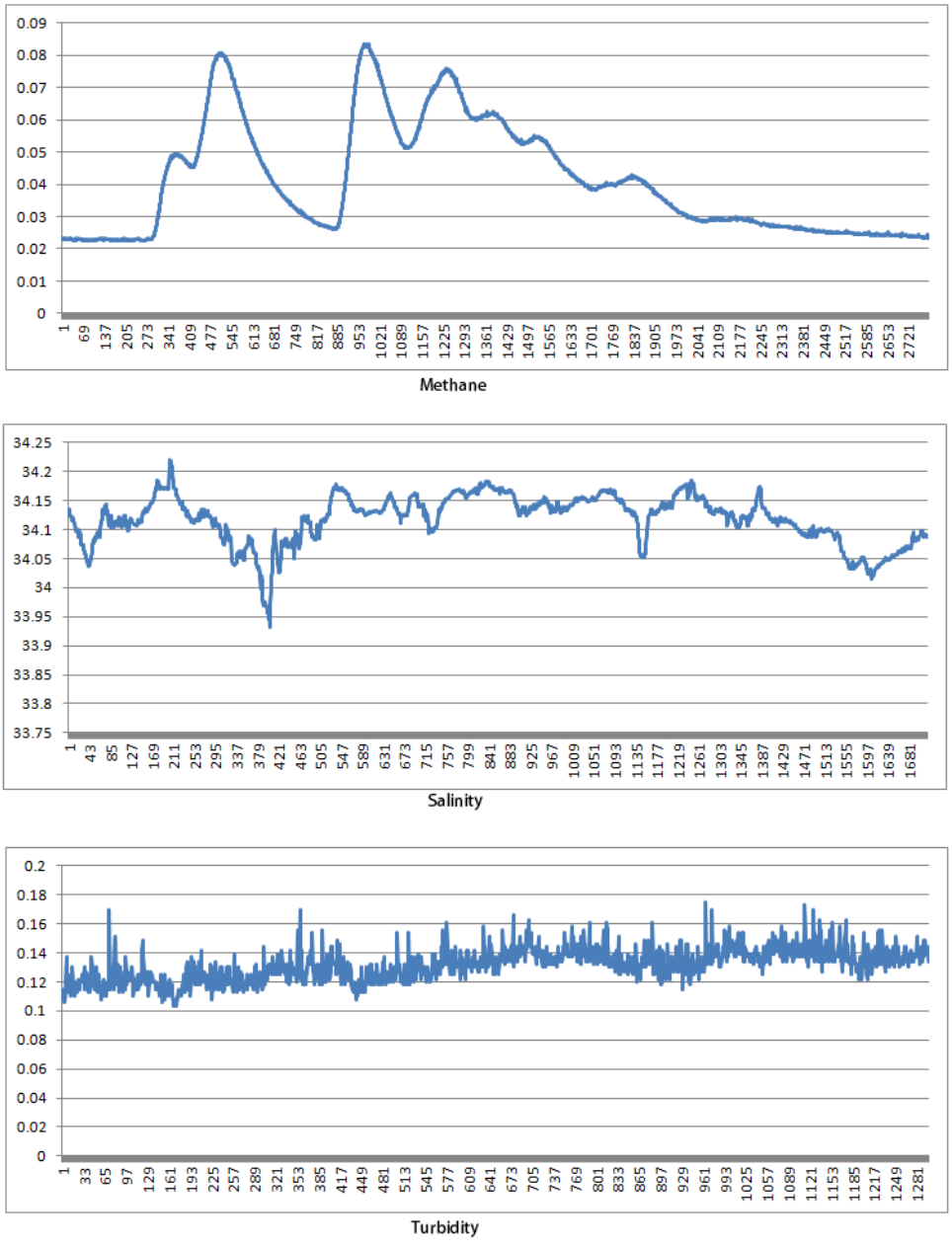

Figure 41 . Synchronous methane (µmol/litre), salinity (ppt) and turbidity (NTU) vs time (seconds) recordings from the HG2 carbonate crust field. No clear relationships between these parameters can be established.

Environmental data such as temperature, salinity, turbidity, and visibility were recorded simultaneously with the methane. When plotted on a map, distinct patterns can be recognized when viewing the entire survey. However, there are no clear relations between levels of

methane and e.g. turbidity and salinity when looking at a time series from the passing of HG2 (Fig. 41).

The CH_4 levels recorded by the METS sensor indicates that there is a slight delay in the gas detection, and that elevated levels are recorded for a considerable time after passing the actual leakage site. The initial delay is well illustrated by Fig. 37 and Fig. 38, showing a c. 10-20 second delay in response time after initial contact with the carbonate crust field. The tendency to continue reporting elevated methane levels for a considerable time after passing the leakage site is demonstrated in Fig. 34. HUGIN came in from the W (A), did several lines NW of the field (blue lines), then crossed the crust field moving northeastwards (B), and subsequently did two lines to the W of the field (C) showing elevated levels (red and beige lines), before heading SSE (D). The methane levels increase within 10-20 seconds after passing the crust field, approximately 20 m after passing the central part (Fig. 42).

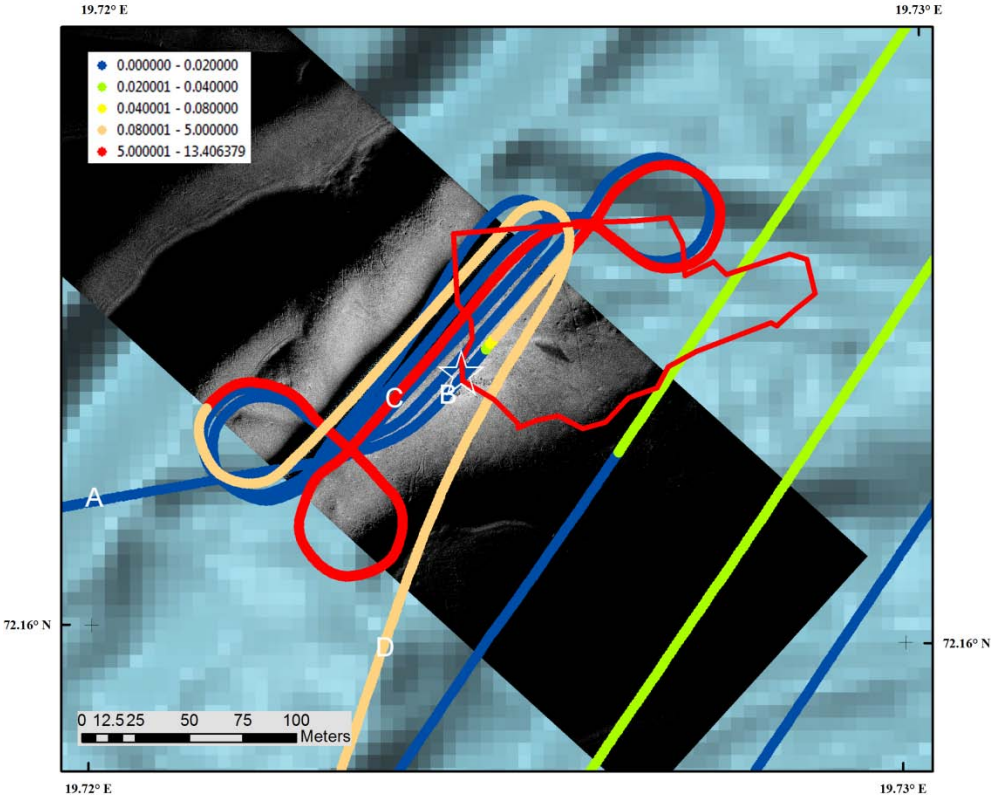

Figure 42. Map showing the HG2 flare site (carbonate crust field) (white star), the gas flare indicated from water column data (red outline), and the methane values from the METS sensor on Hugin. Note that the methane values increase within 10 seconds after passing the carbonate crust. Elevated values are detected for more than 10 minutes after passing the flare site. For several lines, no gas was detected before after passing the flare site.

The methane maximum is reached 138 seconds after passing the crust field (Fig. 43) and the recordings remain elevated above the background level for 14 minutes after the maximum. With a single line passing an active gas leakage site, it could not be excluded that the

recorded, or rather reported methane levels are correct. However, the map (Fig. 42) shows that METS reported high methane levels 20-40 m NW of the crust field after passing the field. There are no indications of elevated methane levels from the lines in the same area before the crust field was passed. This indicates strongly that the elevated levels reported by METS NW of the crust field are not real, but rather due to a "memory effect" in the METS sensor.

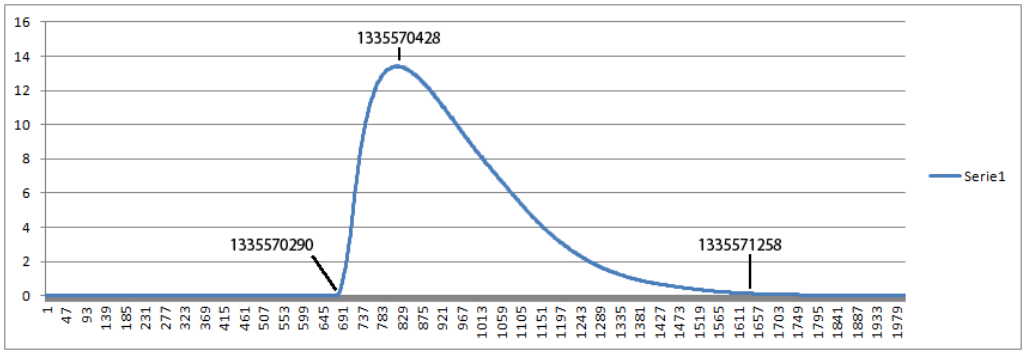

Figure 43. XY plot with methane levels ((µmol/litre),Y axis) versus time (seconds, X axis).The figure shows the time of the initial increase (1335570290), the time for the maximum recorded by METS (1335570428), and the time when the level is close to background levels (1335571258).

In the first survey (Fig. 44), the METS showed several peaks, possibly indicating additional seepage sites outside the 2012.HG2 flare. However, using the results from the second survey (Fig. 42 and Fig. 43), it can be concluded that peaks 1 and 2 in Fig. 44 are caused by the sensor's delay effect, and do not represent seepage at these sites. Peak 3 on the other hand can indicate a flare not detected by the EM710 data.

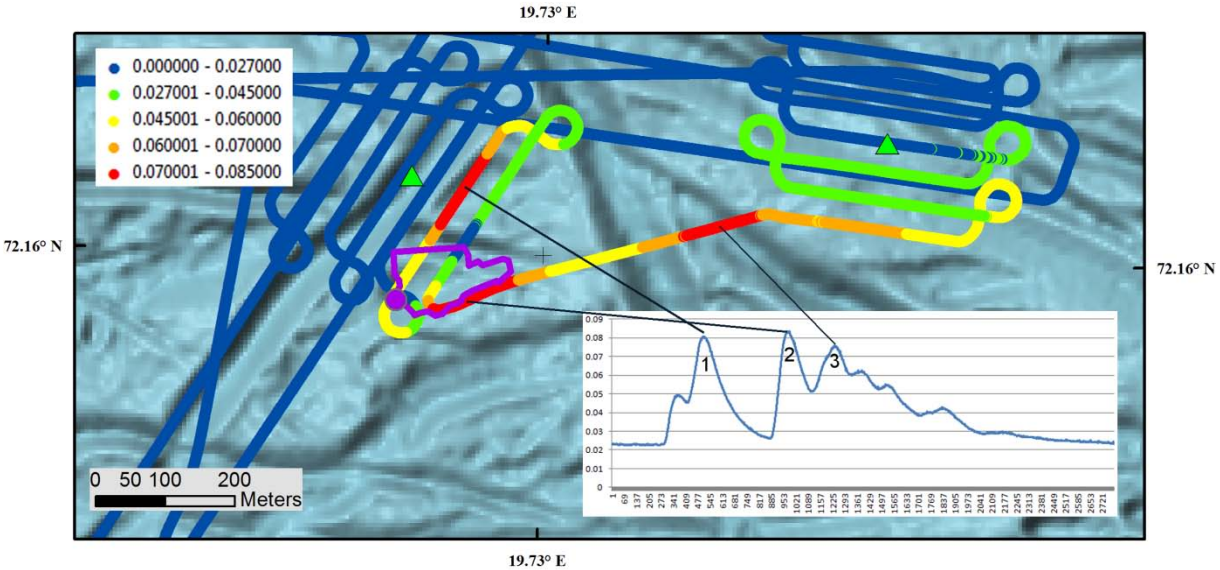

Figure 44. Map over HG2 with colour coded HUGIN track lines showing the methane concentrations recorded by the methane sniffer (METS). The inset plot (lower right) shows an XY plot with methane levels (Y axis) versus time (X axis).

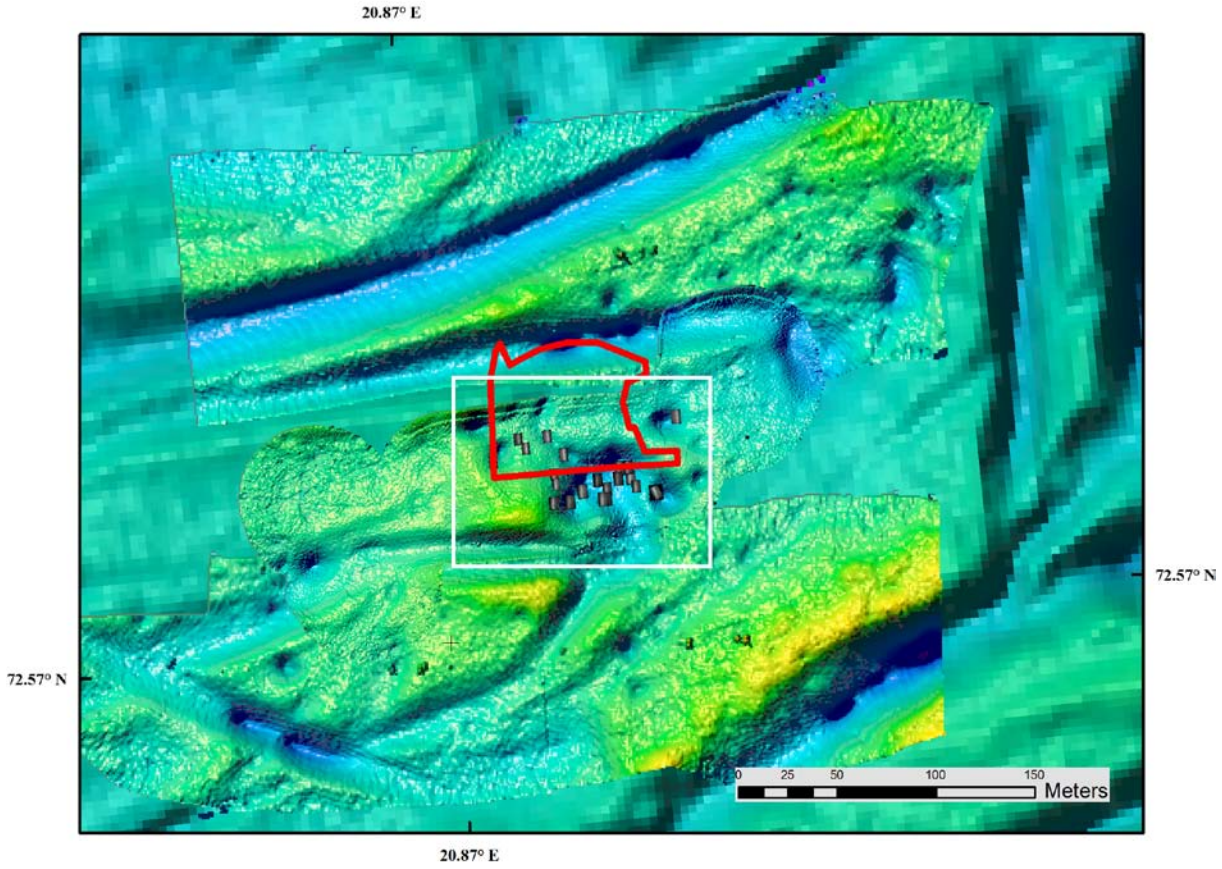

Figure 45. Shaded relief image with data from EM710 and EM2000 (HUGIN) from the eastern flare of Area B (2012.Area_B_1, Table 2, Fig.34) . Water depth varies between 394 and 388 m. The location of the gas flare is indicated by the red outline. Small grey rectangles indicate TFish photos with carbonate crusts and other seep related features. The location of Figure 46 is indicated by the white rectangle.

In Area B, the eastern flare is found just north of a pockmark (Fig. 45) which is 60 m wide and 4-5 m deep. The SAS data (Fig. 46) show that the pockmark is asymmetric with the deepest part in the north. The walls are steep in the northern part, and gentle towards the south. Small pockmarks are abundant along the northern and eastern flanks. Carbonate crusts, filamentuous bacterial mats and small irregular depressions (1-2 m wide, 5-20 cm deep) are found associated with this (Fig. 47). Another shallow pockmark of similar size, but not so deep occur 100 m ENE of the main pockmark

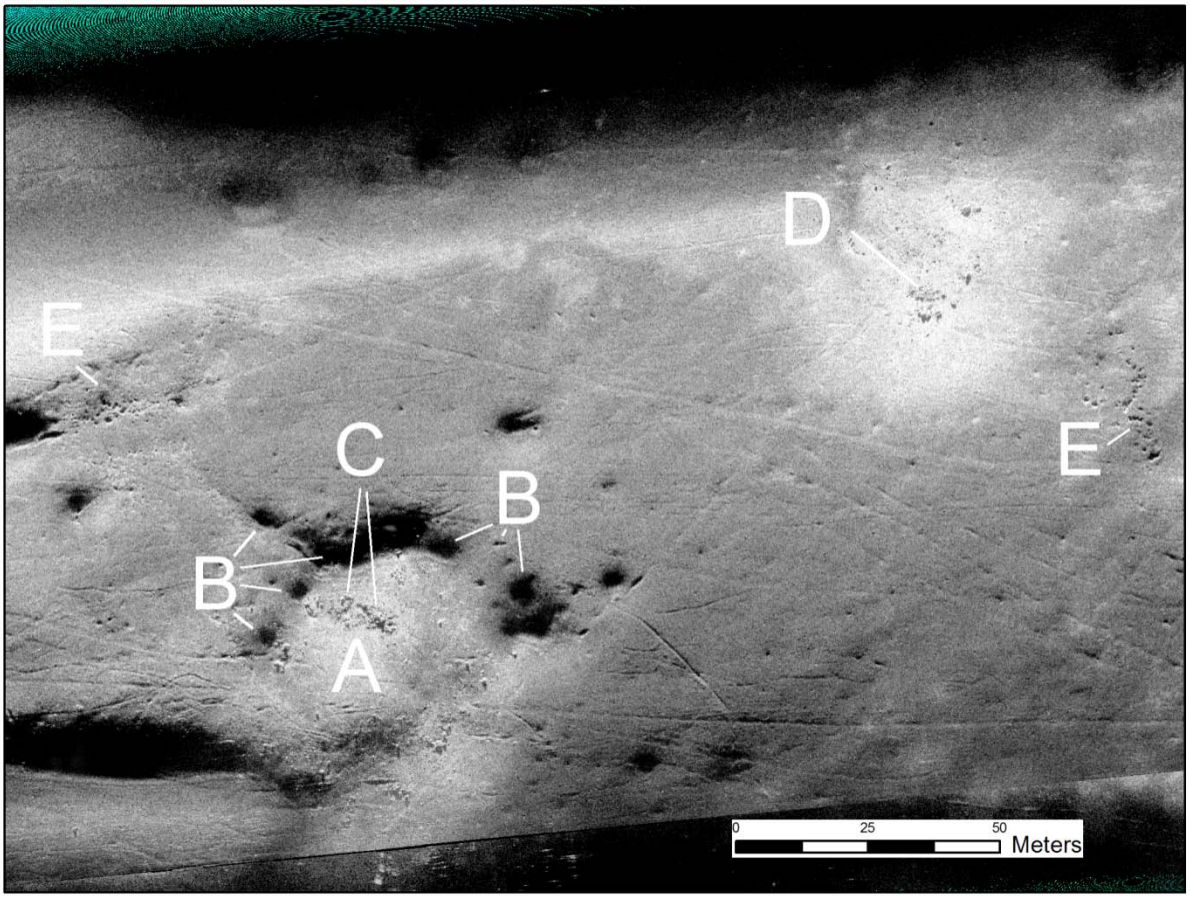

Figure 46. SAS image showing pockmark (A) associated with gas flare, small pockmarks (B) and carbonate crusts (C). Another pockmark with carbonate crust is found at D. Very small pockmarks (E) occur irregularly distributed (see Fig.45 for location).

The western flare in Area B is located in an area with water depths between 395 and 405 meters (Fig. 48) and consists of 4 individual flares in an area of c. 200 x 200 m (Fig. 49). The seabed sediments are generally muddy gravelly sand, with occasional blocks up to 1-2 m. The area is heaviliy incised by iceberg plough marks. Numerous pockmarks occur in plough marks and outside of plough marks, ranging in size from a few decimeters to 20 m. Shapes vary from circular to irregular and angular (Fig. 51). The irregular and angular shapes may indicate rapid expulsion of fluids. Carbonate crusts, irregular depressions usually filled with dark filamentuous mats, and light bacterial mats occur in clusters (Figs. 50 & 52).

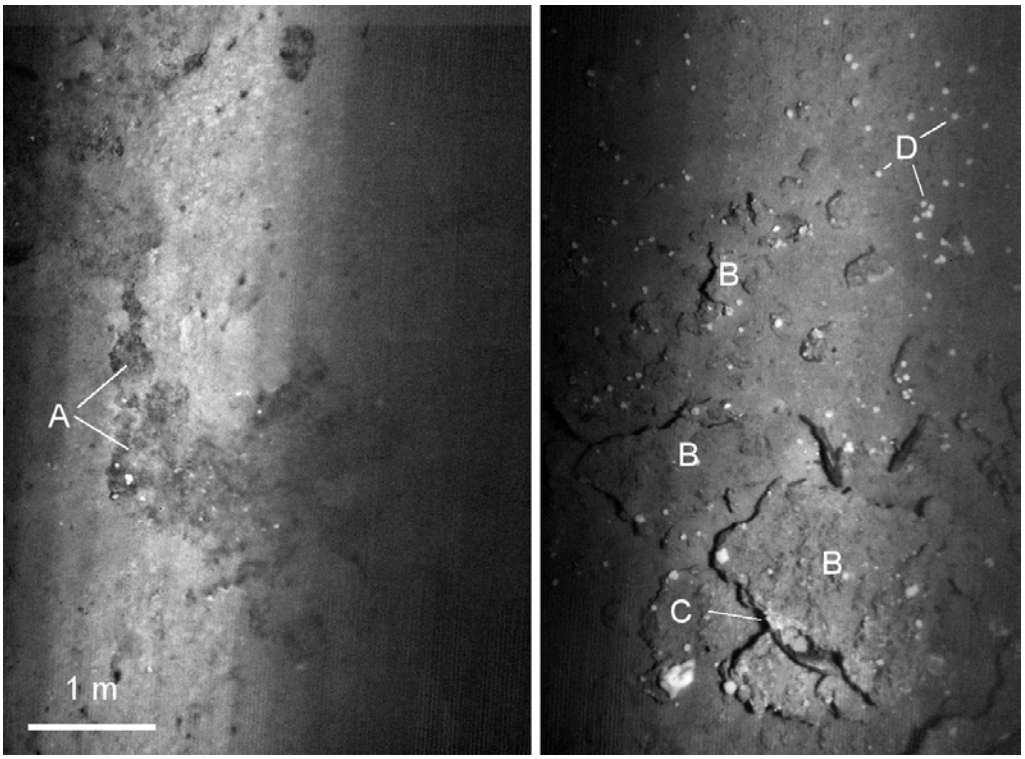

Figure 47. Left photo: Bacterial mats in small depressions (A). Right photo: Carbonate crusts (B), light bacterial mats covering crust (C) and small sponges (D).

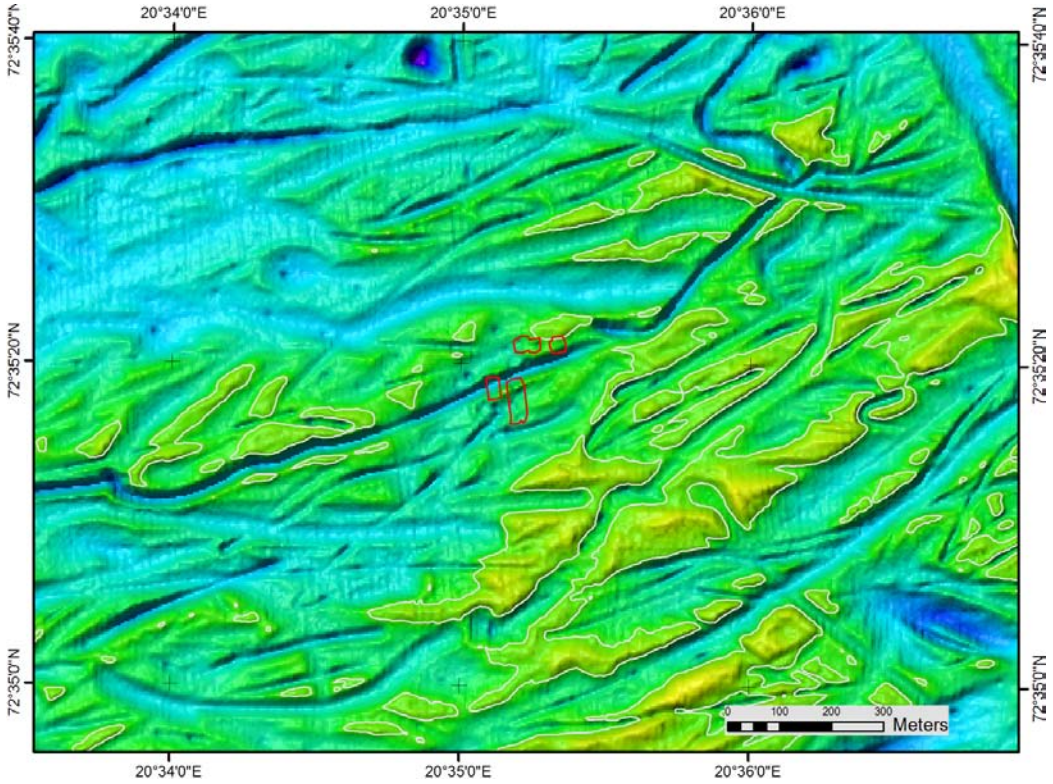

Figure 48. Shaded relief bathymetry from the western flare, Area B. Water depths are between 395 and 405 m. The 400 m contour is shown. Gas flares are shown as red outlines.

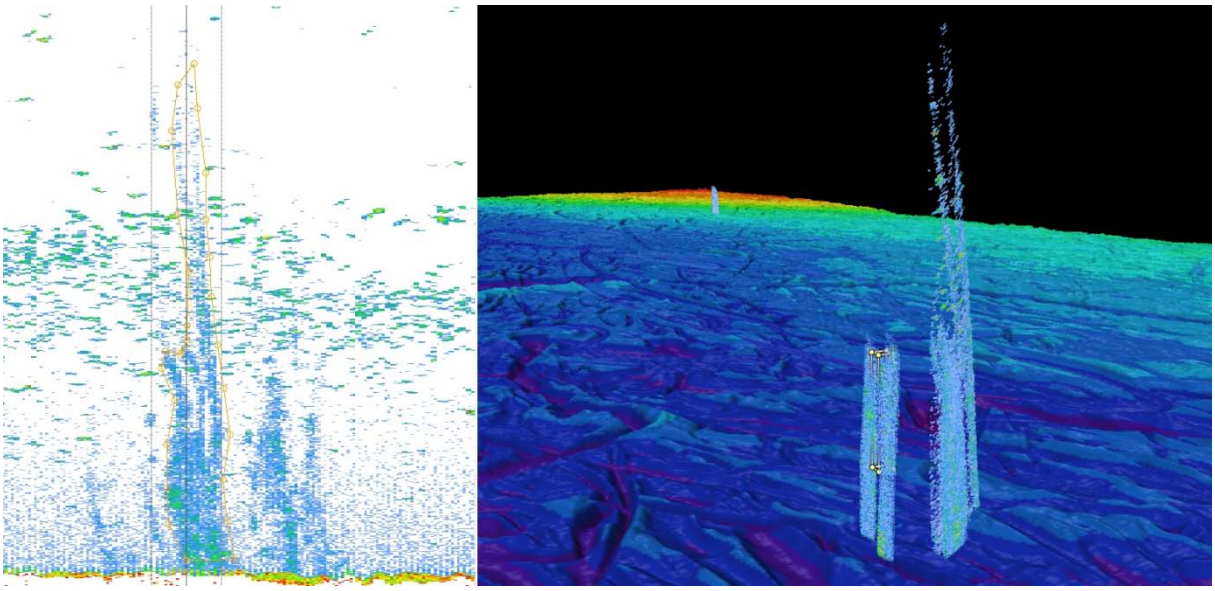

Figure 49. Left: The western gas flare(s) of Area B visualised in Fledermaus Midwater. Right: 3D visualisation of the western gas flare(s). The gas flare is nearly 200 m high. The eastern gas flare can be seen in the background. See Fig. 48 for location.

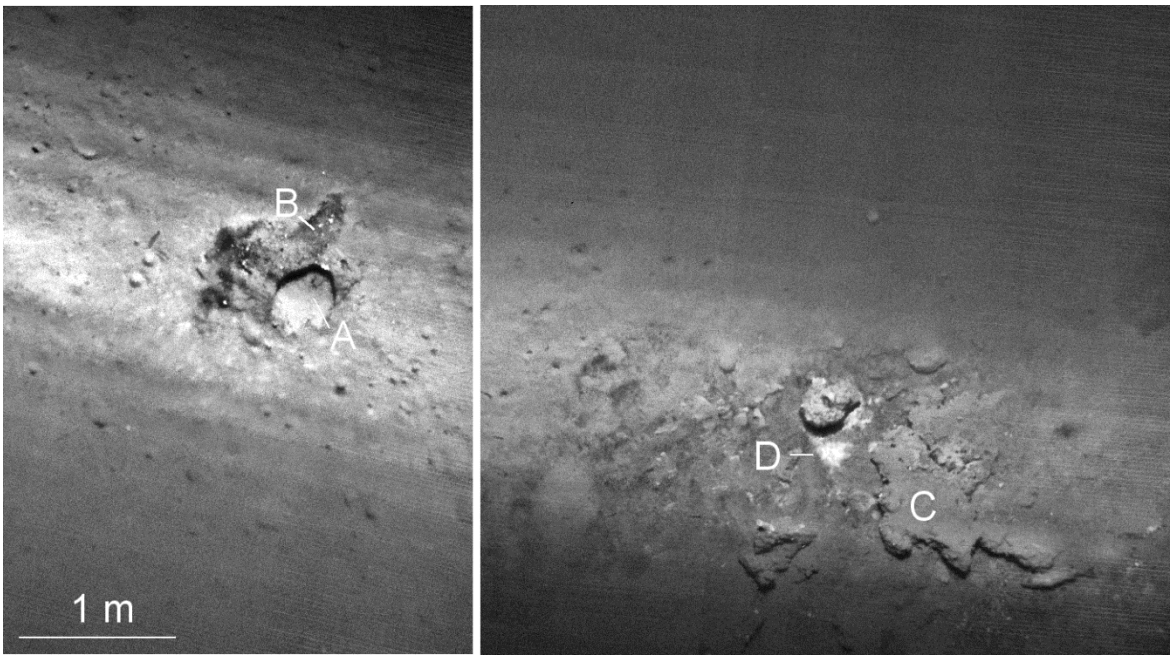

Figure 50. Left: Small, angular pockmark (A) with dark filamentuous mats (B). Right: Carbonate crust (C) and light bacteria mat (D).

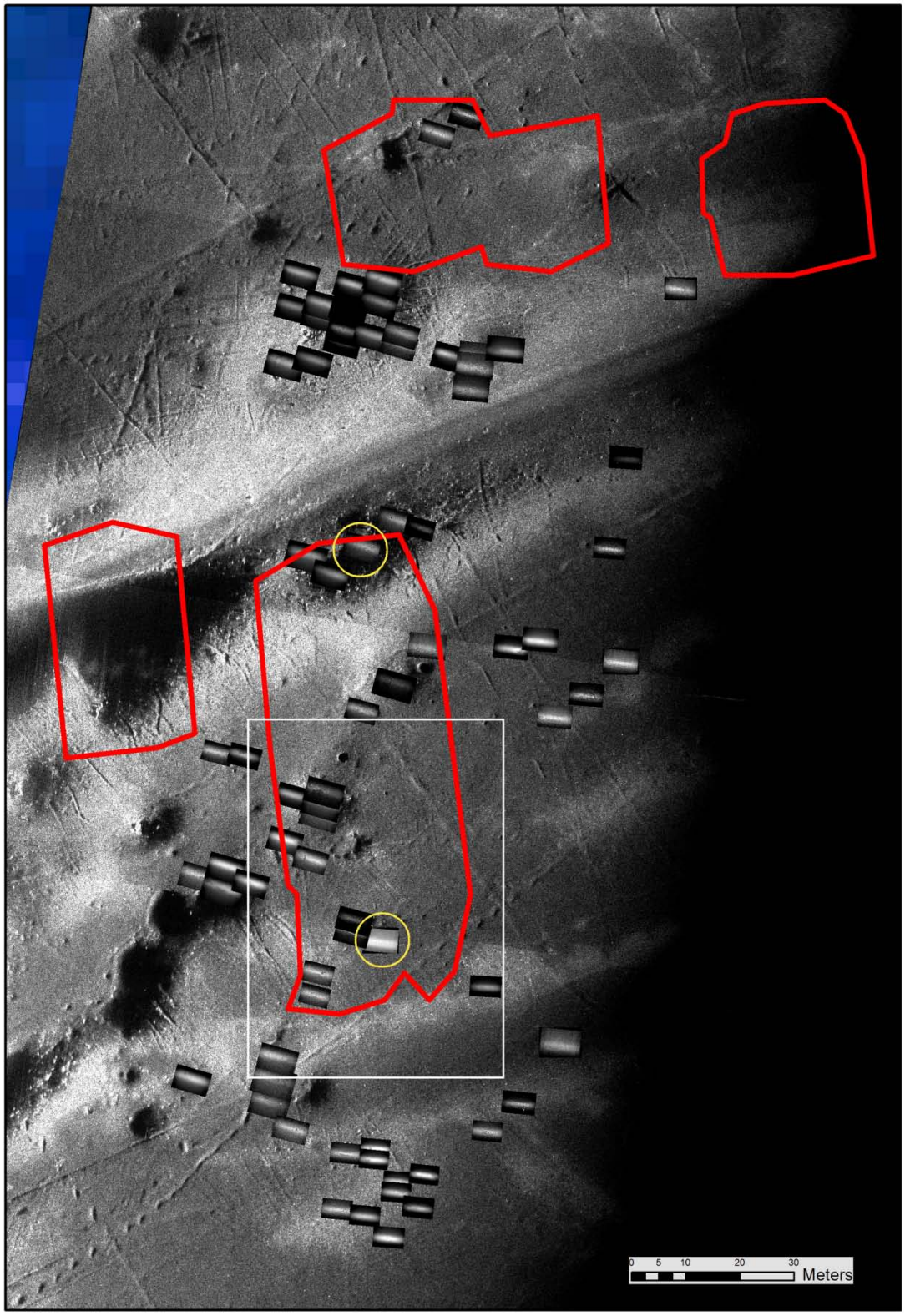

Figure 51. SAS image from the western flare site, Area B. Gas flares are shown as red outlines. Gas bubble locations are marked by yellow circles. TFish images with carbonate crusts and other seep related features are overlain. The location of figure 52 is indicated by the white rectangle.

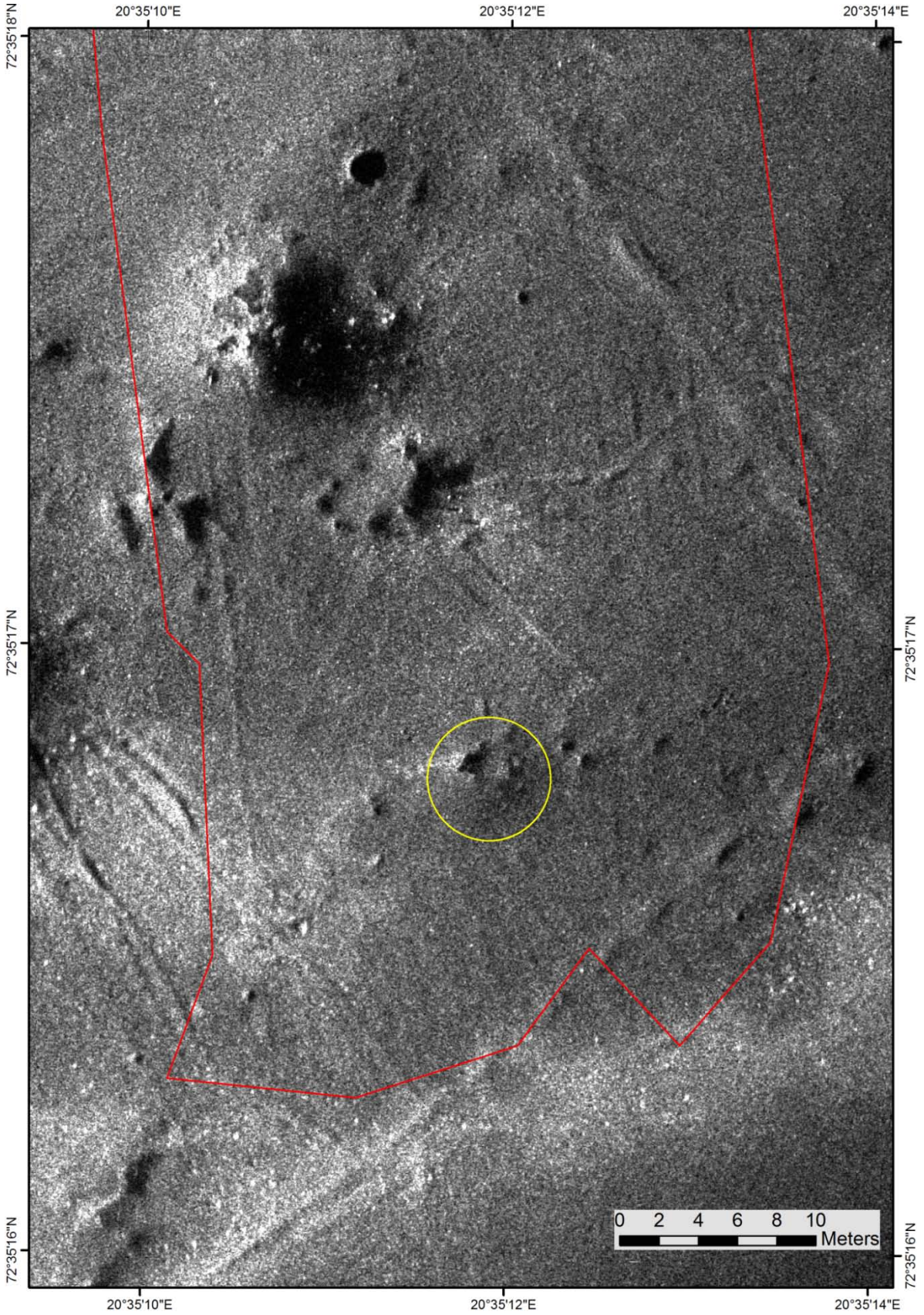

Figure 52. Detailed SAS image showing the southernmost observed gas bubble locality, the outline of the gas flare, and numerous circular to angular pockmarks. Numerous trawl marks (NE-SE, NNW-SSE and N-S) are also visible.

4.4.2. Finnmark Platform

Water column data analyses using the FlederMaus Midwater package indicate 11 possible acoustic gas flares in the area covered by the multibeam data (Figs. 53). The flares are suspicious due to their occurrence in the noisy outer beams of the MBB system. One of the flares is located close to the TFFC (Fig. 53). One of the flare was remapped to verify its presence but without any success indicating that the identified anomalies probably are due to water noise generated by the ship or other electronics within the frequency band of outer beams.

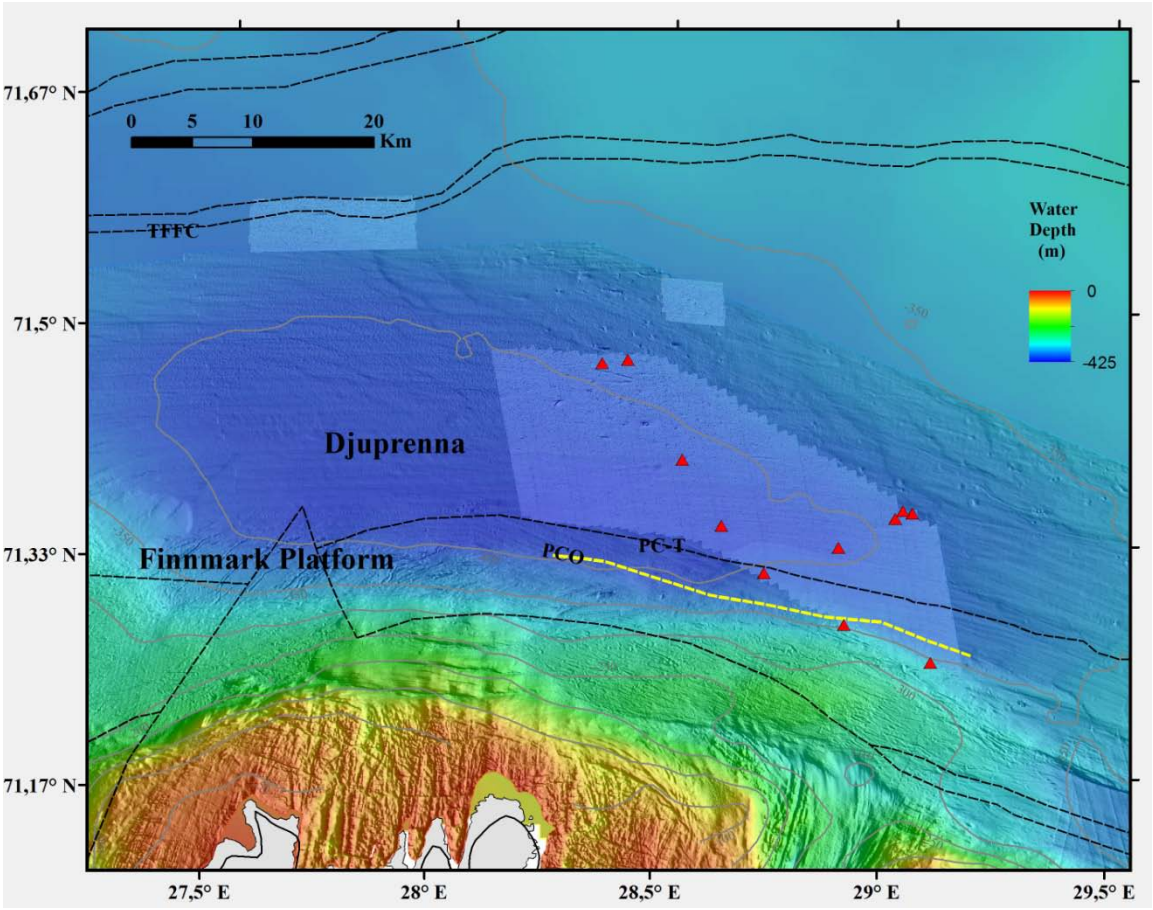

Figure 53. Regional multibeam bathymetry of the Finnmark study area from MAREANO data, multibeam data from the HU Sverdrup II cruise in August 2012 (overlay), bedrock boundaries (black dashed lines), Permo-Carboniferous and Triassic (PC-T) and seafloor outcrop of Permo-Carboniferous bedrock (PCO) mapped from FFI 2D seismic (yellow line).

4.5 **Neotectonic structures**

4.5.1. Loppa High

The new MBB data in Area A and Area B did not indicate occurrence of any neotectonic features.

4.5.2. Finnmark Platform

Two topographic-high diapir like features were observed close to the Permo-Carboniferous to Triassic subcrop boundary on the low resolution bathymetry. These features were remapped with the HUGIN and MBB system, and the new data revealed a ship wreck (Fig. 54).

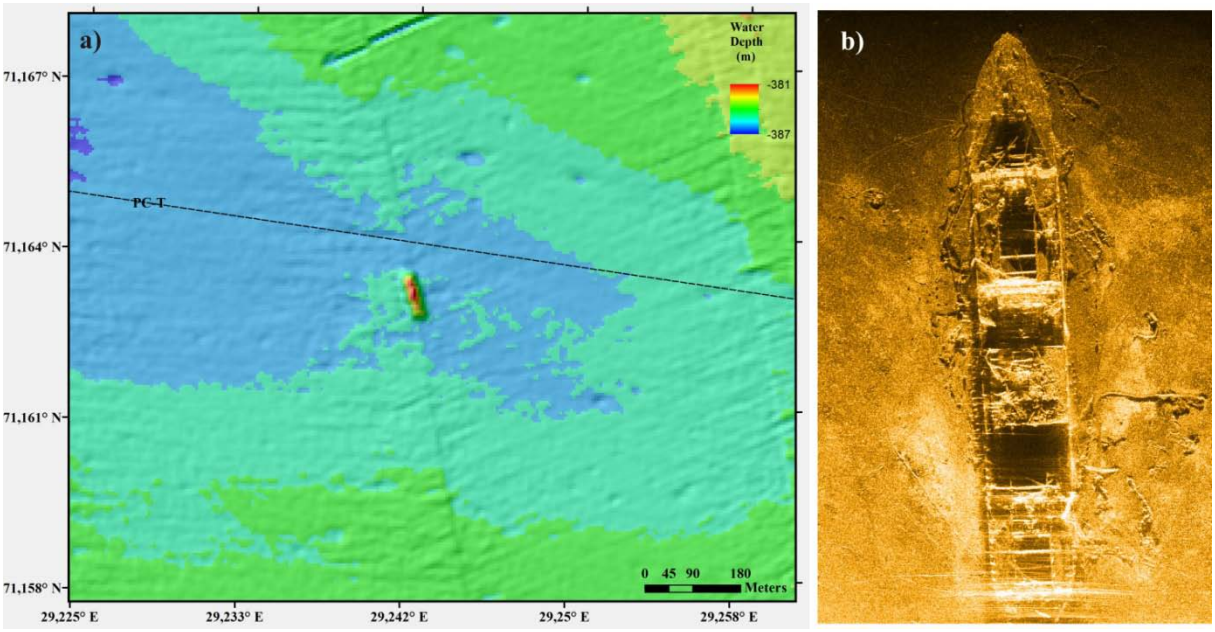

Figure 54. a) Two diapir like features observed on bathymetric data which were later identified to represent a ship wreck. b) HISAS image of the ship.

4.6 **Gas hydrates and fluid flow**

Gas hydrates in offshore areas are often associated with a bottom simulating reflector (BSR) . A BSR is a seismic reflector which sub-parallels the seafloor reflection and is opposite in polarity (Shipley et al., 1979). The BSR indicates an acoustic impedance change across a high velocity layer of gas hydrate containing sediments overlying a gas filled layer (Stoll and Bryan, 1979). The BSR is paralleling the seafloor since the thickness of the gas hydrate stability zone (GHSZ) is primarily decided by the hydrostatic pressure induced by the water column thickness (Sloan, 1990).

The nature and properties of BSRs and their occurrence vary depending on the sedimentary environment and fluid flow (Chand and Minshull, 2003). It is observed in many parts of the world that the BSR depths are determined by the presence of one or more of the gas hydrate inhibitors (NaCl, N_2, warm fluids, isostatic uplift, sliding, deglaciation) or facilitators (CO_2, H_2S, higher order hydrocarbon gases, increase in sea level, subsidence). Hydrates formed from pure methane assume molecular structure I while in the presence of higher order hydrocarbon gases it takes structure II. Structure I and II gas hydrates have different stability conditions and physical properties. Hence, it is complicated to interpret the presence of gas hydrates in areas with mixed gas origin causing disturbed BSRs, or in regions outside the methane hydrate stability field where all the gas hydrate is formed as structure II. The BSR or gas hydrate stability zone is shifted due to changes in sea level, variations in ice thickness or due to influx of warm or salty fluids from below, altering gas hydrate stability conditions.

The present regional gas hydrate stability estimated for structure II hydrates containing higher order hydrocarbon gases for the Barents Sea indicates a ~250 m deep base of the GHSZ covering the study area while the structure I MHSZ is zero using a gas composition consisting of 96% methane, 3% ethane and 1% propane (Chand et al., 2012b). The estimated thickness of the GHSZ in two way time (TWT) in milliseconds (ms) is around 220-270 ms assuming 1990 m/s velocity for the sediments (observed at well 7220/2-1). High amounts of CO_2 (up to 6%) and H_2S (3 ppm) is reported from the Snøhvit area in many wells, indicating that CO_2 and H_2S may be of importance while modelling the gas hydrate stability in this region (NPD, 2005; eg., NPD well report 7021/4-1).

The regional MHSZ estimated for the Barents Sea indicates a base 0 to 250 m below the seafloor depending on the present day bathymetry and bottom water temperature (Chand et al., 2012b). During the last glacial maximum (LGM), about 20 000 ^{14}C years ago, a more than 1200 m thick ice cap covered the SW Barents Sea (Siegert et al., 2001). This made the whole SW Barents Sea stable for methane hydrate with MHSZ depths up to 600 m below the present seafloor (Chand et al., 2012b). The difference between the present MHSZ and that during LGM indicates a change of thickness by up to 600 m. The MHSZ within the Bear Island Trough (BIT) thinned to less than 250 m while most other parts of the southwestern Barents Sea including our study area lie outside the MHSZ. The major change occurred outside the BIT, which made this region prone to release of methane accumulated during the last glaciation as methane hydrates. Our study areas experienced a change in MHSZ of 500 m to zero m during this change in ice thickness.

4.6.1. Loppa High

Gas hydrate modeling was carried out assuming two different gas compositions during the earlier phases of the project (Chand et al., 2008; 2012a). The gas compositions and geothermal gradients observed in the nearby wells were used to assess the gas hydrate stability of the region in more detail. The analysis showed that the gas hydrate stability zone is very shallow and close to the seafloor at the Loppa High, but deepening towards the Tromsø Basin and Sør-Vestnaget Basin/Veslemøy High (Fig. 55). The acquisition of gas from this area using ROV and the results from the gas analysis led to a totally different scenario since the gas leaking is observed to be 100% methane (Table 3). In such a case, the higher order components which could be leaking from the subsurface are most probably adsorbed by the sediments. The gas is observed to have a thermal component in it as indicated by relatively high $\delta^{13}C$ values (Table 4) ruling out a totally biogenic origin (Fig. 56). The study area is also located close to the boundary of the Loppa High where the prograding wedges of glacial debris pinch out causing upward focusing of fluids towards the eastern flank of the Loppa High. The study area is also transected by a large number of regional faults, including the Ringvassøy Loppa Fault Complex and the Asterias Fault, facilitating upward fluid flow.

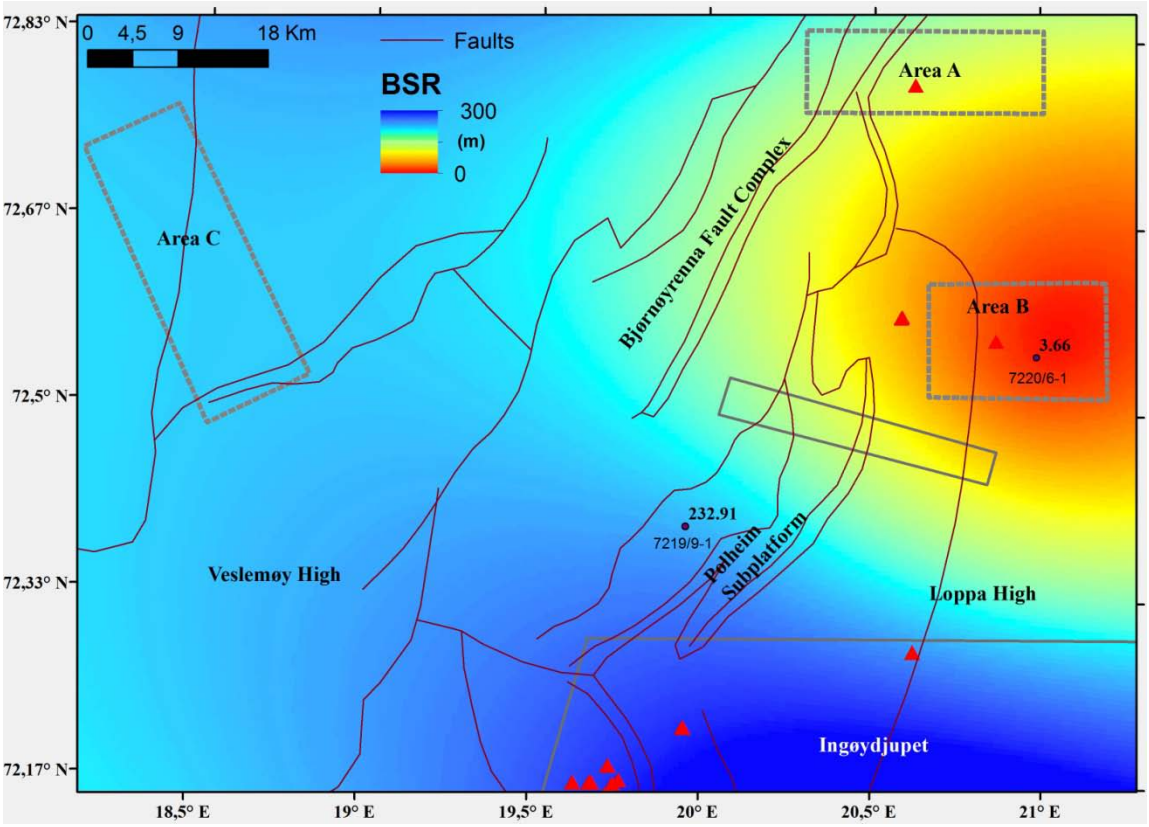

Figure 55. Gas hydrate stability zone map of the Loppa High area showing the shallowing of the gas hydrate stability zone towards the Loppa High from the Tromsø Basin.The gas hydrate stability zone thickness estimated at each well site and well names are also given. Red triangles show locations of gas flares.

Table 3. Gas composition from anlaysis of gas samples collected by ROV in the Loppa High gas flare area.

Well	Sample type	Sample info	APT ID	C1(%THCG)	C2(%THCG)	C6+(%THCG)	CO2(%THCG)	ppm THCG	He(%Total)	N2(%Total)	O2+Ar(%Total)	Ppm Total	C1-nC4(%THCG)	C2-nC4(%THCG)	C5+(%THCG)	Wetness
Barents Sea gas seeps	Gas	P1210031G	103327	100.0	0.0000	0.0042	0.018	658612	0.0075	27.7	5.65	103327	100.0	0.0038	0.0042	0.0038
Barents Sea gas seeps	Gas	P1210038G	103328	100.0	0.0000	0.0000	0.0028	873990	0.0095	11.4	0.85	103328	100.0	0.0038	0.0000	0.0038

Table 4. Gas isotope values of samples collected in the Loppa High area.

Well	Sample type	Sample info	APT ID	C1 δ13C	CO2 δ13C	C1 δD
Barents Sea gas seeps	Gas	P1210031G	103327	-47.8	-17.7	-185
Barents Sea gas seeps	Gas	P1210038G	103328	-47.6		-187

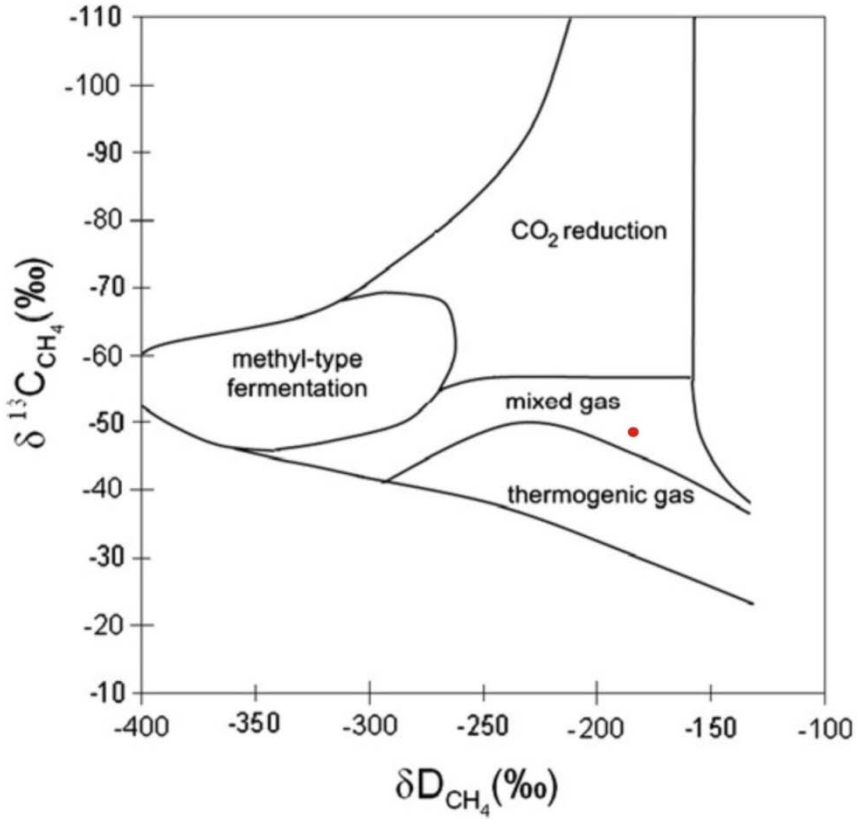

Figure 56. Cross plot of $\delta^{13}C$ and δD values of methane in a gas sample from the Loppa High area (red dot) shown on a diagram of known isotopic fields for bacterial and thermogenic methane (adapted from Whiticar (1990)).

Area C was analysed for gas hydrate stability zone thickness in an attempt to explain the deep, high amplitude reflector (Fig. 57) observed in the area. The gas hydrate stability zone is deeper in Araa C than in Areas A and B, but the deep high amplitude reflector observed in Area C (Fig. 57) cannot be explained with a gas hydrate model. Similar cross cutting reflectors observed at comparable depths along the western Loppa High are interpreted to be due to fluid flow close to the Opal A to Opal CT transition zone. General lithological correlation to information from nearby well (Moe et al ., 1988) and depths indicate top Paleocene, and a similar kind of depositional setting is expected in Area C. Deposition of siliceous ooze in Area C in a similar kind of setting can lead to Opal A being converted to Opal CT at these depths resulting in high amplitude reflector.

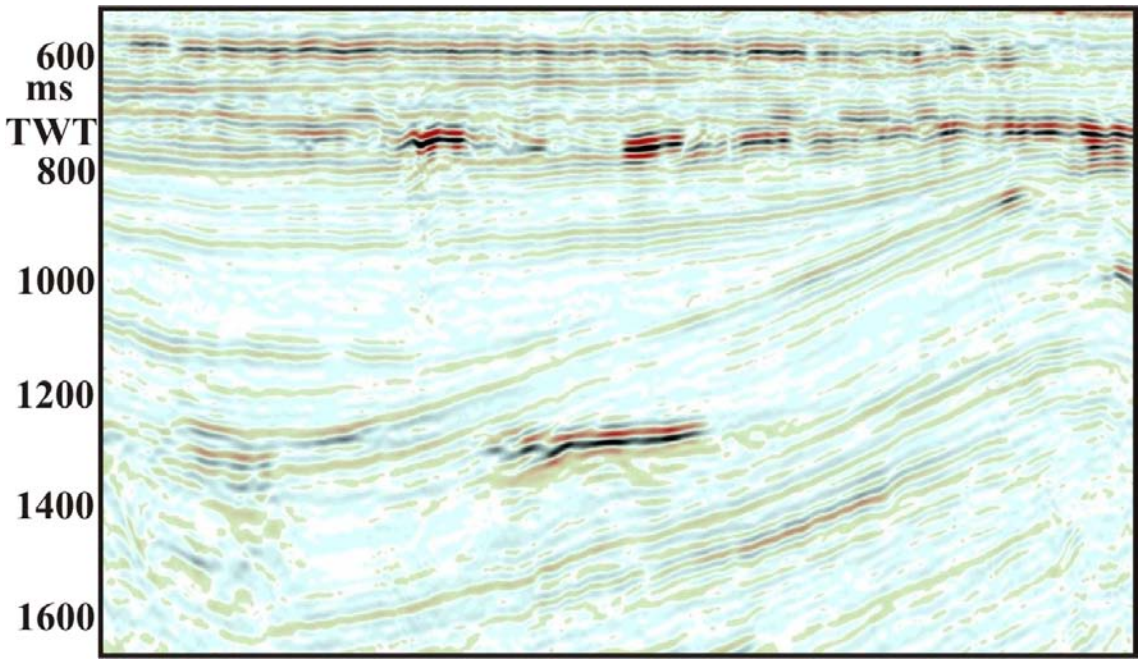

Figure 57. Seismic line from Area C indicating a suspicious high amplitude reflection cutting across stratigraphic layers.

4.6.2. Finnmark Platform

The Finnmark platform study area has also been modelled for gas hydrate stability zone depths using information from the nearby well 7128/4-1. The gas hydrate stability zone is estimated to be around 250 m below the sea floor and deepening towards the Hammerfest Basin (Fig. 58). Seismic sections show older formation subcropping below a thick Quaternary succession (Figs. 59 & 60). The boundary between the Permo-Carboniferous and Triassic cross cuts the southern part of the study area and many units subcrop under the URU creating many possible fluid flow pathways (Fig. 59). The boundary between the Permo-Carboniferous and the Triassic does not indicate fluid flow or seepage neither in the water column nor in subsurface seismic data (Fig. 59). The southern pockmarks boundary appears to coincide with one of the bedrock boundaries. The deepest part of the depression in the

study area appears to be devoid of soft sediments due to relatively high current strength along the steep slopes close to the bedrock outcrop. Detailed high resolution seismic acquired using HUGIN Edgetech sub bottom profiler needs to be analysed before a conclusion can be made. The Quaternay succession thins out north of the study area close to the Jurassic-Cretaceous boundary (Fig. 60).

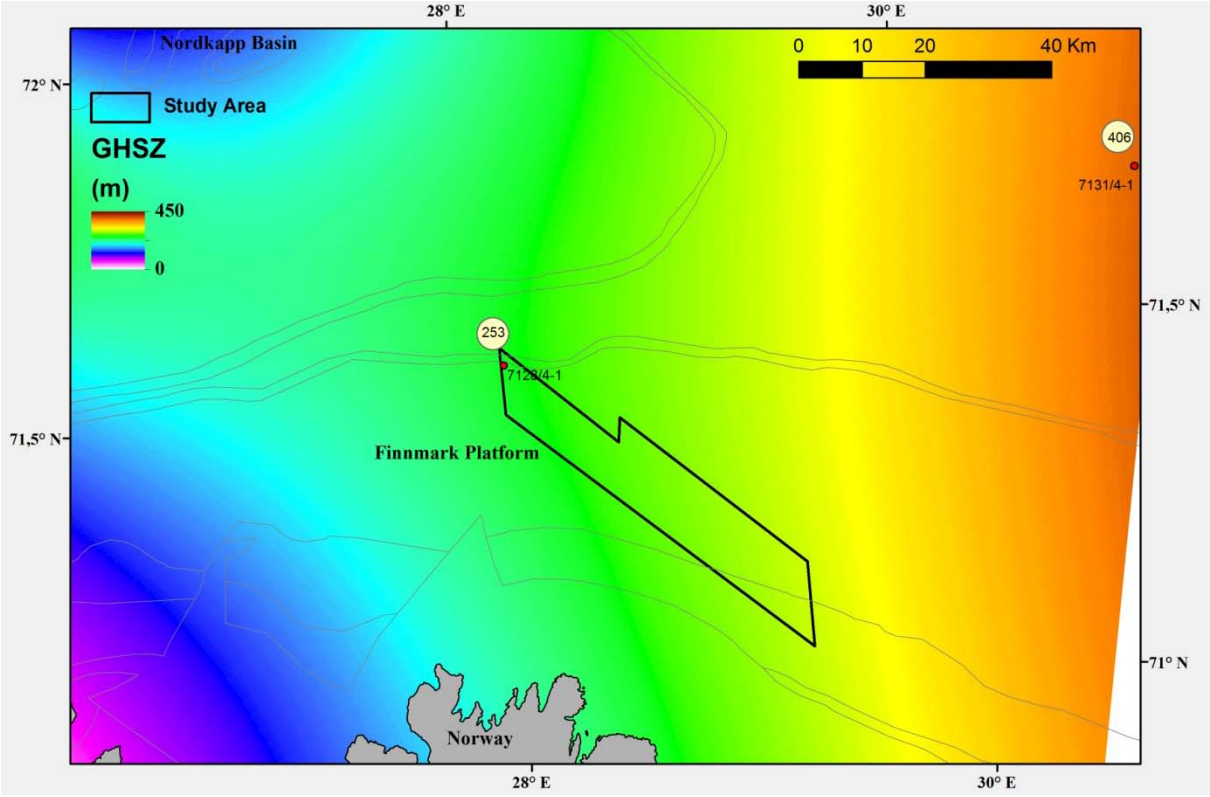

Figure 58. Gas hydrate stability zone in the Finnmark platform study area.The estimated gas hydrate stability zone thickness at well locations and the well names are also shown.

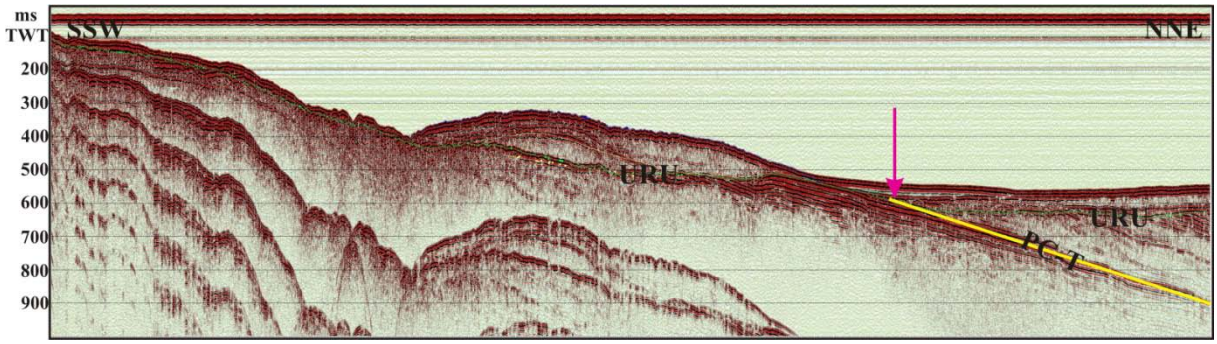

Figure 59 . Seismic line FFI_SB1L57 across the Permo-Carboniferous to Triassic boundary (red arrow). Green line: base Plio-Pleistocene. See Fig. 4 for location.

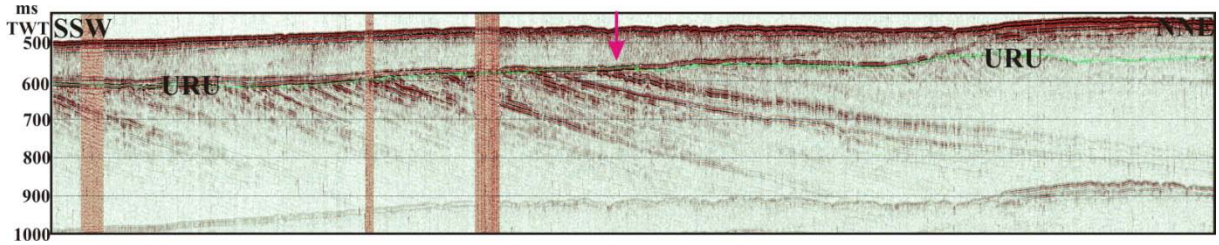

Figure 60 . Seismic line FFI_S6L02 across the Jurassic-Cretaceous boundary (red arrow). Green line: base Plio-Pleistocene (URU). See Fig. 4 for location.

In both study areas, fluid flow appers to be controlled by dipping strata and open faults resulting from tectonism, isostatic uplift and glacial erosion. The fluid flow model for the study area is complex due to the two stage process which governed the accumulation and release of fluids and gases.

Fluids and methane accumulated as methane hydrates under glaciers during LGM and were later released during the deglaciation which created the pockmarks. This can be confirmed in the Loppa High area, where the pockmarks were formed after deposition of the glaciomarine and the lower part of the postglacial marine succession. The stratigraphic layers in the glaciomarine unit are cut by the pockmarks, indicating that sediments were removed once the gas hydrates started melting after the glaciers retreated from this region. The process has a time delay and probably stopped after some time indicated by a few centimeters of marine sediments in pockmarks. The correlation between sub bottom profiler data and the cores justify this conclusion. Thus the formation of pockmarks can be related to the deglaciation after the LGM.

A second stage of fluid flow, may be related to leakage along regional faults. Concentration of acoustic gas flares along the Ringvassøy Loppa Fault Complex and fluid accumulation along stratigraphic boundaries indicate a focused fluid flow system. This is justified by the findings of new gas flares along the fault complex and also findings of subsurface gas anomalies related to it connected to deeper strata. The focused fluid flow at present is hence concentrated along these open faults and driven by isostatic uplift after the removal of ice load.

5. CONCLUSIONS

1. New multibeam echosounder data from Study area A from Loppa High identified one new gas flare and a large density of pockmarks beyond 400 metre water depths. No neotectonic features were observed in this area.
2. New multibeam echosounder data form Study area B from Loppa High indicated two areas with gas flares. Pockmarks occur in both flare areas. Carbonate crusts, filamentuous bacterial mats and small irregular depressions (1-2 m wide, 5-20 cm deep) occur at the base of the flares. No neotectonic features were identified in this area.
3. New gas flares were discovered in the Polheim Sub-platform area which were not active during the last multibeam acquisition. Some of the previously documented flares were not active during the survey in April 2012. This shows the episodic nature of the gas flares.
4. Carbonate crusts and active gas seepage were documented by the HUGIN surveys using the HISAS synthetic aperture sonar, the TFish photo system and the Mets methane sniffer.
5. Analysis of the methane sniffer data from several lines crossing the gas seeps gave valuable information on the behaviour of the sniffer with regard to response time and the time to get back to background levels after passing gas seepages.
6. ROV cruise of these locations recovered gas and carbonate crust samples. Analysis of gas samples indicated the dominance of a thermogenic component in the seeping gas.
7. Airgun seismic profiles across selected locations verified thickness of Quaternary units, and showed consistency with previously collected data.
8. New multibeam echosounder data collected from the Finnmark Platform did not indicate the presence of any gas flares or neo tectonic features.
9. Gas hydrate modelling in conjunction with other anomalies indicate the GHSZ is shallow in both study areas. The strong dipping reflector observed in Area C can be compared to the Opal A to Opal CT transition boundary observed in the Tromsø basin.

6. REFERENCES

Andreassen, K. & Hansen, T. 1995: Inferred gas hydrates offshore Norway and Svalbard. Norsk Geologisk Tidskrift 45, 10-34.

Andreassen, K., Laberg, J.S. & Vorren, T.O. 2008: Seafloor geomorphology of the SW Barents Sea and its glaci-dynamic implications. Geomorphology 97, 157-177.

Bugge, T., Elvebakk, G., Fanavoll, S., Mangerud, G., Smelror, M., Weiss, H.M., Gjelberg, J., Kristensen, S.E. & Nilsen, K. 2002: Shallow stratigraphic drilling applied in hydrocarbon exploration of the Nordkapp Basin, Barents Sea. Mar. Pet. Geol. 19, 13–37.

Chand, S. & Minshull, T. A. 2003: Seismic constraints on the effects of gas hydrate on sediment physical properties and fluid flow: A review. Geofluids 3, 275-289.

Chand, S., Mienert, J., Andreassen, K., Knies, J., Plassen, L., & Fotland, B. 2008: Gas hydrate stability zone modeling in areas of salt tectonics and pockmarks of the Barents Sea suggest an active hydrocarbon venting system. Marine and Petroleum Geology 25, 625-636.

Chand, S., Thorsnes, T., Rise, L. & Bøe, R. 2009. Shallow Geology and seabed processes, Western Barents Sea. NGU Report 2009.041, pp 71.

Chand, S., Thorsnes, T., Rise, L. & Bøe, R. 2012a: Pockmarks, gas flares, tectonic features and processes leading to their formation, south western Barents Sea. NGU Report 2012.017.

Chand, S., Thorsnes, T., Brunstad, H., Stoddert, D., Bøe, R., Lågstad, P. & Svolsbru, T. 2012b: Huge gas flares, pockmarks and gas accumulation along the Loppa High, SW Barents Sea indicate multiple episodes of formation and fault controlled focused fluid flow. Earth and Planetary Science Letters 331-332, 305-314.

Eldholm, O., Sundover, E., Myhre, A.M. & Faleide, J.I. 1984: Cenozoic evolution of the continental margin off Norway and western Svalbard. In: AM Spencer (ed) Petroleum geology of the North European Margin, Graham and Trotman, London, 3-18.

Eidvin, T. & Riis, F. 1989: Nye dateringer av de tre vestligste borehullene I Barentshavet. Resultater og konsekvenser for den tertiaere hevingen. NPD Contribution 27, 44 pp.

Eidvin, T., Brekke, H., Riis, F. & Rensaw, D.K. 1998: Cenozoic stratigraphy of the Norwegian Sea continental shelf 64^{o}N – 68^{o}N. Norsk Geologisk Tidskrift 78, 125-151.

Eidvin, T., Jansen, E. & Riis, F. 1993: Chronolgy of Tertiary fan deposits off the western Barents Sea: implications for the uplift and erosion history of the Barents Shelf. Marine Geology 112, 109-131.

Faleide, J.I., Solheim, A., Fiedler, A., Hjelstuen, B.O., Andersen, E.S., Vanneste, K. 1996: Late Cenozoic evolution of the western Barents Sea – Svalbard continental margin. Global and Planetary change 12, 53-74.

Hald, M., Saettem, J. & Nesse, E. 1990: Middle and Late Weichselian stratigraphy in shallow drillings from the southwestern Barents Sea: foraminiferal, amino acid and radiocarbon evidence. Norsk Geologisk Tidskrift 70, 241-257.

Knies, J., Matthiessen, J., Vogt, C., Laberg, J.S., Hjelstuen, B.O., Smelror, M., Larsen, E., Andreassen, K., Eidvin, T. & Vorren, T.O. 2009: The Plio-Pleistocene glaciation of the Barents Sea-Svalbard region: a new model based on revised chronostratigraphy. Quaternary Science Reviews 28, 812-829.

Laberg, J. S., Andreassen, K., Knies, J., Vorren, T.O. & Winsborrow, M. 2011: Late Pliocene-Pleistocene development of the Barents Sea Ice Sheet, Geology, 38, 107-110.

Lastochkin, A.N. 1977: Submarine valleys on the northern continental shelf of Europe, Izv. Vsesoy. Geogr. Obsh. 5, 412-417.

Løseth, H., Lippard, S.J., Sættem, J., Fanavoll, S., Fjerdingstad, V., Leith, L.T., Ritter, U., Smelror, M. & Sylta, O. 1992: Cenozoic uplift and erosion of the Barents Sea – evidence from the Svalis Dome area. In: TO Vorren et al (eds) Arctic Geology and Petroleum Potential (Norw. Pet. Soc. Spec Pub. 2, Elsevier Amsterdam, 639-661.

Moe, R.H., Roaldset, E. & Gjelsvik, N. 1988: Siliceous sediments and seismic response – a correlation tool in exploration on Norwegian shelf. Norwegian Petroleum Society, Correlations in Hydrocarbon Exploration, 3-5 October.

Mørk, M.B. & Duncan, R.A. 1993: Late Pliocene basaltic volcanism on the western Barents shelf margin: implications from petrology and ^{40}Ar -^{39}Ar dating of volcani-clastic debris from a shallow drill core. Norsk geologisk Tidskrift 73, 209-225.

Nansen, F. 1904: The bathymetrical features of the North Polar seas with a discussion of the continental shelves and previous oscillations of the shoreline. Norwegian Polar Expeditions 1893-1896, Scientific results, vol. IV, 231pp.

Norwegian Petroleum Directorate, 2005: NPD well report 7021/4-1, http://factpages.npd.no/ReportServer?/FactPages/PageView/wellbore_exploration&rs:Command=Render&rc:Toolbar=false&rc:Parameters=f&NpdId=135&IpAddress=193.156.2.1&CultureCode=nb-no

Nyland, B., Jensen, L.N., Skagen, J., Skarpnes, O. & Vorren, T. O. 1992: Tertiary uplift and erosion in the Barents Sea: Magnitude, timing and consequences. In: RM Larsen and H Brekke, TB Larsen and E Talleraas (eds), Structural and tectonic modeling and its application to petroleum geology, Norw. Pet. Soc. Spec. Publ. 1, Elsevier, Amsterdam, 153-162.

Nøttvedt, A., Berglund, T., Rasmussen, E. & Steel, R. 1988: Some aspects of Tertiary tectonics and sediments along the western Barents shelf. In: Morton AC, and Parson LM, (eds): Early Tertiary volcanism and the opening of the NE Atlantic. Geological Society of London, special publication 39, 421-425.

Oliver, John S., Slattery, Peter N., Silberstein, Mark A., O'Connor, Edmund F. 1984: Gray whale feeding on dense ampeliscid amphipod communities near Bamfield, British Columbia. **Canadian Journal of Zoology,** 1984, Vol. 62, No. 1, 41-49.

Riis, F. & Fjeldskaar, W. 1992: On the magnitude of the late Tertiary and Quaternary erosion and its significance for the uplift of Scandinavia and the Barents Sea. In: RM Larsen, H Brekke, BT Larsen, and E Talleraas (eds): Structural and tectonic modeling and its application to the Petroleum Geology NPF Special Publication 1, 163-185, Elsevier, Amsterdam.

Sheriff, R. 1980: Nomogram for Fresnel zone calculation. Geophysics 45, 968-972.

Shipley, T.H., Houston, M., Buffler, R.T., Shaub, F.J., McMillan, K.J., Ladd, J.W. & Worzel, J.L. 1979: Seismic reflection evidence for the wide spread occurrence of possible gas hydrate horizons on continental slopes and rises. American Association of Petroleum Geologists 63, 2204-2213.

Siegert, M.J., Dowdeswell, J.A., Hald, M., Svendsen, J.I. 2001: Modelling the Eurasian Ice Sheet through a full (Weichselian) glacial cycle. Global and Planetary Change 31, 367-385.
Sloan, E. D. 1990: Clathrate Hydrates of Natural Gases, Marcel Dekker, NewYork.

Sigmond, E.M.O. 1992: Bedrock map of Norway and adjacent ocean areas, NGU.

Solheim, A. & Elverhøi, A. 1985: A pockmark field in the central Barents Sea: gas from petrolgenic source ? Polar Research, 3, 11-19.

Solheim, A. & Kristoffersen, Y. 1984: Sediments above the upper regional unconformity: thickness, seismic stratigraphy and outline of the glacial history, Norsk Polarinstitutt Skrifter 179B, 26pp.

Solheim, A., Faleide, J.I., Andersen, E.S., Elverhøi, A., Forsberg, C.F., Vanneste, K., Uenzelmann-Neben, G. & Channell, J.E.T. 1998: Late Cenozoic seismic stratigraphy and glacial geological development of the east Greenland and Svalbard-Barents Sea continental margins. Quaternary Science Reviews 17, 155-184.

Spencer, A.M., Home, P.C. & Berglund, L.T. 1984: Tertiary structural development of western Barents shelf: Troms to Svalbard. In: AM Spencer (ed) Petroleum geology of the North European Margin, Graham and Trotman, London, 199-210.

Stoll, R.D. & Bryan, G.M. 1979: Physical properties of sediments containing gas hydrates. Journal of Geophysical Research 84, 645-648.

Sættem, J., Rise, L. & Westgard, D.A. 1992: Composition and properties of Glacigenic sediments in the southwestern Barents Sea. Marine Geotechnology 10, 229-255.

Vadakkepuliyambatta, S., Buenz, S., Mienert, J. & Chand, S. 2013: Distribution of sub-surface fluid flow systems in the southwest Barents Sea. Marine and Petroleum Geology (in press).

Vorren, T.O., Hald, M. & Lebesbye, E. 1988: Late Cenozoic environments in the Barents Sea. Paleocenography 3, 601-612.

Vorren, T.O., Kristoffersen, Y. & Andreassen, K. 1986: Geology of the inner shelf west of North Cape. Norsk Geologisk Tidskrift 66, 99-105.

Vorren, T.O., Lebesbye, E., Andreassen, K. & Larsen, B. 1989: Glacigenic sediments on a passive continental margin as exemplified by the Barents Sea. Marine Geology 85, 251-272.

Vorren, T.O., Lebesbye, E. & Larsen, K,B. 1990: Geometry and genesis of the glacigenic sediments in the southern Barents Sea, In: Dowdeswell JA and Scourse JD, (eds) Glacimarine environments, processes and sediments, Geol Soc London, Sp Publ. 53, 309-328.

Vorren, T.O., Richardsen, G., Knutsen, S.M. & Henriksen, E. 1991: Cenozoic erosion and sedimentation in the western Barents Sea. Marine and Petroleum Geology 8, 317-340.

Whiticar, M.J. 1990: A geochemical perspective of natural gas nad atmospheric methane. In: Durand B & Behar F, (eds.) Advances in organic geochemistry, Pergamon press, Oxford, pp. 531-547,

Winsborrow, M.C.M., Andreassen, K., Corner, G.D., Laberg, J.S. 2010: Deglaciation of a marine-based ice sheet: Late Weichselian palaeo-ice dynamics and retreat in the southern Barents Sea reconstructed from onshore and offshore glacial geomorphology. Quaternary Science Reviews, 29, 424-442-

WOD, 2005: World Ocean Database, (2005) http://www.nodc.noaa.gov/General/temperature.html.

Norges geologiske undersøkelse
Postboks 6315, Sluppen
7491 Trondheim, Norge

Besøksadresse
Leiv Eirikssons vei 39, 7040 Trondheim

Telefon 73 90 40 00
Telefax 73 92 16 20
E-post ngu@ngu.no
Nettside www.ngu.no

Geological Survey of Norway
PO Box 6315, Sluppen
7491 Trondheim, Norway

Visitor address
Leiv Eirikssons vei 39, 7040 Trondheim

Tel (+ 47) 73 90 40 00
Fax (+ 47) 73 92 16 20
E-mail ngu@ngu.no
Web www.ngu.no/en-gb/